Epigenetic Regulation of Keratinocytes in Normal and Pathologic Wound Healing

by

Jadie Yoonjoo Moon

A dissertation submitted in partial fulfillment
of the requirements for the degree of
Doctor of Philosophy
(Immunology)
in the University of Michigan
2026

Doctoral Committee:

Professor Katherine E. Gallagher, Co-Chair
Professor Bethany B. Moore, Co-Chair
Professor Johann E. Gudjonsson
Professor J. Michelle Kahlenberg
Professor Mary O'Riordan

Jadie Yoonjoo Moon

jdymoon@umich.edu

ORCID iD: 0000-0001-9451-6806

© Jadie Yoonjoo Moon 2026

Dedication

To my parents, my brother, and my husband, for always believing in me. Your unconditional love and support have pushed me to become a better person and scientist every day.

Acknowledgements

I would like to express my deepest gratitude to my academic advisor, Dr. Katherine Gallagher, for her exceptional mentorship and unwavering support throughout my Ph.D. training. Dr. Gallagher continually pushed me to grow as a scientist by encouraging me to pursue grants, awards, conferences, and publication in high-impact journals. I began my graduate training uncertain of my potential, but through her trust, guidance, and belief in my abilities, I gained confidence in myself as an independent scientist. I am especially grateful for her support of my long-term career goals, including her encouragement to pursue a biotechnology internship during my Ph.D. as I prepare to return to industry. Her mentorship has shaped both my scientific development and my professional trajectory.

I am incredibly thankful to the members of the Gallagher laboratory, who created a supportive, collaborative, and intellectually stimulating environment. I am particularly grateful to Dr. Amrita Joshi, our lab manager, whose positivity, technical expertise, and constant willingness to help have been invaluable. Her mentorship and support in both experimental techniques and scientific problem-solving made even the most challenging experiments manageable. I would also like to thank Dr. Sonya Wolf-Fortune, who served as my primary lab mentor during the early years of my Ph.D. She not only taught me foundational keratinocyte biology techniques but also went above and beyond to provide thoughtful guidance on presentations, abstract writing, and navigating graduate school despite her busy schedule. I extend my sincere thanks to all current and former members of the Gallagher lab for their collaboration and camaraderie. In particular, I would

like to thank Amber L. Estor, my first undergraduate mentee, whose rapid growth, curiosity, and increasing independence have been a source of pride and joy to witness.

I am grateful to my thesis committee members, Dr. Johann Gudjonsson, Dr. Beth Moore, Dr. Michelle Kahlenberg, and Dr. Mary O'Riordan, for their continued guidance throughout my graduate training. Their insightful feedback, willingness to share protocols and critical resources, and thoughtful advice greatly strengthened this work. I deeply appreciate their encouragement of my long-term goal of becoming an industry scientist and their support at every stage of my Ph.D.

I would not be where I am today without the unwavering support of my family. I am profoundly thankful to my parents, Woojin Moon and Jeonghee Moon, and my brother, Jake Moon, for always listening to my struggles, lifting me up, and believing in me—especially from afar in Korea and New York. Despite the distance, their constant encouragement and confidence in my ability to complete this journey never wavered. I would also like to express my heartfelt gratitude to my parents-in-law, Daeyeal Park and Eunjoo Lew, who have welcomed me as their own daughter and provided a loving home to return to during the holidays each year. Their warmth and genuine curiosity about my work have meant more to me than words can express.

Finally, I owe my deepest gratitude to my husband, Shihyung Park. He moved across the country from California to Michigan with me to support my pursuit of a Ph.D., and together we navigated the challenges of adapting to a new environment, building a life, and adopting our cat, Hoochoo. Through every high and low, he listened patiently, offered thoughtful advice, pushed me to be better, and believed in me when I struggled to believe in myself. I will always be grateful for his sacrifices and immeasurable support, and I am excited to begin the next chapter of our lives together after the completion of this Ph.D.

Table of Contents

Dedication ii

Acknowledgements iii

List of Figures ix

Abstract xii

Chapter 1 – Introduction 1

1.1 Normal Wound Healing 1

1.1.1 Phases of Wound Healing 2

1.2 Wound Healing in Type 2 Diabetes 11

1.2.1 Epidemiology 12

1.2.2 Clinical Manifestations 12

1.2.3 Current Treatments 14

1.2.4 Future Directions 15

1.3 Epigenetic Regulation of Cell Plasticity in Wounds 15

1.4 Keratinocyte Crosstalk with Immune and Stromal Cells 18

1.4.1 Keratinocyte-Macrophage Crosstalk 18

1.4.2 Keratinocyte-Fibroblast Crosstalk 21

1.4.3 Keratinocyte-Endothelial Cell Crosstalk 22

1.4.4 Keratinocyte-T Cell Crosstalk 23

1.4.5 Other Keratinocyte Communication Networks 24

1.5 Rationale and Specific Aims 26

Chapter 2 – IL-17A Is Increased in Diabetic Wounds and Impairs Keratinocyte Function via Histone Demethylase JMJD3 31

2.1 Abstract 31

2.2 Introduction 32

2.3 Materials and Methods 35

2.3.1 Study Approval 35

2.3.2 Mice 35

2.3.3 Wound-Healing Assessment 36

2.3.4 Primary Keratinocyte Isolation 37

2.3.5 N/TERT Human Keratinocyte Culture 37

2.3.6 Scratch Wound Assay 38

2.3.7 Keratinocyte Proliferation Assay 39

2.3.8 RNA Extraction 39

2.3.9 PCR Array Analysis 39

2.3.10 siRNA Knockdown 40

2.3.11 Murine Bulk RNA Sequencing Analysis 40

2.3.12 Chromatin Immunoprecipitation Assay 40

2.3.13 Enzyme Linked Immunosorbent Assay (ELISA) 41

2.3.14 Western Blot 42

2.3.15 Histology and Immunofluorescence 42

2.3.16 Flow Cytometry 43

2.3.17 Magnetic-Activated Cell Sorting (MACS) of Murine Wound Monocyte, $CD4^+$ T cell, and Fibroblast Isolates 45

2.3.18 Human Wound Isolation 46

2.3.19 Human Bulk RNA-Seq and ScRNA-Seq Analyses 47

2.3.20 Statistics 48

2.3.21 Data Availability 48

2.4 Results 49

2.4.1 IL-17A Signaling in Keratinocytes Controls Wound Repair via Regulation of Migratory and Inflammatory Genes 49

2.4.2 IL-17A Signaling Upregulates Expression of the Histone Demethylase, JMJD3, via a TRAF6/NFκB Pathway 55

2.4.3 *Jmjd3* Directly Regulates Anti-Migratory and Inflammatory Genes in Wound Keratinocytes in Response to IL-17A and Direct Inhibition of *Jmjd3* in Keratinocytes Improves Migration / Wound Closure Rate 58

2.4.4 Human and Murine Diabetic Wounds Display Increased IL-17A Signaling, JMJD3, and Expression of Anti-Migratory / Inflammatory Genes in Wound Keratinocytes 62

2.4.5 Disruption of the IL-17A/JMJD3 Cascade in Diabetic Wound Keratinocytes Improves Wound Repair via Decreased Expression of Anti-Migratory / Inflammatory Genes 70

2.5 Discussion 81

Chapter 3 – Histone Methyltransferase SETDB2 Modulates Keratinocyte Inflammatory Cytokine Production in Diabetic Wounds by an IFNβ/JAK/STAT Mechanism 88

3.1 Abstract 88

3.2 Introduction 89

3.3 Materials and Methods 91

3.3.1 Study Approval 91

3.3.2 Mice 92

3.3.3 Wound-Healing Assessment 92

3.3.4 Primary Keratinocyte Isolation 93

3.3.5 RNA Extraction 93

3.3.6 PCR Array Analysis 94

3.3.7 Murine Bulk RNA Sequencing Analysis 94

3.3.8 Chromatin Immunoprecipitation Assay 94

3.3.9 Enzyme Linked Immunosorbent Assay (ELISA) 95
3.3.10 Western Blot 95
3.3.11 Histology 96
3.3.12 Human Wound Isolation 96
3.3.13 Human ScRNA-Seq Analysis 97
3.3.14 Statistics 98
3.3.15 Data Availability 98
3.4 Results 98
3.4.1 IFNβ Decreases Inflammatory Cytokine Gene Expression via *Setdb2* in Keratinocytes 98
3.4.2 IFNβ Regulates *Setdb2* in Keratinocytes via JAK/STAT1 102
3.4.3 SETDB2 Expression Is Decreased While Inflammatory Cytokine Gene Expression Is Increased in Diabetic Keratinocytes 105
3.4.4 Manipulation of IFNβ/SETDB2 Axis in Keratinocytes Results in Decreased Inflammation and Improved Wound Healing 108
3.5 Discussion 110
Chapter 4 – Discussion and Future Directions 116
4.1.1 Summary of Dissertation Findings 116
4.1.2 Keratinocyte Epigenetic Regulation in Chronic Wounds 117
4.1.3 WHSC1 as a Potential Epigenetic Regulator of Keratinocyte Proliferation 119
4.1.4 Broader Impact and Translational Implications 126
4.1.5 Limitations and Future Directions 128
4.1.6 Conclusions 130
Bibliography 132

List of Figures

Figure 1-1: Stages of normal and chronic wound repair 1

Figure 1-2: Keratinocyte functions in wound healing 6

Figure 1-3: Epigenetic modifications that alter cells in wounds 17

Figure 2-1: IL-17A signaling in keratinocytes controls wound repair via regulation of migratory and inflammatory genes 51

Figure 2-2: Neutralizing IL-17A-induced chemokines does not impact keratinocyte migration 54

Figure 2-3: Expression of *Jmjd3* is upregulated in response to IL-17A in keratinocytes 56

Figure 2-4: IL-17A signaling upregulates expression of the histone demethylase, JMJD3, via a TRAF6/NFκB pathway 57

Figure 2-5: *Jmjd3* directly regulates anti-migratory and inflammatory genes in wound keratinocytes in response to IL-17A and direct inhibition of *Jmjd3* in keratinocytes improves migration / wound closure rate 60

Figure 2-6: The role of JMJD3 on keratinocyte proliferation is minimal 62

Figure 2-7: Human and murine diabetic wounds display increased IL-17A signaling, JMJD3, and expression of anti-migratory / inflammatory genes in wound keratinocytes 65

Figure 2-8: Spatial and kinetic data of IL-17A and K27me3 display increasing IL-17A and decreasing K27me3 levels in diabetic wounds throughout the course of wound healing 65

Figure 2-9: Spatial single cell RNA-sequencing analysis of keratinocyte-immune cell interactions in human diabetic wounds 67

Figure 2-10: Expression of JMJD3-mediated target genes is increased at the protein level in diabetic wounds 69

Figure 2-11: Pharmacological modulation of JMJD3 *in vivo* in diabetic murine model (*db/db*) results in improved wound healing 71

Figure 2-12: Keratinocyte-specific IL-17A signaling deficiency ($Il17ra^{fl/fl}K14^{cre+}$) does not result in improved healing in the non-diabetic setting 72

Figure 2-13: Disruption of the IL-17A/JMJD3 cascade in diabetic wound keratinocytes improves wound repair via decreased expression of anti-migratory / inflammatory genes 74

Figure 2-14: Histomorphometric analysis of wound contraction and myofibroblast transition in DIO *Il17ra*$^{fl/fl}$ *K14*$^{cre+}$ mice 75

Figure 2-15: Single cell RNA-sequencing of mice with a keratinocyte-specific deletion of IL-17A signaling (*Il17ra*$^{fl/fl}$ *K14*$^{cre+}$) demonstrate decreased anti-migratory and inflammatory gene expression in wound keratinocytes and decreased T cell infiltration 77

Figure 2-16: Keratinocyte-specific deletions of IL-17A signaling or JMJD3 result in increased reparative immune and fibroblast phenotypes in wounds..... 80

Figure 2-17: Single cell RNA-sequencing of mice with a keratinocyte-specific deletion of IL-17A signaling (*Il17ra*$^{fl/fl}$ *K14*$^{cre+}$) demonstrate increased myofibroblast transition in wound fibroblasts..... 81

Figure 2-18: Schematic of IL-17A-mediated JMJD3 regulation of keratinocyte functions in normal and diabetic wound keratinocytes..... 83

Figure 3-1: IFNβ decreases inflammatory cytokine gene expression via *Setdb2* in keratinocytes 101

Figure 3-2: Confirmation of decreased Setdb2 expression in keratinocyte-specific *Setdb2*-deficient mice (*Setdb2*$^{fl/fl}$ *K14*$^{cre+}$) 102

Figure 3-3: IFNβ regulates *Setdb2* in keratinocytes via JAK/STAT1 104

Figure 3-4: SETDB2 expression is decreased while inflammatory cytokine gene expression is increased in diabetic keratinocytes 107

Figure 3-5: Manipulation of IFNβ/SETDB2 axis in keratinocytes results in decreased inflammation and improved wound healing 109

Figure 3-6: Schematic of IFNβ-mediated SETDB2 regulation of keratinocyte inflammatory cytokine gene expression in normal and diabetic wound keratinocytes 111

Figure 4-1: HiCa-differentiated keratinocytes display decreased proliferation rates and proliferative gene expression 120

Figure 4-2: HiCa-differentiated keratinocytes display decreased *Whsc1* 121

Figure 4-3: WHSC1 gene expression is increased in proliferative keratinocytes in human wounds 122

Figure 4-4: siRNA targeting and pharmacological inhibition of *Whsc1* results in decreased proliferative gene expression via reduction of K36me2 123

Figure 4-5: Pharmacological inhibition of *Whsc1* results in decreased proliferation and wound closure rates 124

Figure 4-6: Inhibition of calcium signaling results in increased *Whsc1* and proliferative gene expression 125

Figure 4-7: Pharmacological inhibition of WHSC1 results in delayed wound repair 126

Abstract

Type 2 diabetes (T2D) mellitus affects over 500 million people worldwide and is associated with profound impairments in wound healing, leading to chronic non-healing ulcers that represent a major cause of morbidity and healthcare burden. While the pathophysiology of diabetic wound healing has been extensively studied, the epigenetic mechanisms driving keratinocyte dysfunction in this context remain incompletely understood. Keratinocytes, the primary cellular component of the epidermis, serve dual roles as both structural barriers and active immune regulators during wound repair. This dissertation investigates how cytokine-driven epigenetic modifications disrupt keratinocyte function in T2D wounds, contributing to impaired re-epithelialization and chronic inflammation.

The central hypothesis of this work is that aberrant cytokine signaling in the diabetic wound microenvironment induces pathological epigenetic remodeling in keratinocytes, altering their capacity for migration, proliferation, and inflammatory regulation. Through investigation of histone-modifying enzymes and their downstream transcriptional regulation, this research examines mechanisms by which keratinocyte epigenetic states become disrupted in diabetic wounds.

The first part of this study demonstrates that interleukin-17A (IL-17A), which is elevated in diabetic wounds, drives keratinocyte dysfunction through induction of the histone demethylase Jumonji domain–containing protein 3 (JMJD3). Using primary murine keratinocytes and human diabetic wound samples, we show that IL-17A signaling through IL-17 receptor A/C complexes

activates downstream Act1/TRAF6/NF-κB pathways, resulting in increased JMJD3 expression and activity. JMJD3-mediated removal of repressive histone H3 lysine 27 trimethylation (H3K27me3) at promoters of anti-migratory genes (*Itga3*, *Timp1*) and inflammatory chemokines (*Cxcl1*, *Cxcl3*, *Cxcl5*, and *Ccl20*) leads to increased transcription of these targets, promoting an anti-migratory and pro-inflammatory keratinocyte phenotype. Single-cell RNA sequencing of human wounds revealed elevated JMJD3 expression in diabetic keratinocytes compared to their controls, consistent with altered migration and inflammatory gene signatures. Pharmacologic inhibition or genetic knockdown of JMJD3 partially restored keratinocyte migratory capacity *in vitro,* while diabetic keratinocyte-specific JMJD3-deficient mice exhibited improved wound repair *in vivo*, supporting a role for aberrant JMJD3 activity in delaying re-epithelialization in diabetic wounds.

The second part of this study defines a complementary epigenetic mechanism involving interferon-β (IFNβ)-mediated regulation of the histone methyltransferase SET domain bifurcated 2 (SETDB2). In non-diabetic wounds, IFNβ signaling activates JAK/STAT pathways in keratinocytes, inducing SETDB2 expression and promoting deposition of repressive H3K9 trimethylation (H3K9me3) marks at inflammatory gene loci, thereby suppressing excessive cytokine production. However, IFNβ levels are decreased in diabetic wounds, leading to decreased SETDB2 activity and loss of H3K9me3-mediated repression. As a result, keratinocytes from diabetic wounds exhibit increased expression of pro-inflammatory cytokines including *Il1b*, *Tnf*, and *Il23a*. Lastly, *in vivo* subcutaneous administration of IFNβ in diabetic mice improved wound closure and reduced inflammatory gene expression in keratinocytes. Together, these findings indicate that impaired IFNβ-SETDB2 signaling contributes to increased inflammatory responses in diabetic wound keratinocytes.

These findings suggest a dysregulated epigenetic state in diabetic keratinocytes characterized by both excessive inflammatory activation and insufficient repressive control. IL-17A-mediated JMJD3 activity promotes anti-migratory and inflammatory gene expression, while decreased IFNβ-mediated SETDB2 activity fails to suppress inflammatory programs. Together, these alterations skew keratinocytes toward a persistent inflammatory state that is incompatible with efficient wound closure.

Overall, this dissertation provides mechanistic insight into how cytokine-driven epigenetic remodeling contributes to keratinocyte dysfunction in diabetic wound healing. By identifying JMJD3 and SETDB2 as key mediators linking inflammatory signaling to chromatin regulation in keratinocytes, this work establishes a framework for understanding how epigenetic imbalance perpetuates wound chronicity and highlights chromatin-modifying enzymes as potential targets for therapeutic intervention in chronic diabetic wounds.

Chapter 1 – Introduction

1.1 Normal Wound Healing

Wound healing represents a fundamental biological process essential for organismal survival, orchestrating the restoration of tissue integrity following injury through precise spatiotemporal coordination of cellular, molecular, and biochemical cascades. This complex regenerative response has evolved over time to rapidly seal breaches in an organism's outermost barrier, prevent infection, and restore functional tissue architecture. In mammals, cutaneous wound healing proceeds through four overlapping yet distinct phases—hemostasis, inflammation, proliferation, and remodeling—each characterized by specific cellular activities, molecular signatures, and regulatory mechanisms that collectively determine healing outcomes (1, 2) (Figure 1-1). The success of this process depends critically upon the coordinated interactions between multiple cell types including platelets, immune cells, keratinocytes, fibroblasts, and endothelial cells, which communicate through complex networks of cytokines, chemokines, growth factors, and extracellular matrix (ECM) molecules (3).

Portions of this chapter have been published:

Moon JY & Gallagher KA. Wound healing. In D. S. Tyler (Ed.), *Sabiston Textbook of Surgery: The biological basis of modern surgical practice* (22nd ed.). Elsevier. 2025 Aug 27.

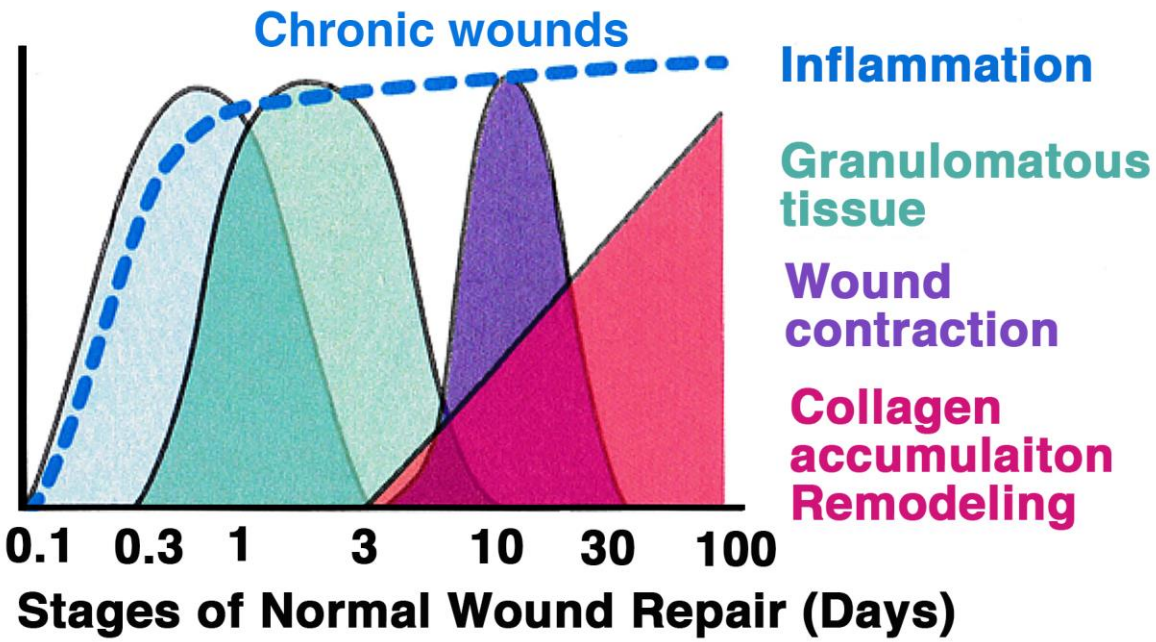


Figure 1-1: Stages of normal and chronic wound repair
Normal repair consists of overlapping phases of inflammation, granulomatous tissue formation or re-epithelialization, wound contraction, and remodeling. However, chronic wounds display prolonged inflammation and lack of transition between the different phases of healing.

At the molecular level, wound healing involves the sequential activation of thousands of genes regulated through transcriptional, post-transcriptional, and epigenetic mechanisms that ensure appropriate cellular responses at each healing phase. Transcription factors including HIF-1α, NF-κB, AP-1, and STATs orchestrate phase-specific gene expression programs, while chromatin remodeling complexes, histone-modifying enzymes, and DNA methyltransferases establish permissive or restrictive chromatin states that determine cellular plasticity and differentiation (4). The integration of these regulatory layers enables cells to rapidly respond to injury signals while maintaining tissue homeostasis and preventing aberrant healing responses such as excessive scarring or chronic inflammation (see Figure 1-1). Understanding these normal wound healing mechanisms provides the foundation for identifying pathological alterations that

underlie impaired healing in disease states, particularly type 2 diabetes mellitus (T2D) where multiple aspects of this coordinated response become dysregulated.

1.1.1 Phases of Wound Healing

1.1.1.1 Hemostasis

The hemostatic phase initiates immediately following tissue injury, representing the body's primary response to vascular damage and the first step in the wound healing cascade. Within seconds of injury, exposed subendothelial collagen and tissue factor trigger the coagulation cascade, leading to rapid platelet adhesion, activation, and aggregation at the wound site (5). Activated platelets undergo dramatic morphological changes, extending filipodia and releasing their granular contents including adenosine diphosphate, thromboxane A2, and calcium ions that amplify platelet recruitment and activation (5). Simultaneously, the extrinsic and intrinsic coagulation pathways converge to generate thrombin, which catalyzes the conversion of fibrinogen to fibrin, creating a provisional matrix that serves as both a hemostatic plug and a scaffold for migrating cells during subsequent healing phases (5).

Beyond their hemostatic function, activated platelets serve as critical initiators of the inflammatory response through the release of α-granules containing platelet-derived growth factor (PDGF), transforming growth factor-β (TGF-β), vascular endothelial growth factor (VEGF), and numerous chemokines including CXCL4 and CCL5 (6). PDGF, existing in multiple isoforms (PDGF-AA, -BB, -AB, -CC, -DD), functions as a potent mitogen and chemoattractant for fibroblasts, smooth muscle cells, and inflammatory cells, establishing concentration gradients that guide cellular migration into the wound bed (7). TGF-β, predominantly released as a latent complex requiring activation by proteases or integrins, initiates multiple signaling cascades through SMAD-dependent and SMAD-independent pathways that regulate inflammation, ECM

deposition, and cellular differentiation throughout healing (8). The fibrin-platelet plug also serves as a reservoir for these growth factors and their sustained release, maintaining bioactivity over days to weeks following injury (7).

1.1.1.2 Inflammation

The inflammatory phase, overlapping with hemostasis and extending for 2-5 days post-injury, represents a critical period where immune cells clear debris, combat infection, and establish the cellular milieu necessary for tissue repair (5). This phase is characterized by the sequential recruitment of neutrophils followed by monocytes/macrophages, and is orchestrated through overlapping chemokine gradients and adhesion molecule expression patterns on activated endothelium (9). Initial inflammatory signals including IL-1β, TNF-α, and IL-6 are produced by damaged epithelial cells, activated platelets, and tissue-resident immune cells, creating a pro-inflammatory microenvironment that promotes leukocyte extravasation through increased vascular permeability and endothelial activation (9).

Neutrophils, the first leukocytes to infiltrate wounds in large numbers, arrive within hours of injury guided by chemokines including CXCL1, CXCL2, and CXCL8 (IL-8 in humans), as well as complement components and bacterial products if present (10). These professional phagocytes eliminate pathogens through multiple mechanisms including phagocytosis, degranulation releasing antimicrobial peptides and proteases, and formation of neutrophil extracellular traps (NETs) that capture and neutralize microorganisms (10). While essential for preventing infection, neutrophil-derived proteases including elastase, cathepsin G, and matrix metalloproteinases (MMPs) can cause collateral tissue damage if not appropriately regulated (10, 11). The resolution of neutrophil infiltration through apoptosis and efferocytosis by macrophages represents a critical

checkpoint in transitioning from inflammation to proliferation, with impaired neutrophil clearance contributing to chronic wound formation (12).

Monocytes begin infiltrating the wound within 48-96 hours, differentiating into macrophages that assume diverse functional phenotypes depending on environmental cues. Classical M1 macrophages, activated by interferon-γ, lipopolysaccharide, and damage-associated molecular patterns (DAMPs), produce high levels of pro-inflammatory cytokines including IL-1β, TNF-α, IL-6, and IL-12, along with reactive oxygen and nitrogen species that provide antimicrobial defense (13). These M1 macrophages also express high levels of MHC class II molecules and co-stimulatory molecules, enabling antigen presentation and adaptive immune activation when necessary (14-16). The subsequent transition to alternatively activated M2 macrophages, driven by IL-4, IL-13, and TGF-β signaling, marks the resolution of inflammation and initiation of tissue repair. M2 macrophages produce anti-inflammatory mediators including IL-10 and TGF-β, growth factors such as VEGF and PDGF, and ECM remodeling enzymes that collectively promote angiogenesis, fibroblast activation, and re-epithelialization (14).

1.1.1.3 Proliferation

The proliferative phase, typically occurring 3-10 days post-injury, encompasses the coordinated processes of re-epithelialization, angiogenesis, and granulation tissue formation that restore tissue continuity and establish provisional matrix architecture (17). This phase involves tight regulation of cellular cooperation, with keratinocytes migrating to resurface the wound, endothelial cells forming new blood vessels, and fibroblasts synthesizing ECM components that provide structural support and regulate cellular behavior (18). The transition from inflammation to proliferation requires precise temporal regulation of growth factor expression, protease activity,

and cellular differentiation programs that transform the wound from a hostile inflammatory environment to a regenerative niche supporting tissue reconstruction (17).

Keratinocytes are epidermal cells primarily responsible for re-epithelialization during the proliferative phase and serve as a physical barrier in the skin. However, keratinocytes are also integral to driving and regulating cutaneous immunity (Figure 1-2). Previously, keratinocytes were thought to be passive cells, however, keratinocytes are highly active cells that are conditioned to respond to environmental stimuli as they express a range of pattern recognition receptors (PRRs) and cytokine receptors. They can detect pathogen-associated molecular patterns (PAMPs) such as bacterial or fungal cell wall components (e.g., LPS) and single- and double-stranded RNA and DNA present on viral species through their PRRs (19). In response, keratinocytes can initiate immune responses via activation of signaling pathways and secrete various antimicrobial peptides (AMPs) and cytokine mediators (19, 20). These factors contribute to host-pathogen defense as well as regulation of immune cell function and phenotypes. Following cutaneous injury, keratinocytes secrete type I interferons (IFNs) such as IFN-α, IFN-β, and IFN-κ (19, 21). Previous understanding of the role of type I IFNs was limited to transduction of anti-viral signaling pathways. However, IFN-κ has been shown to be a critical cytokine for tissue repair by initiating early inflammation upon injury. IFN-κ polarizes wound macrophages towards an inflammatory (M1) phenotype, initiating early and acute inflammation. Keratinocytes also release pro-inflammatory cytokines such as IL-1, IL-6, IL-8, and TNF-α to activate immune cells and recruit them to the wound site (21). Keratinocytes produce IL-7 and IL-15 which are important growth factors for T lymphocytes of the adaptive immune system that aid in the resolution of wounds (19, 22). Additionally, keratinocytes secrete chemokine factors that promote migration of distinct leukocytes to the wound site. In response to mechanical injury, keratinocytes secrete CXCL1, CXCL5, which play an

important role in recruiting neutrophils and macrophages that are the major players during early phases of wound repair (19, 20). Keratinocytes also produce CCL20 that recruits cells of the adaptive immune system that are associated with wound healing (23, 24). These dynamic interactions between keratinocytes and immune cells can drive inflammatory responses that are necessary for protection against pathogens and proper tissue repair. However, overproduction of these factors can result in dysregulated inflammation and poor wound healing as seen in chronic diabetic wounds.

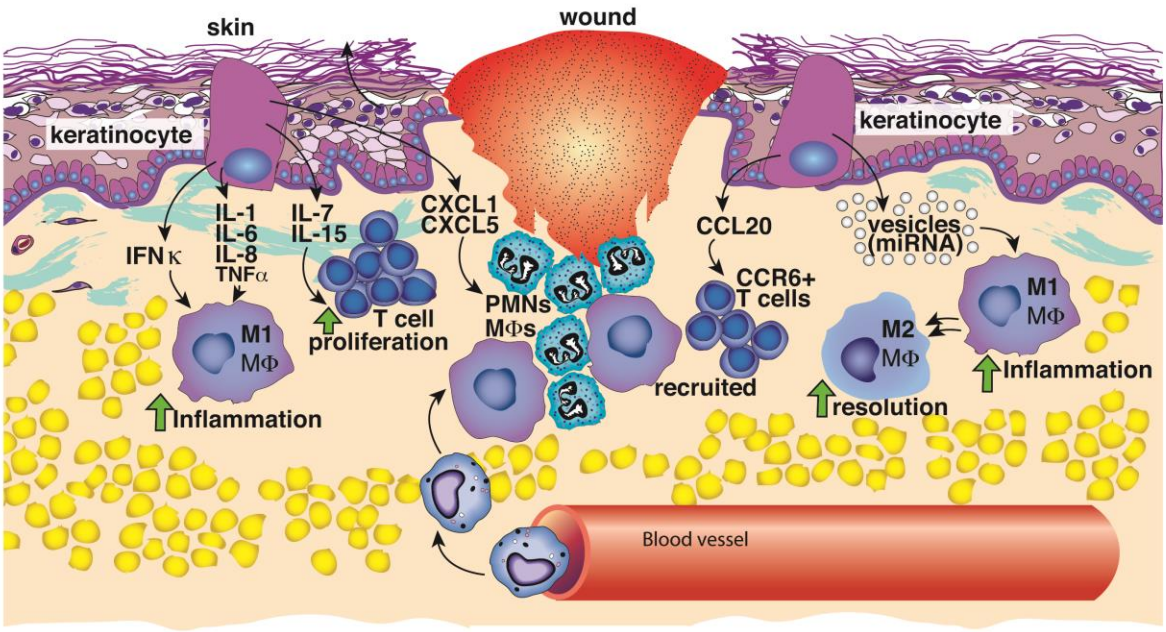


Figure 1-2: Keratinocyte functions in wound healing
Keratinocytes produce cytokines, chemokines, and extracellular vesicles in response to external stimuli in the wound environment to recruit immune cells or alter their functions and phenotypes.

Additionally, keratinocytes can communicate with other cell types by delivering cargo such as protein, lipids, DNA, and RNA via extracellular vesicles (EVs) (25-27). Keratinocyte secretion of EVs promotes cutaneous wound healing, as it allows direct cell-cell communication with wound-associated cells (28, 29). Keratinocytes release exosomes, which is a class of EVs,

containing miRNA to influence macrophage plasticity (25, 28). In vivo inhibition of keratinocyte-secreted exosomes has been shown to cause a significant increase of macrophages of a pro-inflammatory (M1) phenotype rather than a proresolution phenotype (M2) (28). Keratinocytes can actively control the fate and function of macrophages in the wound, demonstrating that bi-directional cell-cell communication between structural and immune cells is necessary for efficient wound healing.

The ultimate goal of the proliferative phase is to achieve a tightly sealed skin barrier through re-epithelialization and secure attachment to the basement membrane. The epidermis serves as a physical barrier to prevent fluid loss and bacterial invasion. Tight cell junctions within the epithelium contribute to its impermeability, and the basement membrane zone gives structural support and provides attachment between the epidermis and the dermis. The basement membrane zone consists of several layers that secure the epidermodermal interface and connect the lamina densa to the dermis: 1) lamina lucida, consisting of laminin and heparan sulfate; 2) lamina densa, containing type IV collagen; and 3) anchoring fibrils, consisting of type IV collagen (30).

The basal layer of the epidermis attaches to the basement membrane zone by hemidesmosomes. Initially, the wound is rapidly sealed by clot formation and then by epithelial cell migration across the defect. Keratinocytes located at the basal layer of the residual epidermis or in the depths of epithelium-lined dermal appendages migrate to resurface the wound. Epithelialization involves a sequence of changes in wound keratinocytes—detachment, migration, proliferation, differentiation, and stratification (30, 31). If the basement membrane zone is intact, epithelialization proceeds more rapidly. The cells are stimulated to migrate. Attachments to neighboring and adjoining cells and to the dermis are loosened, as demonstrated by intracellular

tonofilament retraction, dissolution of intercellular desmosomes and hemidesmosomes linking the epidermis to the basement membrane, and formation of cytoplasmic actin filaments (30, 32).

Epidermal cells express integrin receptors that allow them to interact with ECM proteins such as fibronectin (30, 31, 33). The migrating cells dissect the wound by separating the desiccated eschar from viable tissue. This path of dissection is determined by the integrins that the epidermal cells express on their cell membranes (33). Degradation of the ECM, required if epidermal cells are to migrate between the collagenous dermis and fibrin eschar, is driven by epidermal cell production of collagenase (MMP-1) and plasminogen activator, which activates collagenase and plasmin (30, 31). The migrating cells are also phagocytic and remove debris in their path. Cells behind the leading edge of migrating cells begin to proliferate. The epithelial cells move in a leapfrog and tumbling fashion until the edges establish contact. If the basement membrane zone is not intact, it will be repaired first. The absence of neighboring cells at the wound margin may be a signal for the migration and proliferation of epidermal cells. Local release of EGF, TGF-α, and KGF and increased expression of their receptors may also stimulate these processes (31). Topical application of keratinocyte growth factor-2 (KGF-2) in young and aged animals has been shown to accelerate re-epithelialization (34). Basement membrane proteins, such as laminin, reappear in a highly ordered sequence from the margin of the wound inward (31). After the wound is completely reepithelialized, the cells become columnar and stratified again while firmly attaching to the reestablished basement membrane and underlying dermis.

1.1.1.4 Angiogenesis

Angiogenesis, the formation of new blood vessels from existing vasculature, represents a critical component of the proliferative phase, restoring oxygen and nutrient delivery to the healing tissue. Hypoxia within the wound center stabilizes hypoxia-inducible factor-1α (HIF-1α), a master

transcriptional regulator that induces expression of pro-angiogenic factors including VEGF-A, VEGF-C, angiopoietin-2, and stromal-derived factor-1α (SDF-1α/CXCL12) (35). VEGF-A, the predominant angiogenic factor, signals through VEGFR-2 on endothelial cells to promote proliferation, migration, and tube formation, while also increasing vascular permeability that facilitates plasma protein extravasation and provisional matrix formation (35). The angiopoietin-Tie2 system provides complementary regulation, with angiopoietin-1 promoting vessel maturation and stabilization through pericyte recruitment, while angiopoietin-2 facilitates vessel sprouting and remodeling in conjunction with VEGF signaling (36, 37).

Endothelial tip cells, specialized cells at the leading edge of sprouting vessels, extend filopodia guided by VEGF gradients and express high levels of PDGF-B to recruit pericytes that stabilize nascent vessels. Behind tip cells, stalk cells proliferate to elongate the vessel sprout, while expressing Notch ligands that maintain tip cell identity through lateral inhibition (38). The basement membrane surrounding new vessels undergoes continuous remodeling, with endothelial cells and pericytes depositing laminin, collagen IV, and perlecan while MMPs including MMP-2 and MMP-9 facilitate matrix degradation necessary for vessel sprouting (39, 40). Integrin receptors, particularly αvβ3 and α5β1, mediate endothelial cell adhesion to provisional matrix components including fibrin, fibronectin, and vitronectin, providing survival signals and regulating migration directionality (41). The maturation of new vessels involves recruitment of mural cells, basement membrane assembly, and establishment of tight junctions that restore barrier function, ultimately creating a functional vascular network that persists into the remodeling phase (38).

1.1.1.5 Remodeling

The remodeling phase, which can extend for months to years following initial injury, involves the systematic reorganization of ECM architecture, reduction in cellularity, and maturation of scar tissue that determines final wound strength and appearance. This phase is characterized by a shift from collagen III to collagen I deposition, with increasing cross-linking and alignment of collagen fibers along tension lines that progressively increase tensile strength (42). The initial granulation tissue, rich in fibronectin, hyaluronic acid, and collagen III, undergoes proteolytic remodeling mediated by MMPs including collagenases (MMP-1, MMP-8, MMP-13), gelatinases (MMP-2, MMP-9), and stromelysins (MMP-3, MMP-10) whose activity is precisely regulated by tissue inhibitors of metalloproteinases (TIMPs) to prevent excessive degradation (42).

Myofibroblasts, differentiated from resident fibroblasts under TGF-β1 stimulation and mechanical tension, express α-smooth muscle actin (α-SMA) that enables wound contraction through stress fiber formation and focal adhesion maturation. These specialized cells synthesize abundant ECM proteins while simultaneously reorganizing matrix architecture through tractional forces that align collagen fibers and reduce wound area (43). The eventual disappearance of myofibroblasts through apoptosis, dedifferentiation, or senescence marks the transition to mature scar formation, though mechanisms controlling myofibroblast fate remain incompletely understood. The balance between ECM synthesis and degradation during remodeling determines whether healing results in minimal scarring, hypertrophic scarring, or keloid formation, with TGF-β/SMAD signaling, mechanical forces, and genetic factors influencing outcomes (44). Despite extensive remodeling, scar tissue never fully recapitulates normal skin architecture, achieving at best 70-80% of original tensile strength and lacking appendages including hair follicles, sebaceous

glands, and sweat glands that require developmental programs not activated during adult wound healing (44).

1.2 Wound Healing in Type 2 Diabetes

Type 2 diabetes mellitus (T2D) represents one of the most significant global health challenges of the 21st century, affecting approximately 537 million adults worldwide with projections suggesting this number will rise to 783 million by 2045 (45). The epidemic proportions of T2D, driven by increasing obesity rates, sedentary lifestyles, and aging populations, impose enormous burdens on healthcare systems through both direct costs of disease management and indirect costs from complications including cardiovascular disease, nephropathy, retinopathy, and impaired wound healing. Among these complications, diabetic foot ulcers (DFUs) represent a particularly devastating consequence, affecting 15-25% of individuals with diabetes during their lifetime and preceding 85% of lower extremity amputations (46). The five-year mortality rate following diabetic foot amputation approaches 50%, exceeding that of many cancers and highlighting the urgent need for improved understanding and treatment of diabetic wound healing impairment (46, 47).

The pathophysiology of impaired wound healing in T2D involves complex interactions between metabolic, vascular, neurological, immunological, and cellular dysfunctions that collectively disrupt the normal healing cascade. Chronic hyperglycemia, the hallmark of diabetes, induces widespread cellular and molecular alterations including advanced glycation end product (AGE) formation, polyol pathway activation, protein kinase C activation, and oxidative stress that damage tissues and impair cellular functions (48). These metabolic derangements affect all cell types involved in wound healing, from circulating immune cells exposed to hyperglycemic conditions to resident keratinocytes and fibroblasts that exhibit altered proliferation, migration,

and synthetic capabilities. The concept of metabolic memory, wherein transient hyperglycemic episodes induce persistent cellular dysfunction through epigenetic modifications, suggests that even periods of good glycemic control may not fully restore normal wound healing capacity (49).

1.2.1 Epidemiology

The epidemiology of diabetic foot complications reveals striking disparities across populations, with higher incidence rates in males, elderly individuals, those with longer diabetes duration, and individuals from lower socioeconomic backgrounds who may have limited access to preventive care (50). Geographic variations in DFU prevalence reflect differences in diabetes management, healthcare infrastructure, and genetic susceptibility, with rates ranging from 1.5% in some European populations to over 11% in certain African and North American cohorts (51). The economic burden of diabetic foot disease is staggering, with annual costs exceeding $13 billion in the United States alone, driven by prolonged hospitalizations, repeated surgical interventions, rehabilitation services, and lost productivity (52). These statistics underscore that diabetic wound healing impairment represents not merely a medical challenge but a significant public health crisis requiring comprehensive approaches addressing prevention, early intervention, and novel therapeutic development.

1.2.2 Clinical Manifestations

Clinical manifestations of diabetic foot ulcers reflect the multifactorial pathogenesis, with neuropathy, ischemia, and infection forming the pathological triad underlying most cases. Peripheral neuropathy, affecting up to 50% of individuals with long-standing diabetes, involves sensory, motor, and autonomic nerve dysfunction that collectively predispose to ulceration (53). Sensory neuropathy eliminates protective sensation, allowing unrecognized trauma from pressure, friction, or thermal injury to initiate tissue breakdown. Motor neuropathy causes intrinsic foot

muscle atrophy and imbalances that alter biomechanics, creating abnormal pressure points prone to callus formation and subsequent ulceration. Autonomic neuropathy reduces sweating and alters skin blood flow regulation, resulting in dry, cracked skin vulnerable to infection and impaired thermoregulation that compromises tissue perfusion.

Peripheral arterial disease affects roughly half of patients with diabetic foot ulcers, as diabetes accelerates atherosclerosis through endothelial dysfunction, increased inflammation, abnormal lipid metabolism, and enhanced platelet activation (54). In diabetes, atherosclerotic disease most commonly involves infrapopliteal vessels, leading to occlusion of the tibial and peroneal arteries, limited collateral formation, and impaired distal perfusion. Microvascular dysfunction further worsens tissue ischemia by reducing capillary blood flow and oxygen delivery, even when larger vessels remain unobstructed. As a result, accurate vascular assessment in diabetic feet requires multiple diagnostic approaches, including ankle-brachial index, toe pressures, and transcutaneous oxygen measurements, since arterial calcification can render standard measures unreliable.

Immunological impairment in T2D affects both innate and adaptive immune responses, creating vulnerability to infection and impeding normal inflammatory resolution required for healing progression. Neutrophil dysfunction in diabetes includes impaired chemotaxis, reduced phagocytosis, defective oxidative burst, and delayed apoptosis that collectively compromise antimicrobial defense while perpetuating inflammation (55). Monocytes and macrophages exhibit reduced migration, impaired phagocytosis, and dysregulated cytokine production, with persistent pro-inflammatory M1 polarization and failure to transition to pro-healing M2 phenotypes (15, 16, 56). T cell responses show reduced proliferation, altered subset distributions with decreased regulatory T cells, and impaired cytokine production that disrupts coordination of adaptive

immunity. These immunological defects create a paradox of chronic inflammation with immunodeficiency, where persistent low-grade inflammation damages tissues while failing to provide effective antimicrobial defense or support tissue repair (57, 58).

1.2.3 Current Treatments

Current treatments for diabetic foot ulcers remain inadequate, with standard care achieving healing in only 24-30% of cases at 12 weeks and approximately 50% at 20 weeks (59). The foundation of DFU management involves offloading to reduce mechanical stress, with total contact casting considered the gold standard but often underutilized due to practical limitations and contraindications. Debridement to remove necrotic tissue, biofilm, and hyperkeratotic edges remains essential for creating a healing-conducive wound environment, though optimal frequency and extent remain debated (60). Local wound care utilizing moisture-retentive dressings, antimicrobial agents when indicated, and negative pressure wound therapy for appropriate wounds provides symptomatic management but rarely addresses underlying pathophysiology (61).

Advanced therapies attempting to address specific deficiencies in diabetic wounds have shown mixed results in clinical trials. Growth factor therapy, exemplified by recombinant human platelet-derived growth factor (becaplermin), provides modest improvements in healing rates but requires careful patient selection and has not achieved widespread adoption due to cost and marginal efficacy (62). Cell-based therapies including autologous platelet-rich plasma, mesenchymal stem cells, and bioengineered skin substitutes show promise in selected cases but lack robust evidence from large randomized trials and face regulatory and practical implementation challenges (63). Hyperbaric oxygen therapy, aimed at correcting tissue hypoxia, demonstrates benefit in specific subgroups but requires significant resources and patient commitment (64). The limited success of current treatments highlights critical knowledge gaps in

understanding diabetic wound pathophysiology and the need for novel therapeutic approaches targeting fundamental mechanisms of healing impairment.

1.2.4 Future Directions

Future directions in diabetic wound healing research increasingly focus on precision medicine approaches that recognize the heterogeneity of DFUs and the need for personalized treatment strategies. Biomarker development aims to identify molecular signatures predicting healing trajectories, enabling risk stratification and treatment selection based on individual wound characteristics (65). Epigenetic therapies targeting DNA methylation, histone modifications, and non-coding RNAs offer potential to reverse diabetes-induced cellular reprogramming and restore normal healing capacity. Epigenetic alterations in diabetic wounds reveal multiple druggable targets—including histone demethylases, DNA methyltransferases, and chromatin remodeling complexes—that could be modulated to enhance healing (66). Combination therapies addressing multiple aspects of healing impairment simultaneously, such as improving perfusion while modulating inflammation and supporting keratinocyte function, may prove more effective than single-agent approaches.

1.3 Epigenetic Regulation of Cell Plasticity in Wounds

Different cell types can exhibit specific gene expression profiles leading to distinct functions and phenotypes due to epigenetic modifications that control downstream protein expression patterns. Epigenetics is defined as heritable changes in gene transcription that are not caused by mutations or permanent changes in the genetic code. This is caused by modifications to chromatin that can lead to activation or silencing of genes. In steady-state conditions, genes are stably regulated, whether they are repressed or activated in a cell- or tissue-specific manner. However, under disease conditions, the epigenetic machinery can become dysregulated. Changes

in the external stimuli including toxic chemicals, environmental pollutants, diet, etc. can also contribute to epigenetic modifications.

There are three main types of epigenetic modifications: histone modification, DNA modification, and ATP-dependent remodeling. The former two have been well studied in the context of wound healing (16, 67). Cell plasticity during tissue repair is partly regulated epigenetically and determines downstream reparative functions. Histone methylation and demethylation play critical roles in macrophage polarization during wound healing (Figure 1-3). Methylation of a histone activates or represses transcription depending on the number of methyl groups added and their location on the histone tail, and chromatin modifying enzymes (CMEs) are responsible for this process. For example, methyltransferase mixed lineage leukemia-1 (MLL1) adds methyl groups to the histone 3 lysine 4 (H3K4) site, resulting in an open chromatin structure, promoting transcription of pro-inflammatory cytokines in macrophages (68). In contrast, Setdb2 is a methyltransferase that adds a trimethyl group on the histone 3 lysine 9 (H3K9) site and renders the promoter region inaccessible for transcription factor binding, silencing inflammatory gene transcription in macrophages (15). Another CME that regulates macrophage inflammatory phenotype is histone demethylase Jumonji domain-containing protein 3 (JMJD3) that removes the repressive trimethyl group on the histone 3 lysine 27 (H3K27) site, resulting in opening of chromatin and increasing IL-6, TNF-α, IL-1β transcription (69). Expression and activity of these CMEs can be altered in a dysregulated state such as diabetic wound healing, leading to impaired transition of inflammatory macrophage (M1) phenotype to an immunoregulatory phenotype (M2).

Histone modifications also occur in structural cells like keratinocytes. JMJD3 regulates differentiation, pro-inflammatory cytokine, MMP, and growth factor gene expression in keratinocytes during early phases of wound healing (70). Additionally, MLL1 activity in

keratinocytes is critical for production of IFN-κ that induces early inflammation during tissue repair by polarizing macrophages towards a M1 phenotype (21).

DNA methylation is predominantly associated with transcriptional repression and is regulated by DNA methyltransferases (DNMTs) that transfer a methyl group to the cytosine ring of DNA (see Figure 1.3) (71). The methylation occurs at clusters of CpG islands in gene promoter regions, directly impeding transcription factor binding. DNMT1 and DNMT3b can activate macrophages and bone marrow progenitor cells to become inflammatory (M1), although their exact role in wound healing is unclear (72, 73).

Further investigation into specific upstream pathways of epigenetic regulation of wound-associated cells and their downstream functions may lead to development of cell-specific targeted therapies for pathologic wound healing.

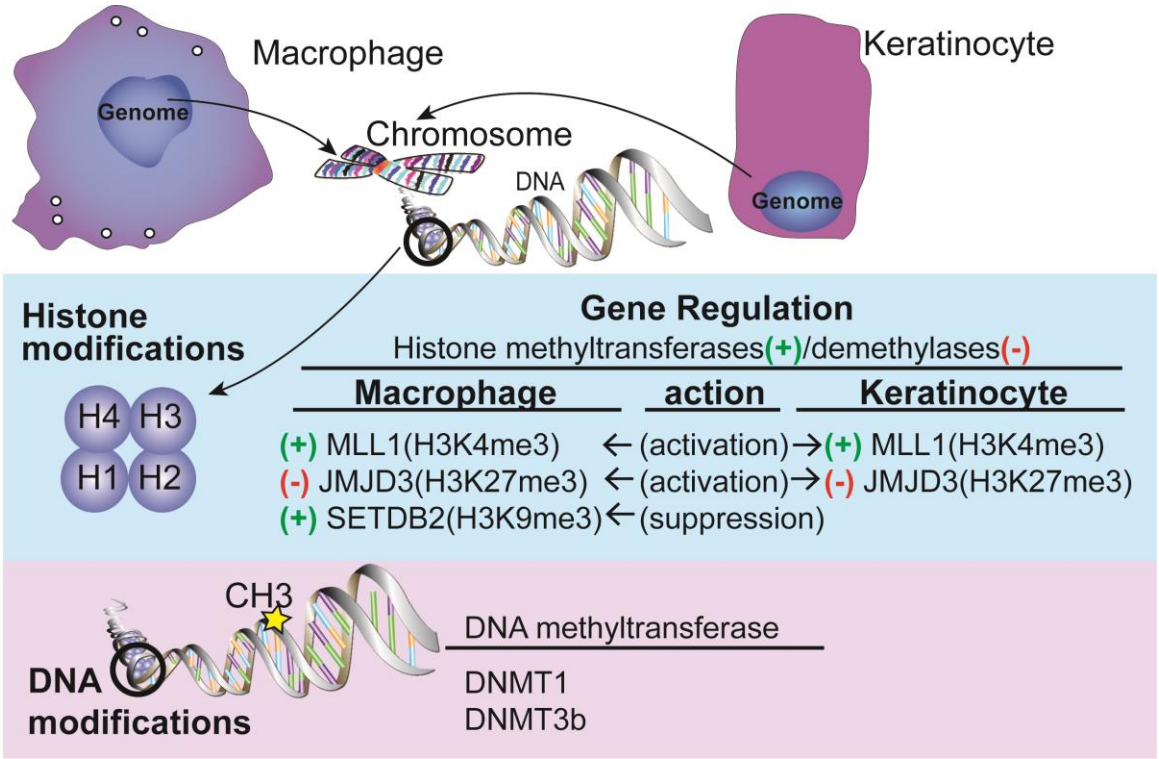


Figure 1-3: Epigenetic modifications that alter cells in wounds
Histone modifications associated with influencing macrophage and keratinocyte phenotypes. DNA modifications associated with influencing macrophage plasticity. Jumonji domain-containing protein (JMJD); Mixed-lineage leukemia (MLL); SET domain bifurcated (SETDB); DNA methyltransferases (DNMT).

1.4 Keratinocyte Crosstalk with Immune and Stromal Cells

The orchestration of wound healing depends critically upon complex bidirectional communication networks between keratinocytes and surrounding immune and stromal cells, with these interactions determining whether wounds progress through normal healing phases or develop chronic inflammation and impaired repair. Keratinocytes, positioned at the interface between the external environment and internal tissues, serve as both sensors of tissue damage and coordinators of cellular responses through production of diverse signaling molecules including cytokines, chemokines, growth factors, antimicrobial peptides, and extracellular vesicles (3). This communication network extends beyond simple ligand-receptor interactions to encompass metabolic coupling, mechanical signaling, and transfer of functional molecules through gap junctions and extracellular vesicles, creating an integrated tissue response system that maintains homeostasis and enables regeneration.

1.4.1 Keratinocyte-Macrophage Crosstalk

The keratinocyte-macrophage axis represents a fundamental regulatory circuit in wound healing, with bidirectional signaling determining inflammatory intensity, duration, and resolution. Keratinocytes shape macrophage recruitment, activation, and polarization through sequential production of chemokines and cytokines that evolve throughout healing phases. Initial keratinocyte production of CCL2, CCL3, and CCL4 establishes chemotactic gradients that guide monocyte infiltration, while CXCL1, CXCL3, CXCL5, and CXCL8 (IL-8 in humans) production recruits neutrophils that influence subsequent macrophage phenotypes through release of granule contents and formation of neutrophil extracellular traps (74). The keratinocyte-derived alarmin IL-1α, constitutively expressed and released upon cell damage, serves as a primary danger signal that

activates tissue-resident macrophages and dendritic cells through IL-1 receptor signaling, triggering MyD88-dependent inflammatory cascades (75).

Recent mechanistic studies from our lab have revealed that diabetic wound keratinocytes actively reprogram macrophage phenotypes through cytokine-epigenetic signaling cascades with important implications for healing outcomes (76). Increased IL-1α production by diabetic keratinocytes signals through IL-1 receptor on macrophages to induce the histone demethylase JMJD3, which removes repressive H3K27me3 marks from the *Nlrp3* gene promoter, driving sustained NLRP3 inflammasome expression and creating a positive feedback loop of chronic inflammation (76). This keratinocyte-initiated epigenetic reprogramming of macrophages establishes a self-perpetuating inflammatory state resistant to normal resolution signals. The therapeutic interruption of this circuit through IL-1 receptor antagonism, MyD88 inhibition, or JMJD3 targeting offers potential to break the chronic inflammatory cycle characteristic of diabetic wounds.

The reciprocal influence of macrophages on keratinocyte function involves both direct signaling through secreted factors and indirect effects through modification of the wound microenvironment. Macrophage-derived TNF-α and IL-1β activate NF-κB and AP-1 signaling in keratinocytes, inducing expression of additional inflammatory mediators, matrix metalloproteinases, and adhesion molecules that perpetuate inflammation and tissue remodeling (77). The transition of macrophages from M1 to M2 phenotypes dramatically alters their influence on keratinocytes, with M2 macrophages producing TGF-β, PDGF, and VEGF that promote keratinocyte migration, proliferation, and differentiation required for re-epithelialization (77, 78). IL-10 production by M2 macrophages suppresses keratinocyte inflammatory gene expression

while enhancing production of antimicrobial peptides and growth factors that support barrier restoration (79).

Extracellular vesicles mediate sophisticated intercellular communication between keratinocytes and macrophages, transferring proteins, lipids, and nucleic acids that modulate recipient cell functions (see Figure 1.2). Keratinocyte-derived exosomes contain inflammatory mediators including IL-1β, TNF-α, and various chemokines that can activate macrophages and perpetuate inflammation (26). These vesicles also carry functional mRNAs encoding cytokines, growth factors, and transcription factors that can be translated in recipient cells, along with regulatory miRNAs that modulate gene expression. In diabetic wounds, keratinocyte-derived exosomes are not only reduced in number but exhibit dramatically altered composition, with decreased RNA content and deficient proteins/lipids that fail to promote appropriate macrophage responses (28). Specifically, diabetic keratinocyte exosomes lack key cargo required to induce M2 polarization, instead maintaining macrophages in persistent inflammatory states that impede healing progression (28).

Conversely, macrophage-derived exosomes provide critical metabolic and regulatory support to keratinocytes during wound healing. Hypoxia-induced mitochondrial depletion in wound-edge keratinocytes is compensated by macrophage exosomes enriched with TOMM70 (translocase of outer mitochondrial membrane 70), which restores mitochondrial biogenesis and powers keratinocyte migration (27). This metabolic rescue mechanism involves transfer of mitochondrial proteins, mitochondrial DNA, and factors promoting mitochondrial biogenesis including PGC-1α activators (27). The transfer of functional mitochondria or mitochondrial components between cells represents an emerging paradigm in tissue repair, with macrophages

serving as metabolic donors supporting energetically demanding processes like migration and proliferation in keratinocytes.

1.4.2 Keratinocyte-Fibroblast Crosstalk

The keratinocyte-fibroblast crosstalk represents another critical axis coordinating wound healing, with reciprocal signaling regulating ECM production, wound contraction, and tissue architecture restoration. Keratinocytes produce multiple factors that regulate fibroblast behavior including TGF-β1 that promotes myofibroblast differentiation; PDGF that stimulates fibroblast proliferation and migration; and CTGF (connective tissue growth factor) that enhances ECM synthesis (3). The spatial organization of these signals creates gradients that guide fibroblast recruitment and activation, with wound-edge keratinocytes producing different factor combinations than migrating or proliferating keratinocytes. Keratinocyte-derived IL-1 and TNF-α initially maintain fibroblasts in an inflammatory, matrix-degrading state through induction of MMPs and suppression of collagen synthesis, while later production of TGF-β and PDGF shifts fibroblasts toward matrix production and wound contraction (3).

Fibroblasts reciprocally regulate keratinocyte behavior through production of growth factors and basement membrane components that control proliferation, migration, and differentiation. Fibroblast-derived FGF-7 (KGF) and FGF-10 specifically signal through FGFR2-IIIb on keratinocytes to promote proliferation and migration, with expression increasing dramatically following injury (80). Fibroblast-derived HGF (hepatocyte growth factor) activates c-Met signaling in keratinocytes, promoting survival, proliferation, and migration while suppressing terminal differentiation (81). The production of basement membrane components including laminin-332, collagen IV, and collagen VII by fibroblasts provides adhesive substrates that guide keratinocyte migration and establish epithelial-mesenchymal boundaries (82). The ECM

itself serves as a signaling platform, with fibroblast-deposited fibronectin, vitronectin, and tenascin-C providing adhesive and signaling cues that regulate keratinocyte behavior through integrin engagement and growth factor presentation (83).

In diabetic conditions, the keratinocyte-fibroblast communication network becomes disrupted through multiple mechanisms. Hyperglycemia and AGE accumulation alter both keratinocyte signal production and fibroblast responsiveness, with reduced growth factor expression, excessive protease activity, and impaired ECM synthesis (84). Diabetic keratinocytes produce reduced levels of FGF-7 and PDGF while overproducing inflammatory mediators that maintain fibroblasts in dysfunctional states (85). Diabetic fibroblasts exhibit reduced responsiveness to keratinocyte-derived signals due to receptor downregulation, impaired signal transduction, and epigenetic reprogramming that alters transcriptional responses (85, 86). The excessive production and reduced degradation of ECM components by diabetic fibroblasts creates a stiff, poorly organized matrix that impedes keratinocyte migration and perpetuates chronic wound states (87).

1.4.3 Keratinocyte-Endothelial Cell Crosstalk

The interaction between keratinocytes and endothelial cells orchestrates angiogenesis essential for wound healing, with keratinocyte-derived signals initiating and guiding vessel formation while endothelial cells provide oxygen and nutrients supporting keratinocyte survival and function. Keratinocytes represent a major source of pro-angiogenic factors in wounds, producing VEGF-A under hypoxic conditions through HIF-1α stabilization, along with angiopoietin-1, FGF-2, and PDGF that collectively promote endothelial cell survival, proliferation, and tube formation (35). The production of these factors shows spatial heterogeneity, with hypoxic wound-center keratinocytes producing high VEGF levels while wound-edge keratinocytes express

different angiogenic factor profiles (35, 88, 89). Keratinocyte-derived chemokines including CXCL12 (SDF-1α) recruit endothelial progenitor cells from circulation, while IL-8 promotes endothelial cell proliferation and tube formation through CXCR2 signaling (90).

Endothelial cells influence keratinocyte behavior through production of basement membrane components, growth factors, and establishment of oxygen gradients that regulate keratinocyte metabolism and gene expression. The endothelial production of laminin-511 provides critical adhesive and survival signals for basal keratinocytes through α3β1 and α6β4 integrin engagement (91). Endothelial-derived factors including endothelin-1 regulate keratinocyte proliferation and pigmentation, while NO production influences keratinocyte differentiation and antimicrobial peptide expression (92). The restoration of angiogenesis alters keratinocyte metabolism, shifting from glycolytic to oxidative metabolism that supports differentiation and barrier formation (93, 94). In diabetes, impaired angiogenesis due to reduced growth factor production, endothelial dysfunction, and defective progenitor cell recruitment creates persistent hypoxia that maintains keratinocytes in stressed, dysfunctional states unable to support normal re-epithelialization.

1.4.4 Keratinocyte-T Cell Crosstalk

The communication between keratinocytes and T cells extends beyond classical antigen presentation to encompass diverse regulatory interactions that shape wound healing outcomes. γδ T cells, enriched in epithelial tissues, establish close associations with keratinocytes through E-cadherin interactions and respond to keratinocyte stress signals including MICA/B and Rae-1 through NKG2D receptor engagement (95). These unconventional T cells produce growth factors including IGF-1 and FGF-7 that directly promote keratinocyte proliferation and survival, while their production of IL-17A and IL-22 enhances antimicrobial peptide expression and maintains

barrier integrity (96). The depletion of γδ T cells significantly impairs re-epithelialization, demonstrating non-redundant roles in supporting keratinocyte function beyond conventional immunity.

Keratinocytes actively shape T cell responses through production of cytokines and chemokines that influence T cell recruitment, differentiation, and function. Keratinocyte-derived TSLP (thymic stromal lymphopoietin) promotes Th2 differentiation while suppressing Th1 and T_H17 responses, establishing an anti-inflammatory environment conducive to healing (97). The production of IL-23 by activated keratinocytes maintains T_H17 responses that, while providing antimicrobial defense, can perpetuate inflammation if not appropriately regulated (98). Keratinocyte expression of PD-L1 following IFN-γ exposure provides negative regulation of T cell responses, preventing excessive inflammation and tissue damage. The chemokine production by keratinocytes, including CCL-20 that recruits T_H17 cells and CCL17/CCL22 that attract Th2 cells, creates specialized microenvironments that shape local immune responses (24, 99).

1.4.5 Other Keratinocyte Communication Networks

The impact of hyperglycemia, reactive oxygen species (ROS), and advanced glycation end products (AGEs) on keratinocyte crosstalk networks in diabetes involves both direct cellular effects and disruption of signaling mechanisms. High glucose conditions directly impair keratinocyte production of growth factors and cytokines through multiple mechanisms including osmotic stress, metabolic dysfunction, and epigenetic reprogramming (100). The accumulation of AGEs on ECM proteins and cell surface receptors alters adhesion, migration, and signaling, with AGE-RAGE (receptor for AGE) interactions activating pro-inflammatory pathways that perpetuate tissue damage (101). ROS generation, enhanced in diabetic conditions through multiple sources including mitochondrial dysfunction, NADPH oxidases, and AGE-RAGE signaling,

damages cellular components and dysregulates redox-sensitive signaling pathways critical for normal cellular communication (102).

Recent multi-omic and spatial transcriptomic studies have revealed previously unrecognized complexity in keratinocyte communication networks, identifying specialized keratinocyte subpopulations with distinct signaling profiles and spatial organization of cellular interactions. A recent spatiotemporal single-cell analysis study of human wounds have demonstrated that FOSL1+ keratinocytes serve as critical drivers of re-epithelialization through enhanced production of migration-promoting factors and ECM remodeling enzymes (89). The study identified sequential waves of cellular interactions, with pro-inflammatory macrophages initially supporting keratinocyte activation, followed by fibroblast-mediated support during migration, demonstrating a "relay-race" pattern of cellular cooperation (89). Comparison with diabetic foot ulcers revealed disrupted spatial organization of these cellular interactions, with failed keratinocyte migration correlating with aberrant immune cell positioning and signaling.

The identification of multiple keratinocyte states with distinct transcriptional programs challenges the traditional view of uniform epithelial responses and suggests opportunities for targeted therapeutic intervention. Single-cell transcriptomic analyses have revealed CXCL10-high keratinocyte populations enriched for interferon-responsive genes and inflammatory mediators, accompanied by reduced proliferative capacity, consistent with roles in immune modulation rather than tissue expansion (103-105). STAT3 signaling in keratinocytes has been shown to regulate inflammatory responses and wound repair, highlighting its importance in coordinating epithelial–immune interactions during healing (106). In contrast, KLF4 regulates keratinocyte differentiation and cell fate decisions, contributing to epidermal maturation and homeostasis (107). The spatial and temporal distribution of these keratinocyte states during wound healing suggests functional

specialization across distinct wound microenvironments (105). Disruption of the emergence or maintenance of these states in diabetes may contribute to impaired repair and represents a potential avenue for therapeutic intervention.

1.5 Rationale and Specific Aims

Overall Rationale

The goal of this dissertation was to advance our understanding of the epigenetic mechanisms that regulate keratinocyte function in both normal and pathological wound repair, with a particular focus on type 2 diabetic wounds. Although epigenetic regulation in immune cells has been extensively studied, far less is known about how chromatin-modifying enzymes shape keratinocyte behavior, despite keratinocytes being the primary drivers of re-epithelialization and key coordinators of cutaneous immunity. Type 2 diabetic wounds are characterized by chronic inflammation and impaired keratinocyte migration that together prevent normal tissue repair, yet the molecular mechanisms underlying this dysfunction remain incompletely defined. This work addresses a critical gap in knowledge by examining how inflammatory cytokine signaling pathways converge on keratinocyte-specific epigenetic regulators to alter inflammatory gene expression and migratory programs. Specifically, this dissertation focuses on two complementary epigenetic mechanisms: IL-17A-driven induction of the histone demethylase JMJD3, which promotes inflammatory gene transcription through removal of repressive H3K27 trimethylation, and IFNβ/JAK/STAT-mediated regulation of the histone methyltransferase SETDB2, which suppresses inflammatory gene expression via H3K9 trimethylation. Dysregulation of these opposing epigenetic pathways in diabetic conditions creates a persistent inflammatory state that impairs keratinocyte function and perpetuates wound chronicity, highlighting keratinocyte-specific chromatin regulation as a promising therapeutic target for restoring normal wound healing.

Aim 1: Chapter 2 – IL-17A is increased in diabetic wounds and impairs keratinocyte function via histone demethylase JMJD3

IL-17A has emerged as a critical mediator of pathological inflammation in diabetic wounds. Our preliminary studies identified elevated IL-17A levels and a predominant T_H17 signature in human diabetic wound tissue compared to non-diabetic controls. Given that IL-17A is known to regulate keratinocyte function in other inflammatory skin conditions and signals through the ACT1/TRAF6 pathway—a major activator of NFκB-mediated inflammation—we investigated its role in diabetic keratinocyte dysfunction. We found that IL-17A directly impairs keratinocyte migration while increasing production of inflammatory mediators, particularly CXCL1, CXCL3, CXCL5, and CCL-20, which further compromise wound healing. The rationale for focusing on JMJD3 as a downstream epigenetic mediator stems from our single-cell RNA sequencing data showing increased JMJD3 expression in diabetic wound keratinocytes. As JMJD3 removes repressive H3K27me3 marks to activate gene transcription, its upregulation provides a mechanistic link between IL-17A signaling and persistent inflammatory gene expression in diabetic keratinocytes.

The central hypothesis of this study was that IL-17A signaling through the ACT1/TRAF6 pathway induces JMJD3 expression in diabetic wound keratinocytes, leading to removal of repressive H3K27me3 marks and subsequent activation of inflammatory genes that impair keratinocyte migration and perpetuate wound inflammation. The sub-aims include the following: 1) To characterize the IL-17A/ACT1/TRAF6 signaling axis in diabetic wound keratinocytes and determine how this pathway regulates JMJD3 expression at both transcriptional and post-translational levels; 2) To define the epigenetic changes mediated by JMJD3, including H3K27me3 alterations at anti-migratory and inflammatory gene promoters in normal and diabetic

keratinocytes; 3) To evaluate the functional consequences of keratinocyte-specific JMJD3 deletion on wound healing parameters, including re-epithelialization rates, inflammatory chemokine production, and keratinocyte-immune and keratinocyte-stromal cell interactions in diabetic wound models.

These studies established that IL-17A-induced JMJD3 expression represents a critical contributor to diabetic wound pathology. By demonstrating that therapeutic targeting of this pathway improves keratinocyte migration and reduces inflammatory cytokine production, this work identifies JMJD3 as a promising therapeutic target for diabetic wounds.

Aim 2: Chapter 3 – Histone methyltransferase SETDB2 modulates keratinocyte inflammatory cytokine production in diabetic wounds by an IFNβ/JAK/STAT mechanism

While Aim 1 focused on mechanisms that activate inflammatory gene expression, this aim investigated an opposing epigenetic mechanism that normally functions to suppress inflammation. Our single-cell RNA sequencing revealed that SETDB2, a histone methyltransferase that catalyzes repressive H3K9 trimethylation, is significantly decreased in diabetic wound keratinocytes. This loss of SETDB2-mediated repression allows for aberrant activation of inflammatory genes, IL-1β, TNF-α, and IL-23. The rationale for studying SETDB2 regulation through IFNβ/JAK/STAT signaling emerged from our preliminary data showing that IFNβ treatment induces SETDB2 expression in wound keratinocytes. As type I interferons can have both pro- and anti-inflammatory effects depending on context, understanding how IFNβ regulates keratinocyte SETDB2 provides insight into a previously unrecognized anti-inflammatory mechanism that is compromised in diabetic wounds.

The central hypothesis of this study was that loss of SETDB2 expression in diabetic wound keratinocytes results from impaired IFNβ/JAK/STAT signaling, leading to insufficient H3K9me3-

mediated repression of NFκB target genes and consequent overproduction of inflammatory mediators that impair wound healing. The subaims include the following: 1) To determine the molecular mechanisms through which IFNβ/JAK/STAT signaling regulates SETDB2 expression, including identification of specific STAT transcription factors controlling SETDB2 transcription in keratinocytes; 2) Characterize SETDB2-dependent H3K9me3 deposition at inflammatory gene promoters in wound keratinocytes, comparing normal and diabetic conditions; 3) To assess the therapeutic potential of restoring SETDB2 expression or activity in diabetic wounds, examining effects on re-epithelialization and inflammatory cytokine production.

This work revealed that SETDB2 functions as a critical epigenetic checkpoint for keratinocyte inflammation, with its loss in diabetic conditions contributing to increased inflammatory signaling. By demonstrating that restoration of SETDB2 expression through JAK/STAT pathway modulation improves wound healing outcomes, these studies identified a novel therapeutic strategy for managing diabetic wound inflammation.

Concluding Perspective

Together, these two aims provide a framework for examining how distinct epigenetic mechanisms that regulate gene activation and repression—specifically JMJD3-mediated H3K27 demethylation and SETDB2-mediated H3K9 trimethylation—are altered in diabetic wound keratinocytes. The studies presented here suggest that IL-17A-associated induction of JMJD3 contributes to increased anti-migratory and inflammatory gene expression, while decreased IFNβ/JAK/STAT-dependent SETDB2 activity may limit repression of inflammatory gene expression in diabetic wounds. In combination, these alterations are consistent with a keratinocyte chromatin state biased toward prolonged inflammatory signaling, which may contribute to delayed wound repair.

The findings in the following chapters advance our understanding of molecular pathways that contribute to keratinocyte dysfunction in diabetic wounds and highlight epigenetic regulators as potential points of intervention. While further work is required to establish therapeutic efficacy, modulation of these chromatin-modifying enzymes or their upstream signaling pathways may represent a strategy to rebalance inflammatory responses in chronic wounds. More broadly, these studies provide a conceptual framework that may be applicable to other inflammatory skin conditions in which altered keratinocyte gene regulation contributes to disease pathology.

Chapter 2 – IL-17A Is Increased in Diabetic Wounds and Impairs Keratinocyte Function via Histone Demethylase JMJD3

2.1 Abstract

IL-17A is a cytokine critical for tissue repair, but in excess, it prolongs inflammation and impairs healing. In type 2 diabetic (T2D) wounds, keratinocyte functions, including migration and inflammation, are disrupted, though mechanisms remain unclear. Here, we demonstrate that IL-17A regulates keratinocyte dysfunction via induction of the histone demethylase Jumonji domain-containing protein 3 (JMJD3) through a TRAF6/NFκB pathway. JMJD3 removes repressive histone 3 lysine 27 (H3K27me3) marks at anti-migratory (*Itga3, Timp1*) and inflammatory (*Ccl20, Cxcl1, Cxcl3, Cxcl5*) gene promoters, increasing transcription. Human and murine diabetic wounds exhibit elevated IL-17A signaling, JMJD3, and expression of associated anti-migratory and inflammatory genes compared to controls. Importantly, keratinocyte-specific deletion of IL-17A signaling or JMJD3 in diabetic mice improves wound healing and decreases expression of JMJD3 target genes. These findings reveal an IL-17A/JMJD3-mediated mechanism driving keratinocyte dysfunction in T2D wounds and highlight the therapeutic potential of targeting this axis to enhance wound repair.

Portions of this chapter have been published:

Moon JY, Wolf SJ, Joshi AD, Zhang H, Shadiow J, Bauer TM, Mangum KD, Hughes LD, Audu CO, Melvin WJ, Barrett EC, Rocco S, Saldana de Jimenez G, Estor AL, Nelapudi M, Li Q, Bogle R, Levi B, Davis FM, Obi AT, Moore BB, Tsoi LC, Gudjonsson JE, Gallagher KA. IL-17A is increased in diabetic wounds and impairs keratinocyte function via histone demethylase JMJD3. *Nature Communications*, 17(1):780 (2025).

2.2 Introduction

Wound healing progresses through discrete yet overlapping stages where impaired progression through these phases results in pathologic healing. Keratinocytes are non-immune resident cells in the skin that play key roles (proliferation, migration, inflammation, differentiation) primarily during the re-epithelialization and remodeling phases of wound repair. In normal wound repair, keratinocytes migrate as a sheet towards the wound site and proliferate during the re-epithelialization phase (108, 109). During remodeling, they produce matrix metalloproteinases (MMPs) and tissue inhibitors of MMPs (TIMPs) to restructure the extracellular matrix and terminally differentiate to form a protective outer layer of the epidermis (110). Directional/collective cell migration, rather than random/individual cell migration, is crucial for proper wound closure and is achieved partly via integrin-mediated adhesion and regulation of matrix topography (111). Although previously thought to be passive cell types that solely act as a physical barrier, keratinocytes are now recognized as highly active cells that respond to external stimuli throughout all stages of wound healing (20). In response to the cytokine milieu in the wound environment, keratinocytes produce inflammatory cytokines and chemokines that promote inflammation and recruit immune cells (19, 20); however, an alteration in the cytokine milieu can result in impaired keratinocyte functions (21, 76, 112). Our lab and others have found that keratinocytes display impairments in migration, proliferation, and other functions during the re-epithelialization phase in nonhealing type 2 diabetic (T2D) wounds (21, 76, 113); however, the precise molecular mechanisms that regulate keratinocyte function in normal or pathologic repair remain unclear.

T2D wounds are often characterized by a late prolonged inflammatory phase due, in part, to pathologic production of inflammatory cytokines by both immune and non-immune cells (76, 114-118). Importantly, serum IL-17A levels have been shown to be increased in diabetic patients, providing a potential mediator for the chronic low-grade inflammation seen in non-healing diabetic wounds (119-121). Our lab and others have identified that IL-17A is increased in diabetic wound tissue as well as in other tissues/organs (blood, pancreas, kidneys, etc.) (57, 115, 120-122). This is highly relevant since increased IL-17A has been shown to impair inflammatory cyto/chemokine production, proliferation, and differentiation functions in epithelial cells in other chronic inflammatory disease processes (i.e., psoriasis, Crohn's disease, chronic obstructive pulmonary disease) (123-125). Despite this, the effects of excessive IL-17A on keratinocyte function have not been examined in tissue repair. Further, the molecular mechanisms by which IL-17A signaling in keratinocytes controls their function is unknown. In this regard, epigenetic modifications have been shown to regulate changes in gene expression and, hence, cell function in the setting of tissue repair (15, 68, 126). Epigenetic modifications have been well studied in immune cells during tissue repair, but considerably less is known about epigenetic modifications in non-immune cells during the wound healing process. Although not well-studied in keratinocytes, NFκB-mediated cytokine expression has been recently found to be regulated upstream in keratinocytes by chromatin-modifying enzymes (CMEs) (70). Additionally, certain transcriptional factors have been shown to regulate keratinocyte migration-related genes during wound re-epithelialization possibly via recruitment of CMEs (127). Despite these reports, studies on epigenetic regulation of wound keratinocyte function in the setting of normal or dysregulated wound repair are limited.

Here, we demonstrate that increased IL-17A signaling in the diabetic wound environment alters keratinocyte functions including migration and inflammation that are necessary for tissue

repair. Using *in vitro* and *in vivo* assays, we identified that increased IL-17A signaling in keratinocytes leads to decreased wound closure rates via increase in expression of anti-migratory (i.e., *Itga3, Timp1*) and inflammatory (i.e., *Ccl20, Cxcl1, Cxcl3,* and *Cxcl5*) genes. Using multiple keratinocyte-specific murine models (*Il17ra*$^{fl/fl}$ *K14*$^{cre+}$, *Traf6*$^{fl/fl}$ *K14*$^{cre+}$, *Jmjd3*$^{fl/fl}$ *K14*$^{cre+}$), we identified that IL-17A signaling upregulates the CME, JMJD3, in keratinocytes, and that JMJD3 is regulated upstream in keratinocytes via a TRAF6/NFκB pathway. Chromatin immunoprecipitation (ChIP) analysis of JMJD3-mediated demethylation of the repressive H3K27me3 mark on *Itga3, Timp1, Ccl20, Cxcl1, Cxcl3,* and *Cxcl5* gene promoters in keratinocytes stimulated with IL-17A revealed a decrease in H3K27me3 contributing to increased gene expression. Importantly, treatment with a pharmacological inhibitor specific for JMJD3 decreased *Itga3, Timp1, Ccl20, Cxcl1, Cxcl3,* and *Cxcl5* gene expression and protein abundance in IL-17A-stimulated keratinocytes, resulting in improved keratinocyte migration rates. As a translational corollary, single-cell RNA-Sequencing (scRNA-Seq) in keratinocytes from T2D and non-T2D human wounds revealed increased *JMJD3* as well as *ITGA3, TIMP1, CCL20, CXCL1, CXCL3,* and *CXCL5* in keratinocytes from T2D patients compared with non-T2D controls. Importantly, keratinocyte-specific diabetic murine models deficient in IL-17A signaling or JMJD3 displayed increased wound repair and decreased *Itga3, Timp1, Ccl20, Cxcl1, Cxcl3,* and *Cxcl5* gene expression in keratinocytes *in vivo*. Our findings reveal that expression of anti-migratory and inflammatory genes is regulated by an IL-17A/TRAF6/JMJD3-mediated mechanism and manipulation of this pathway in keratinocytes may improve wound repair in the setting of diabetes.

2.3 Materials and Methods

2.3.1 Study Approval

All experiments using human samples were approved by the IRB at the University of Michigan (IRB#: HUM00098915) and were conducted in accordance with the principles in the Declaration of Helsinki. All mice used were on a C57BL/6 background. We used 2 diabetic models, diet-induced obesity (DIO) and *db/db,* which were used in acute and/or chronic wound models. DIO mice were generated by feeding mice with a high fat diet (HFD) for 12 – 16 weeks to simulate a "prediabetic" state that is physiologically similar to humans; mice were used at 20 weeks of age or older. Female C57BL/6J mice do not develop glucose intolerance/insulin resistance metabolic syndrome or "prediabetes" on a high-fat diet; therefore, they cannot be used in this T2D model. For *db/db* mice, both male and female mice were used in experiments starting at 7 weeks of age. Mice were housed at the University of Michigan Biomedical Sciences and Research Building in the Unit for Laboratory and Animal Medicine (ULAM)—a pathogen free animal facility. Mouse experiments were conducted with approval from our Institutional Animal Care and Use Committee (IACUC; Protocol no. PRO00009811) and all regulatory and safety standards were strictly adhered to.

2.3.2 Mice

All mice were housed at University of Michigan animal facilities. C57BL/6J, *db/db*, *db/+*, *K14*$^{cre+}$ mice were purchased from The Jackson Laboratory at 6 - 7 weeks of age and maintained in breeding pairs in Unit for Laboratory Animal Medicine (ULAM) facilities. *Il17ra*$^{fl/fl}$ mice [RRID:IMSR_JAX:030849] on a C57BL/6J background were a gift from B. Moore (University of Michigan). *Traf6*$^{fl/fl}$ mice [RRID:IMSR_JAX:030849] on a C57BL/6J background were a gift from S. Soleimanpour (University of Michigan) (128). *Jmjd3*$^{fl/fl}$ mice were created as previously

reported by our laboratory (129). *Il17ra*$^{fl/fl}$, *Traf6*$^{fl/fl}$, *Jmjd3*$^{fl/fl}$ mice were then bred with *K14*$^{cre+}$ [RRID:IMSR_JAX:018964] mice from the Jackson Laboratory to obtain mice expressing keratinocytes deficient in IL-17RA, TRAF6, and JMJD3, respectively. Floxed-cre mice were genotyped regularly after birth with custom primers. All mice were housed on a 14-hour light/10-hour dark cycle with free access to food, water, and bedding (Andersons Lab Bedding Bed-o'Cobs combination) at ambient temperatures of 65-75°F (18-23°C) and 40-60% humidity.

2.3.3 Wound-Healing Assessment

Mice were anesthetized with isoflurane using a vaporizer with the station flowmeter set at 2.0 liters per minute (LPM). Mice were depleted of hair on their dorsum via Veet (Reckitt Benckiser), and two 6 mm punch biopsy wounds were created per mouse (130). For the chronic wound-healing model, a splinted full-thickness wound was used to minimize wound contracture (130). Briefly, a 6 mm full-thickness excisional wound was created on the shaved dorsum of the anesthetized mice. A 10 mm doughnut-shaped silicone splint was then centered on the wound and fixed to the skin using interrupted 6-0 nylon sutures (Ethicon). In GSK-J4 rescue experiments, 1 mg/kg GSK-J4 (Tocris, Catalog 4594) or 100 µL DMSO control injection was performed s.c. at 2 points along the wound edge, as described previously by our group (131). An iPad camera (8-megapixel) was used to take digital photographs daily. The wound surface area was calculated using ImageJ software (NIH) and was expressed as percentage of original wound size/time. The wounds were collected at the indicated time points and immediately snap-frozen and placed at –80°C for RNA isolation, prepared for keratinocyte isolation or placed in formalin for histology. For wound keratinocyte isolation experiments, 6 mm wound biopsies were obtained, encompassing a 2 mm margin around the wound.

Some wounds were harvested and formalin fixed overnight, followed by embedding the tissue in paraffin. Murine tissue slides were stained with H&E (132). The wound diameter was obtained by calculating the distance between leading wound epithelial edges compared with the maximum diameter of the wound. Images were taken using a Zeiss Axioskop 2 microscope.

2.3.4 Primary Keratinocyte Isolation

Primary keratinocytes were isolated from the tails or wounds of mice (133). First, skin from tails and wounds was incubated in 1% trypsin for 1.5 hours and 2 hours, respectively, at 37°C. Following incubation, the epidermis from tails and wounds was peeled off, and epidermal cells (containing primarily keratinocytes) were agitated off into high-calcium (HiCa) medium (8% nonmixed FBS in EpiLife, with 60 μM Ca^{2+} (Gibco)). Next, primary keratinocytes from the tail were cultured in low-calcium (LoCa) medium (8% mixed FBS in EpiLife, with 60 μM Ca^{2+} (Gibco), at 0.05 mM final Ca^{2+} concentration) for 1 - 2 days at 37°C. Following isolation of primary keratinocytes (tail) and wounds, cells were harvested for RNA or fixed in 1% paraformaldehyde for ChIP.

2.3.5 N/TERT Human Keratinocyte Culture

N/TERT human keratinocyte cell line was a gift from J. Gudjonsson (University of Michigan) that was used with permission from James G. Rheinwald (Brigham and Women's Hospital, Boston, Massachusetts, USA) (134). N/TERT human keratinocytes were cultured in Keratinocyte Serum-Free Medium (Gibco) supplemented with 30 μg/mL bovine pituitary extract and 0.2 ng/mL human epidermal growth factor. Cells were maintained below 60% confluency and used for scratch wound assays at passages less than 10 to ensure consistent behavior and viability.

2.3.6 Scratch Wound Assay

N/TERT human keratinocytes or cultured primary keratinocytes isolated from tails of mice were subjected to scratch wound assays (135, 136). Briefly, cells were grown to 90 – 95% confluency at 37°C. Since IL-17A increases proliferation in keratinocytes (123), cells were pre-treated with a mitosis inhibitor, Mitomycin C (10 μg/mL), for 2 hours to eliminate the contribution of cell proliferation to gap closure and to specifically assess changes in migration (135). Mitomycin C medium was removed, and keratinocytes were washed once with HBSS (without Ca^{2+}, Mg^{2+}). P20 pipette tips were used to scratch the wells horizontally and vertically. A new tip was used for each scratch. Wells were washed with 1XHBSS and appropriate medium (containing peptide stimuli, inhibitors, etc.) was added. For neutralizing antibody experiments in murine keratinocytes, IgG isotype control (R&D, Cat# AB-108-C, Lot# ES4524111) or a combination of anti-mouse anti-CCL-20 (R&D, Cat# AF760-SP, Lot# CZQ1024101), anti-CXCL-1 (R&D, Cat# AF-453-SP, Lot# VF062403), anti-CXCL-3 (R&D, Cat# AF5568-SP, Lot# CDEO022502B), and anti-CXCL-5 (R&D, Cat# AF433-SP, Lot# BCH032502A) at 1 μg/mL was used. For neutralizing antibody experiments in human keratinocytes, IgG isotype control (R&D, Cat# AB-108-C, Lot# ES4524111) or a combination of anti-human anti-CCL-20 (R&D, Cat# AF360-SP, Lot# ATU0824011), anti-CXCL-1 (R&D, Cat# AF275-SP, Lot# BEP082503A), and anti-CXCL-5 (R&D, Cat# AF254-SP, Lot# ARO0424101) at 1 μg/mL was used. 0 hr, 8 hr, 12 hr, 24 hr, or 48 hr images of the same sections of each well were taken using an inverted microscope (EVOS Cell Imaging System). Wound gap area was measured using ImageJ (NIH) software and comparisons were made using images taken at the same location of each well. Percentage of initial gap area was calculated using the following formula: $\%\text{Initial Wound Area} = \frac{\text{Area at 8,12,24,or 48 hr}}{\text{Area at 0 hr}} \times 100\%$

2.3.7 Keratinocyte Proliferation Assay

Primary keratinocytes isolated from our murine models with the keratinocyte-specific JMJD3 deficiency (*Jmjd3*$^{fl/fl}$ *K14*$^{cre+}$) and their littermate controls (*Jmjd3*$^{fl/fl}$ *K14*$^{cre-}$) were seeded at identical densities (400,000 cells / mL), cultured for 24, 48 hours, and alamarBlue (Invitrogen) reagent was added to get viability readouts at each timepoint after 4 hours of incubation at 37°C. Viability readouts or fluorescence intensities were compared to that of the initial timepoint to calculate proliferation rates or % initial viability at each timepoint. A subset of cells from each group was pre-treated with Mitomycin C (10 μg/mL) for 2 hours and washed with HBSS (without Ca^{2+}, Mg^{2+}).

2.3.8 RNA Extraction

Total RNA extraction was performed with TRIzol (Invitrogen) using manufacturer's directions. RNA was extracted using chloroform, isopropanol and ethanol. Superscript III Reverse transcriptase (ThermoFisher Scientific) kits were used to synthesize cDNA from extracted RNA. cDNA primers for *Jmjd3* (Mm01332680), *Fgf2* (Mm01285715), *Mmp2* (Mm00439498), *Itga3* (Mm00442910), *Timp1* (Mm01341361), *Ccl20* (Mm01268754), *Cxcl1* (Mm04207460), *Cxcl3* (Mm01701838), *Cxcl5* (Mm00436451), and 18s (no. 4318839) were purchased from Applied Biosciences. RT-PCR was conducted with 2x Taqman Fast PCR mix and run on a 7500 Real-Time PCR system (Applied Biosciences), and data was then reviewed in a relative quantification analysis to the 18s ribosomal RNA. All samples were assayed in triplicate. Data was then compiled in Excel (Microsoft) and presented using Prism software (GraphPad version 10.2.2).

2.3.9 PCR Array Analysis

Keratinocytes were isolated from tails of C57BL/6 mice, cultured, and stimulated with rIL-17A (40 ng/mL) for 1 hour. RNA was isolated and DNase digested using the RNAeasy mini kit,

and reverse transcription was performed using the RT^2 first strand kit (QIAGEN). Gene expression was analyzed using PCR array PAMM-085Z (Qiagen), which includes PCR primers for 84 chromatin-modifying enzymes. Data were analyzed using the PCR Array Data Analysis Web Portal.

2.3.10 siRNA Knockdown

Primary murine keratinocytes were transfected with 1 μM siRNA (Dharmacon Cat# E-063799-00-0005) targeted to *Jmjd3* or a non-targeting control (NTC) siRNA for 72 hours. Accell Delivery Medium (Dharmacon Cat# D-001910-01-05) was used as the transfection reagent.

2.3.11 Murine Bulk RNA Sequencing Analysis

Keratinocytes were isolated from tails of C57BL/6 mice, cultured, and stimulated with rIL-17A (40 ng/mL) for 5 hours. Keratinocytes were isolated from day 5 wounds from *db/+* and *db/db* mice. RNA isolation was performed using a RNeasy Kit (Qiagen) with DNase digestion. Library construction and analysis of reads was performed as described previously (56). Briefly, reads were trimmed using Trimmomatic and mapped using HiSAT2 (137, 138). Read counts were performed using the feature-counts option from the subRead package followed by the elimination of low reads, normalization and differential gene expression using edgeR (139, 140). Differential expression was performed on mapped reads using the taqwise dispersion algorithm in edgeR.

2.3.12 Chromatin Immunoprecipitation Assay

Chromatin immunoprecipitation assay was performed as described previously using a kit purchased from Abcam (ab500) (141). Briefly, following *ex vivo* studies, keratinocytes were cross linked in 1% formaldehyde for 10 min at RT and pellets stored at -80°C until analyzed. Following manufacturer's instructions, cells were lysed for 10 min on ice in an SDS-containing lysis buffer

(Abcam), supplemented with a protease inhibitor cocktail (Abcam), sonicated to generate 100-300 base pair fragments. Five percent of the total chromatin volume was put aside for the input control. The rest of the chromatin was subsequently incubated with antibodies against JMJD3 (Cat# ab169197, Lot# GR3263105-3, Abcam) at 3 µg/sample, trimethylated H3K27 (Active Motif, Cat# 39155, Lot# 16021022) at 1 µg/sample, or rabbit polyclonal IgG (Diagenode, Cat# C15410206, Lot# RIG002C) at 1 or 3 µg/sample overnight at 4°C. This was followed by addition of Protein A sepharose beads (Abcam) for 1 hour at 4°C. The pellet was washed, and a DNA purifying slurry (Abcam) was added. The eluates were reverse cross linked for 10 min at 98°C, followed by a proteinase K digestion for 30 min at 55°C and 10 min at 98°C. Precipitated DNA was analyzed by quantitative real time PCR on a Taqman 7500 sequence detection system. The following primers were used to amplify DNA in samples: *Itga3*: (forward) 5' GGGCTGCAAAGATCTCAAAC 3' and (reverse) 5' GCCACCACTATGTAAACCCA 3', *Timp1*: (forward) 5' CCAGGGAATACTCCTGCATC 3' and (reverse) 5' CTCAGGCAGGACACAATCTT 3', *Ccl20*: (forward) 5' TCACCACCATCTTTGGACTG 3' and (reverse) 5' ACAACATGACAGAGGTGTCC 3', *Cxcl1*: (forward) 5' AGGGACCTAACCTTGACAGT 3' and (reverse) 5' CTACAGTGATTTGCGGGGAT 3', *Cxcl3*: (forward) 5' GCGAAAAGTACTGGGGTACA 3' and (reverse) 5' ACTCCTGATTGTGACTGCTG 3', *Cxcl5*: (forward) 5' AAACTCCTTCCTTTGGCTCC 3' and (reverse) 5' TGAGGATGCCCTTCTTTTCC 3'

2.3.13 Enzyme Linked Immunosorbent Assay (ELISA)

Keratinocytes were isolated, cultured, scratched, and stimulated in culture for 24 or 48 hours in low-calcium (LoCa) medium. After stimulation, cell free supernatant was collected and analyzed by the University of Michigan Immune Monitoring Shared Resource Core for CCL-20,

CXCL-1, CXCL-5 or specific enzyme immunoassay kits for CXCL-3 (Boster Bio) and TIMP-1 (R&D Systems) according to the manufacturer's instructions.

2.3.14 Western Blot

Cell suspensions were lysed in radioimmunoprecipitation assay (RIPA) buffer (Sigma) and standardized for protein concentrations using a Bradford protein assay (BioRad) to generate a standard curve. Equal amounts of protein were then loaded onto to 4 to 12% sodium dodecyl sulfate gel electrophoresis under reducing conditions. Protein bands were then transferred to nitrocellulose membranes and probed with primary antibodies anti-mouse ITGA3 (Cat# ab190731, Lot# 1043494-4, Abcam, 1:1000), anti-mouse beta actin (Cat# A5316-100UL, Lot# 0000127607, Sigma Aldrich, 1:1000) at 4 °C for 48 hr. For JMJD3 western blots, nuclear extraction was performed using a kit (Active Motif) and lysates were probed with primary antibodies anti-JMJD3 (Cat# ab169197, Lot# GR3263105-3, Abcam, 1 µg/mL) or anti-H3 (Cat# 3638S, Lot# 11, Cell Signaling, 1:1000). All primary antibodies were diluted 1:1000 in 1% BSA in 0.1% Tween Tris-buffered saline (TBS-T) solution. Nitrocellulose membranes were then washed and incubated with horseradish peroxidase−labeled secondary antibody (Cell Signaling) for 1 hr at room temperature and visualized with chemiluminescence (Thermo Fisher Scientific). Blot images were analyzed using NIH ImageJ software to obtain sample densitometry readings normalized to beta actin.

2.3.15 Histology and Immunofluorescence

Tissues were harvested from mice and fixed in 10% formalin for 24 hours then stored in 70% ethanol. Specimens were embedded in paraffin and sectioned onto microscope slides. After deparaffinization, sections underwent Trichrome staining or were processed for immunofluorescence. For histomorphometric analysis of wounds, re-epithelialization rates were calculated as the distance between the two leading epithelial tongues expressed as a percentage of

the initial wound diameter. Wound contraction rates were determined by measuring the distance between the two edges of intact dermis or solid blue collagen bands and expressing this as a percentage of the initial wound diameter. For immunofluorescent staining, slides underwent antigen retrieval in citric acid buffer (pH 6.0). Samples were then permeabilized, blocked, and incubated with primary antibodies, rabbit polyclonal IgG (Diagenode, Cat# C15410206, Lot# RIG002C), anti-cytokeratin14 (Cat# LL002, Abcam, 5 μg/mL), anti-IL-17A (Cat# ab91649, Lot# 1017634-1, Abcam, 5 μg/mL), anti-H3K27me3 (Cat# 39155, Lot# 16021022, Active motif, 2 μg/mL), or anti-αSMA (Cat# A5228-100UL, Lot# 0000348067, Sigma-Aldrich, 2 μg/mL) in blocking solution overnight at 4C in a humidity chamber. The following day, slides were washed in PBS, then incubated with fluorophore-conjugated secondary antibody (Vector Labs, 1:400) in PBS for 2 hours at room temperature or with DAPI. Slides were washed with PBS, mounted, allowed to dry overnight, and then imaged. Images were taken with Nikon Ti2 Widefield Fluorescence Microscope at 20X magnification to capture the wound edge or 4X magnification to capture the whole wound. To quantify αSMA staining, brightness/contrast adjustments and background subtraction were first applied to all images using identical settings. Granulation tissue regions of interest (ROIs) were analyzed in ImageJ. Mean fluorescence intensity (MFI) of αSMA within the ROI was quantified and normalized to DAPI signal.

2.3.16 Flow Cytometry

For T cell analysis, single-cell suspensions from murine wound tissue were prepared and filtered through a 70 μm cell strainer. Cells were stained with BD Horizon™ Fixable Viability Stain 510 (BD Biosciences, Cat# 564406, RRID: AB_2869572) to exclude dead cells. Fc receptors were blocked using anti-CD16/32 (BioXCell, Cat# CUS-HB-197) for 10 minutes on ice. For lineage exclusion, cells were stained with FITC-conjugated anti-CD8 (Invitrogen, Cat# 11-0081-

81, RRID: AB_464915), anti-CD19 (BioLegend, Cat# 115506, RRID: AB_313641), and anti-Gr-1 (BioLegend, Cat# 108406, RRID: AB_313371). For T cell phenotyping, surface markers included CD3 APC (Invitrogen, Cat# 17-0031-82, RRID: AB_469315), and CD4 BV605 (BioLegend, Cat# 100547, RRID: AB_11125962). Following surface staining, cells were fixed in 2% formaldehyde and permeabilized using BD Perm/Wash buffer (BD Biosciences, Cat# 00-8333-56). Intracellular staining was performed with Foxp3 PE (BioLegend, Cat# 126404, RRID: AB_1089117) for regulatory T cells and RORγt PerCP-Cy5.5 (BD Pharmingen, Cat# 562683, RRID: AB_2737720) for T_H17 cells. For myeloid cell analysis, single-cell suspensions from murine wound tissue were similarly prepared and stained with BD Horizon™ Fixable Viability Stain 510 (BD Biosciences, Cat# 564406, RRID: AB_2869572) for viability discrimination. To exclude lymphoid and erythroid lineages, cells were stained with biotin-conjugated antibodies: anti-CD3 (BioLegend, Cat# 100304, RRID: AB_312669), anti-CD19 (BioLegend, Cat# 115504, RRID: AB_313639), and anti-TER-119 (BioLegend, Cat# 116204, RRID: AB_313705). Streptavidin-Pacific Orange (BioLegend, Cat# 405233) was used to label these biotinylated antibodies. Lineage-positive and dead cells were excluded from analysis. Myeloid populations were then identified using: CD45 PE-Cy7 (BioLegend, Cat# 103114, RRID: AB_312979), F4/80 PE (BioLegend, Cat# 111704, RRID: AB_2936728), CD11b APC (BioLegend, Cat# 101212, RRID: AB_312795), Ly6C PerCP (BioLegend, Cat# 128028, RRID: AB_10897805), and Ly6G FITC (BioLegend, Cat# 127606, RRID: AB_1236494). All flow cytometric analyses were performed using FlowJo version 10.10.0 software.

2.3.17 Magnetic-Activated Cell Sorting (MACS) of Murine Wound Monocyte, CD4$^+$ T cell, and Fibroblast Isolates

MACs sorting of wound cell isolates was performed. Wound tissue from mice was digested into single-cell suspensions as described previously. To enrich for monocytes, magnetic-activated cell sorting (MACS) was performed using a two-step process. First, cells were subjected to negative selection to deplete lymphocytes and neutrophils. Briefly, single-cell suspensions were incubated with biotin-conjugated antibodies against lineage markers: anti-mouse CD3 (BioLegend, Cat#100304, RRID: AB_312669), CD19 (BioLegend, Cat#115504, RRID: AB_313639), and Ly6G (BioLegend, Cat#127604, RRID: AB_1186108). Following incubation, cells were labeled with streptavidin-conjugated magnetic particles using the EasySep™ Mouse Streptavidin RapidSpheres™ Isolation Kit (Stemcell Technologies, Cat#19860) according to the manufacturer's instructions. The lineage-negative fraction was then subjected to positive selection for CD11b$^+$ myeloid cells using the EasySep™ Mouse CD11b Positive Selection Kit II (Stemcell Technologies, Cat#18970). The resulting CD11b$^+$ cell population was enriched for monocytes and used for downstream applications. For CD4$^+$ T cell isolation, CD4$^+$ T cells were isolated from single-cell suspensions of murine wound or lymphoid tissues using the EasySep™ Mouse CD4$^+$ T Cell Isolation Kit II (Stemcell Technologies, Cat#18952A). The procedure was performed according to the manufacturer's instructions to positively select for CD4$^+$ T cells. Isolated cells were used for downstream applications such as gene expression analysis. Lastly, to enrich for wound fibroblasts, single-cell suspensions from digested murine wound tissue were subjected to negative selection to remove hematopoietic, endothelial, and epithelial cell populations. Cells were incubated with biotin-conjugated antibodies targeting non-fibroblast lineages: anti-mouse CD45 (BioLegend, Cat#103104, RRID: AB_312969), CD31 (BioLegend, Cat#102404, AB_312899),

EpCAM (BioLegend, Cat#118204, AB_1134178), TER119 (BioLegend, Cat#116204, RRID: AB_313705), and Tie2/CD202b (BioLegend, Cat#124006, RRID: AB_2203221). Labeled cells were then incubated with streptavidin-conjugated magnetic particles and depleted using the EasySep™ Mouse Streptavidin RapidSpheres™ Isolation Kit (Stemcell Technologies, Cat#19860), following the manufacturer's protocol. The resulting lineage-negative cell population was enriched for fibroblasts and used for downstream analysis.

2.3.18 Human Wound Isolation

All experiments using human samples were approved by the IRB at the University of Michigan and were conducted in accordance with the principles in the Declaration of Helsinki. Written informed consent was obtained from all subjects involved in human studies. Human subject data is de-identified and these patients are not followed after the sample is collected. Per our IRB, at initial sample collection, we obtain information on age, sex, and diabetes status. For the bulk RNA sequencing cohort, biopsies from human diabetic wounds (N = 4) versus normal skin samples (N = 38) were collected. For a separate scRNA-Seq cohort, biopsies from human diabetic wounds versus normal skin samples were collected. Within the diabetic patient samples for scRNA-Seq, the average age was 60 years, with all patients having diabetes, hypertension, hyperlipidemia, and coronary artery disease. Within the nondiabetic patient samples, the average age was 70 years, with 50% of patients having hypertension, hyperlipidemia, and coronary artery disease. Wounds were obtained from the lateral edge of wound specimens using an 8 mm punch biopsy tool and processed for RNA extraction and sequencing as described for the murine wounds, and the material was fully consumed during analysis. RNA with RNA integrity number scores of greater than 8 were used, and all values were done with comparison to 28S/18S ratios and other housekeeping genes.

2.3.19 Human Bulk RNA-Seq and ScRNA-Seq Analyses

Single-cell suspensions for scRNA-Seq were generated as follows. Wound tissue from diabetic and non-diabetic patients was collected by punch biopsy and immediately processed. Samples were incubated overnight at 4°C in 0.4% Dispase (Life Technologies, Thermo Fisher Scientific) prepared in HBSS (Gibco, Thermo Fisher Scientific). The epidermal and dermal layers were then separated. The epidermis was enzymatically digested with 0.25% Trypsin-EDTA (Gibco, Thermo Fisher Scientific) containing 10 U/mL DNase I (Thermo Fisher Scientific) for 1 hour at 37°C, followed by quenching with FBS (Atlanta Biologicals) and filtration through a 70 μm strainer. Dermal tissue was finely minced and digested in 0.2% Collagenase II (Life Technologies, Thermo Fisher Scientific) and 0.2% Collagenase V (MilliporeSigma) for 1.5 hours at 37°C, then passed through a 70 μm strainer. Epidermal and dermal cells were combined in a 1:1 ratio and submitted to the University of Michigan Advanced Genomics Core for scRNA-Seq library generation on the 10x Genomics Chromium platform. Libraries were sequenced on the Illumina NovaSeq 6000 to produce 151 bp paired-end reads. Read trimming and quality control followed standard pipelines (142, 143). Processed reads were aligned to the human reference genome (GRCh37) using STAR (144). Gene-level counts were obtained with HTSeq (145) and normalized using DESeq2 (146), which was also used for differential expression testing with negative binomial models. To expand control sample representation, additional skin biopsy data from our prior study (147) were incorporated. Bulk RNA-seq and scRNA-seq data have been deposited in the Gene Expression Omnibus under accession numbers GSE154556 and GSE154557, respectively. For scRNA-Seq processing, Cell Ranger (10x Genomics) was used for alignment, quality filtering, and quantification. Subsequent normalization, data integration, and clustering were carried out in Seurat (148). Cell identities were assigned by comparing cluster

marker genes with known lineage-specific signatures. Spatial scRNA-Seq data from diabetic (N = 3) and non-diabetic (N = 1) wounds were analyzed to assess keratinocyte proximity to IL-17A-expressing cells using Giotto (v4.2.0). A Delaunay triangulation–based spatial network was constructed with a maximum intercellular distance of 50 μm. Cells with detectable IL-17A transcripts (raw counts > 0) were defined as IL-17A$^+$. Keratinocytes were designated "Near" if they had at least one direct spatial edge connecting to an IL-17A$^+$ cell and "Far" if no such connections were present. Log-normalized expression values for *CXCL1*, *CCL20*, *CXCL3*, *CXCL5*, *ITGA3*, and *TIMP1* were compared across proximity ("Near" vs. "Far") and diabetic status groups.

2.3.20 Statistics

GraphPad Prism software (RRID:SCR_002798) version 10.2.2 was used to analyze the data. Data were analyzed for normal distribution and then statistical significance between multiple groups was determined using a one-way analysis of variance test followed by Newman-Keuls post hoc test. For all single group comparisons, if data passed normality test, we used a two-tailed Student's t test. Otherwise, data were analyzed using the Mann–Whitney *U*-test. All data are representative of at least two independent experiments as detailed in the figure legends. A P value of less than or equal to 0.05 was significant. Values smaller than 0.0001 are reported as $P < 0.0001$.

2.3.21 Data Availability

Source data are provided with this paper. All sequencing data generated in this study have been deposited in the Gene Omnibus (GEO) or Zenodo repositories. The human bulk RNA-sequencing data have been deposited under accession code GSE154556 [https://www.ncbi.nlm.nih.gov/geo/query/acc.cgi?acc=GSE154556], and the human scRNA-sequencing data under accession code GSE154557

[https://www.ncbi.nlm.nih.gov/geo/query/acc.cgi?acc=GSE154557]. The human spatial scRNA-sequencing data of diabetic and non-diabetic wounds are available at [https://doi.org/10.5281/zenodo.17508360]. The mouse bulk RNA-sequencing data of IL-17A-stimulated keratinocytes are available at [https://doi.org/10.5281/zenodo.17504145], and the mouse bulk RNA-sequencing data of *db/+* and *db/db* wounds at [https://doi.org/10.5281/zenodo.17508179]. The mouse scRNA-sequencing data of wounds from keratinocyte-specific IL-17A signaling-deficient mice are available at [https://doi.org/10.5281/zenodo.17508202].

2.4 Results

2.4.1 IL-17A Signaling in Keratinocytes Controls Wound Repair via Regulation of Migratory and Inflammatory Genes

In order for wound repair to progress in an orchestrated fashion, chemokine and cytokine signals must occur at precise times in the wound microenvironment. In this regard, IL-17A and its downstream signaling are essential for wound repair, where it is increased early in wounds and serves to initiate inflammation and promote pathogen clearance (122, 149). It is well-established that delayed or exaggerated chemokine/cytokine-mediated signaling can result in pathologic healing (15, 68, 150). For example, excessive IL-17A in wound tissue has been shown to promote prolonged inflammation in the late phases of wound repair and delay re-epithelialization and remodeling (57). However, the precise cell-specific mechanisms for this IL-17A-mediated impaired re-epithelialization/migration and altered inflammation are unknown. In order to first examine IL-17A signaling in keratinocytes in wound repair, we isolated and cultured basal keratinocytes from C57BL/6 mice as we have previously described (133), stimulated them with or without recombinant mouse IL-17A (rIL-17A) (40 ng/mL), and performed scratch wound assays

over a 48-hour period to compare migration rates. Since IL-17A increases proliferation in keratinocytes (123), we pre-treated them with a mitosis inhibitor, Mitomycin C (10 μg/mL), for 2 hours to eliminate the contribution of cell proliferation to gap closure and to specifically assess changes in migration (135). We found that IL-17A-stimulated keratinocytes displayed a significant increase in percentage of initial gap area, indicating decreased gap closure rates at 48 hours compared to unstimulated controls (Figure 2-1A). To assess translational relevance, we repeated the scratch assay using N/TERT human keratinocytes, which closely mimic primary human keratinocyte epithelialization *in vitro* (151). We confirmed that IL-17A-stimulated human keratinocytes displayed decreased gap closure rates at 8 and 12 hours compared to unstimulated controls (Figure 2-1B).

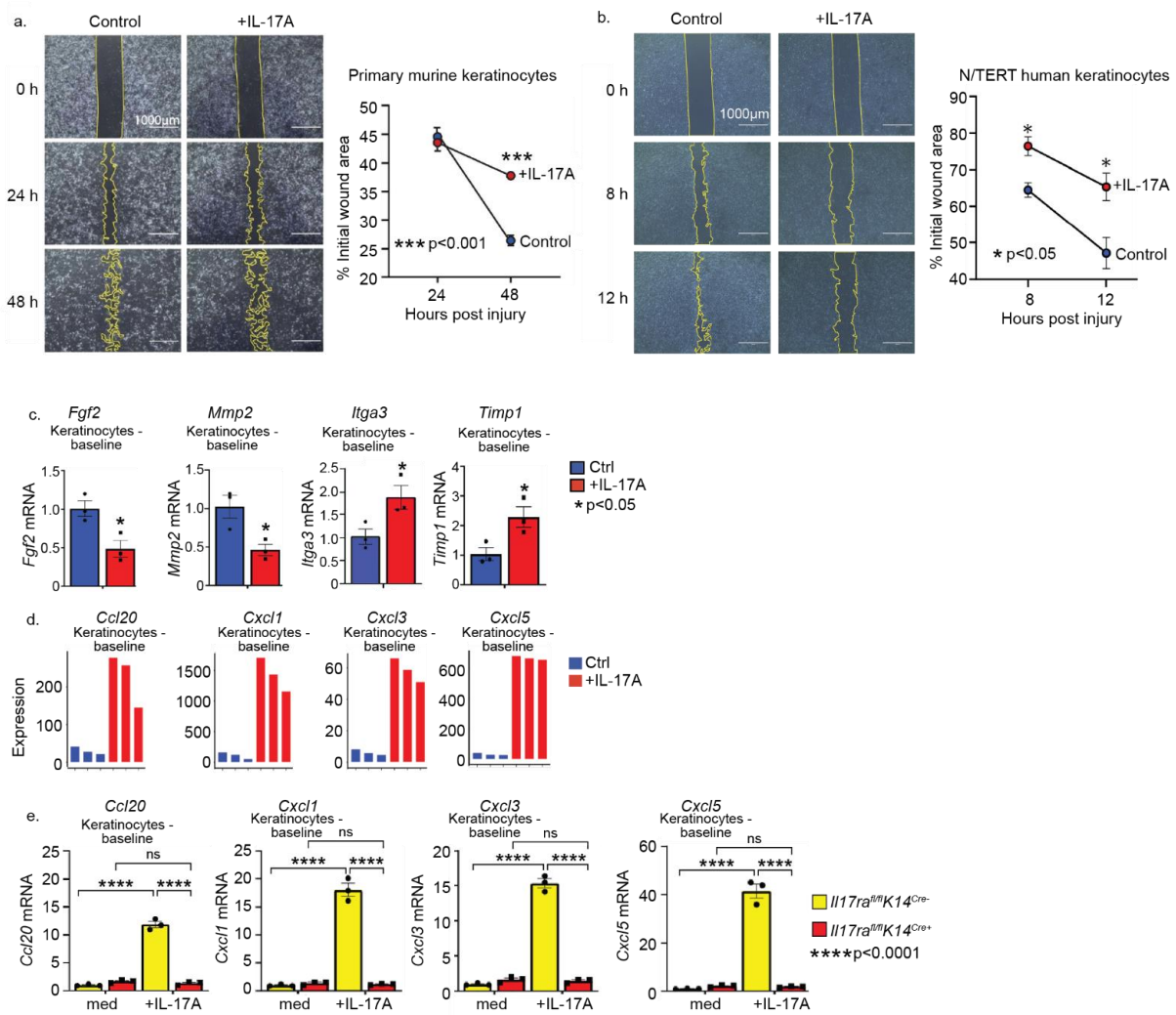


Figure 2-1: IL-17A signaling in keratinocytes controls wound repair via regulation of migratory and inflammatory genes

(A-B) Scratch assays of primary murine (n = 3 biological replicates, p = 0.0003 (48 h)) and N/TERT keratinocytes (n = 3 biological replicates, p = 0.0209 (8 h), p = 0.0324 (12 h)) with (red) or without (blue) IL-17A, n = 3 independent experiments. (C) qPCR analysis of migration-related gene expression in unstimulated (blue) and IL-17A-stimulated (red) keratinocytes. n = 3 biological replicates, *Fgf2*: p = 0.0242, *Mmp2*: p = 0.0274, *Itga3*: p = 0.0454, *Timp1:* p = 0.0374. n = 3 independent experiments. (D) RNA-seq analysis of inflammatory chemokine expression in unstimulated (blue) and IL-17A-stimulated (red) keratinocytes. n = 3 biological replicates. (E) qPCR analysis of inflammatory gene expression in *Il17ra*$^{fl/fl}$ *K14*$^{cre+}$ (red) and *Il17ra*$^{fl/fl}$ *K14*$^{cre-}$ (yellow) keratinocytes. n = 3 biological replicates, *Ccl20:* p < 0.0001 (cre- medium vs. stimulation), p = 0.8426 (cre+ medium vs. stimulation), p < 0.0001 (cre- stimulation vs. cre+ stimulation), *Cxcl1:* p < 0.0001 (cre- medium vs. stimulation), p = 0.9949 (cre+ medium vs. stimulation), p < 0.0001 (cre- stimulation vs. cre+ stimulation), *Cxcl3:* p < 0.0001 (cre- medium vs. stimulation), p = 0.9835 (cre+ medium vs. stimulation), p < 0.0001 (cre- stimulation vs. cre+ stimulation), *Cxcl5:* p < 0.0001 (cre- medium vs. stimulation), p = 0.9983 (cre+ medium vs. stimulation), p < 0.0001 (cre- stimulation vs. cre+ stimulation). n = 3 independent experiments. Data were analyzed for variances, and 2-tailed Student's t tests for (C) and 1-way ANOVA tests for (A-B), (E) were performed. Data are presented as mean ± SEM.

Several genes/proteins play key roles in keratinocyte migration including fibroblast growth factor 2 that accelerates migration by increasing epithelial-to-mesenchymal transition in

keratinocytes (152, 153) and integrin alpha 3 that inhibits migration by promoting cell adhesion (154-157). During ECM remodeling, wound edge keratinocytes control their migration path by modulating expression of MMPs and TIMPs (158), where TIMP-1 is a strong inhibitor of most MMPs including MMP-2, which is linked with keratinocyte migration (110, 159, 160). In normal wound repair, a balance of MMPs/TIMPs is maintained and promotes keratinocyte migration (110); however, in a dysregulated setting, an abnormal increase in TIMP-1 expression decreases keratinocyte migratory capacity (161). To examine the mechanisms underlying delayed wound closure in IL-17A-stimulated keratinocytes, we analyzed gene(s) involved in migration. Upon stimulating cultured murine keratinocytes with rIL-17A (40 ng/mL), we found that expression of pro-migratory genes, fibroblast growth factor 2 (*Fgf2*) and MMP-2 (*Mmp2*) were decreased (110, 152, 153), while expression of anti-migratory genes, integrin alpha 3 (*Itga3*) and TIMP-1 (*Timp1*) were increased compared to their unstimulated controls (Figure 2-1C). In order to identify other keratinocyte genes potentially regulated by IL-17A, we performed bulk RNA-Seq of IL-17A-stimulated murine keratinocytes and found an increase in expression of inflammatory genes *Ccl20, Cxcl1, Cxcl3, Cxcl5* (Figure 2-1D). These chemokines are regulated by IL-17A in keratinocytes in other chronic inflammatory skin diseases (123, 162) and recruit inflammatory cell types such as T_H17 cells, neutrophils, and monocytes (123, 163), driving pathologic inflammation. Next, to further verify that IL-17A signaling regulates these inflammatory genes in keratinocytes, we generated a keratinocyte-specific murine model with a deletion of IL-17 receptor A (*Il17ra*$^{fl/fl}$ *K14*$^{cre+}$) on a C57BL/6 background. Keratinocytes isolated from *Il17ra*$^{fl/fl}$ *K14*$^{cre+}$ and their littermate controls (*Il17ra*$^{fl/fl}$ *K14*$^{cre-}$) were isolated, cultured, and stimulated with rIL-17A for 5 hours, and gene expression was examined. Keratinocytes from *Il17ra*$^{fl/fl}$ *K14*$^{cre+}$ exhibited decreased *Ccl20, Cxcl1, Cxcl3, Cxcl5* compared with littermate controls (Figure 2-1E). Lastly, to

assess whether these chemokines contribute to impaired migration in response to IL-17A, we performed scratch assays using neutralizing antibodies (1 μg/mL) against CCL-20, CXCL-1, CXCL-3, and CXCL-5, or an isotype control, in both murine (Figures 2-2A, B) and human keratinocytes (Figures 2-2C, D). In IL-17A-stimulated keratinocytes, both isotype control and neutralizing antibody treatments resulted in decreased migration, with no rescue observed upon chemokine blockade. These findings suggest that these individual chemokines play a minimal role in mediating IL-17A-induced migration defects. Collectively, these findings indicate that IL-17A signaling in keratinocytes impairs wound closure, likely through the regulation of both migratory and inflammatory genes.

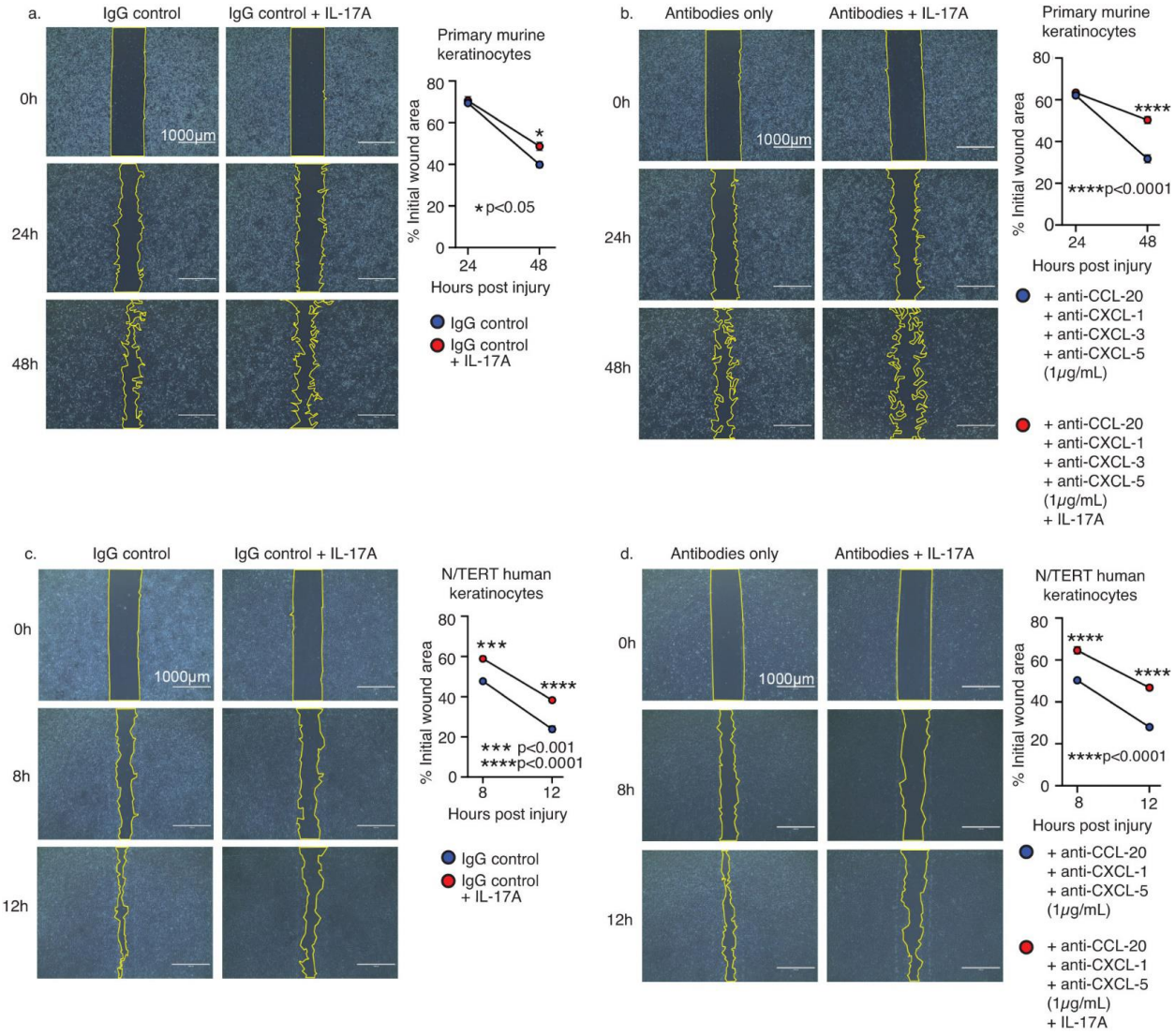
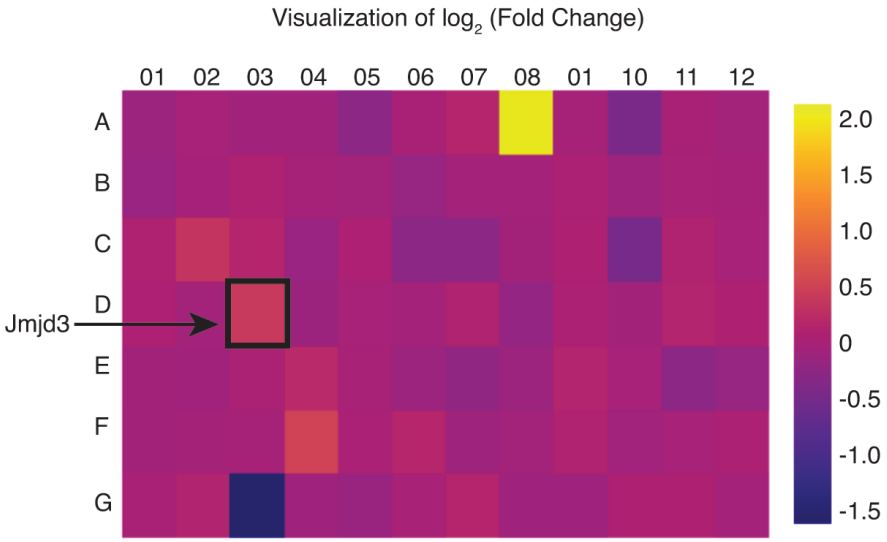


Figure 2-2: Neutralizing IL-17A-induced chemokines does not impact keratinocyte migration
(A) Scratch assay of primary murine keratinocytes treated with IgG control alone (blue) or with IL-17A (red). $n = 3$ biological replicates, $p = 0.0119$ (48 h). (B) Scratch assay of primary murine keratinocytes treated with neutralizing antibodies against CCL-20, CXCL-1, CXCL-3, CXCL-5 alone (blue) or with IL-17A (red). $n = 3$ biological replicates, $p < 0.0001$ (48 h). (C) Scratch assay of N/TERT human keratinocytes treated with IgG control alone (blue) or with IL-17A (red). $n = 3$ biological replicates, $p = 0.0003$ (8 h), $p < 0.0001$ (12 h). (D) Scratch assay of primary murine keratinocytes treated with neutralizing antibodies against CCL-20, CXCL-1, CXCL-5 alone (blue) or with IL-17A (red). $n = 3$ biological replicates, $p < 0.0001$ (8 h), $p < 0.0001$ (12 h). $n = 2$ independent experiments. Data were analyzed for variances, and 1-way ANOVA tests were performed. Data are presented as mean ± SEM.

2.4.2 IL-17A Signaling Upregulates Expression of the Histone Demethylase, JMJD3, via a TRAF6/NFκB Pathway

Epigenetic enzymes have been shown by our group and others to regulate immune cell functions in wound tissue; however, their role in non-immune cells associated with tissue repair is less studied. In order to examine epigenetic alterations in response to IL-17A in keratinocytes, we stimulated murine keratinocytes with rIL-17A (40 ng/mL) and performed a 96-well epigenetic super array (15, 76, 115, 164). We found that the histone demethylase, JMJD3, displayed significant changes in expression in response to IL-17A compared to other epigenetic enzymes examined (Figure 2-3). Next, to confirm our super array results, we examined *Jmjd3* expression via qPCR and western blot in IL-17A-stimulated keratinocytes isolated from C57BL/6 mice and found that IL-17A significantly increases expression of JMJD3 mRNA and protein (Figure 2-4A, B). Prior studies from our group have found that *Jmjd3* expression is abnormally high in diabetic wound macrophages and controls inflammatory gene expression via an H3K27 mechanism (69, 76, 164); however, the role of JMJD3 has not been examined in wound keratinocytes or in response to IL-17A. To further validate that JMJD3 is regulated via an upstream IL-17A signaling pathway, we used our *Il17ra*$^{fl/fl}$ *K14*$^{cre+}$ mice and their littermate controls (*Il17ra*$^{fl/fl}$ *K14*$^{cre-}$), isolated keratinocytes, stimulated them with rIL-17A (40 ng/mL), and examined *Jmjd3* expression. We identified that *Il17ra*$^{fl/fl}$ *K14*$^{cre+}$ keratinocytes were unable to upregulate *Jmjd3* following stimulation with IL-17A (Figure 2-4C), suggesting that the IL-17A signaling pathway is involved in regulating *Jmjd3* expression.



Gene expression, DNA Methylation, Protein detection

Test Group	Control Group	Fold Regulation Threshold	p-value Threshold
IL-17A	Control group	1.3	0.05

Heatmap position	Gene name	Fold Regulation
A08	Ciita	4.63
C02	Hdac5	1.33
D03	Jmjd3	1.38
F04	Setd1a	1.48
A10	Dnmt1	-1.31
C10	Kdm1a	-1.36
G03	Smyd1	-2.95

Figure 2-3: Expression of *Jmjd3* is upregulated in response to IL-17A in keratinocytes
Gene expression of chromatin-modifying enzymes was analyzed using PCR array plates in keratinocytes isolated from C57BL/6 mice stimulated with or without IL-17A for 1 hr. Enzymes that were upregulated (yellow and orange) and downregulated (dark blue) are shown. The threshold was set to a 1.3-fold difference. Data are expressed as fold over control (n = 3 biological replicates).

The primary IL-17A receptor downstream signal pathway involves Act1/TRAF6 complex formation (165-168). TRAF6 signaling has been shown to be responsible for activation of NFκB-mediated pathways involved in chronic inflammation in psoriasis (123); thus, we first examined TRAF6 and its' downstream signaling following IL-17A receptor stimulation. In order to examine

the role of TRAF6 in keratinocytes, we generated a keratinocyte-specific *Traf6*-deficient murine model (*Traf6*$^{fl/fl}$ *K14*$^{cre+}$) (on a C57BL/6 background), and isolated keratinocytes from *Traf6*$^{fl/fl}$ *K14*$^{cre+}$ mice and their littermate controls (*Traf6*$^{fl/fl}$ *K14*$^{cre-}$). Keratinocytes were then stimulated with rIL-17A (40 ng/mL) and examined for *Jmjd3* expression. We found that keratinocytes deficient in TRAF6 were unable to upregulate *Jmjd3* following stimulation with IL-17A (Figure 2-4D). Next, to determine if NFκB alters *Jmjd3* expression, we treated IL-17A-stimulated keratinocytes with a NFκB inhibitor (IKK inhibitor VII, 2 μM) and observed that inhibition of NFκB also resulted in decreased *Jmjd3* expression (Figure 2-4E). This suggests that both TRAF6 and NFκB are important for *Jmjd3* expression. Taken together, these results indicate that IL-17A induces *Jmjd3* in keratinocytes via a TRAF6/NFκB pathway (Figure 2-4F).

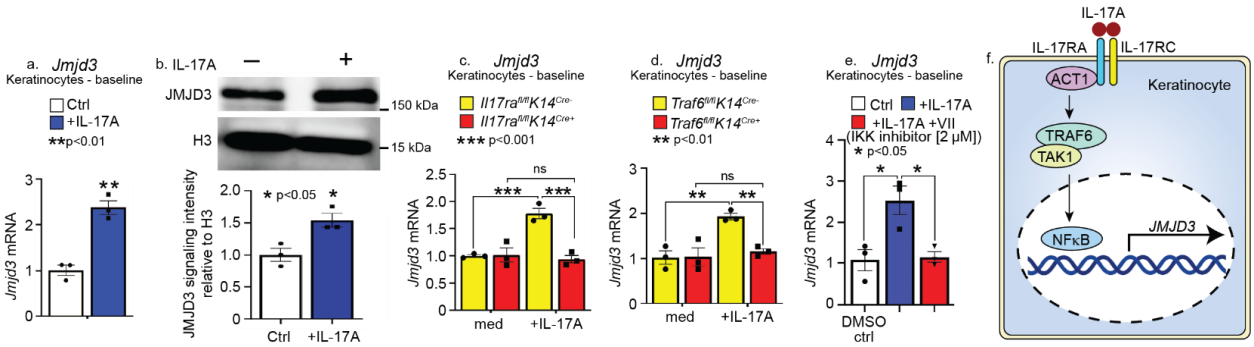


Figure 2-4: IL-17A signaling upregulates expression of the histone demethylase, JMJD3, via a TRAF6/NFκB pathway

(A) *Jmjd3* qPCR analysis of unstimulated (white) and IL-17A-stimulated (blue) keratinocytes. n = 3 biological replicates, p = 0.0021. n = 3 independent experiments. (B) Western blot of JMJD3 expression in unstimulated (white) and IL-17A-stimulated (blue) keratinocytes. n = 3 technical replicates, p = 0.0224. n = 3 independent experiments. Representative densitometry plot shown. (C) *Jmjd3* qPCR analysis of *Il17ra*$^{fl/fl}$ *K14*$^{cre+}$ (red) and *Il17ra*$^{fl/fl}$ *K14*$^{cre-}$ (yellow) keratinocytes. n = 3 biological replicates, p = 0.0008 (cre- medium vs. stimulation), p = 0.9131 (cre+ medium vs. stimulation), p = 0.0005 (cre- stimulation vs. cre+ stimulation), n = 3 independent experiments. (D) *Jmjd3* qPCR analysis of *Traf6*$^{fl/fl}$ *K14*$^{cre+}$ (red) and *Traf6*$^{fl/fl}$ *K14*$^{cre-}$ (yellow) keratinocytes. n = 3 biological replicates, p = 0.0036 (cre- medium vs. stimulation), p = 0.9007 (cre+ medium vs. stimulation), p = 0.0095 (cre- stimulation vs. cre+ stimulation), n = 3 independent experiments. (E) *Jmjd3* qPCR analysis of keratinocytes treated with DMSO only (white), with IL-17A alone (blue), or with IL-17A and IKK inhibitor VII (2 μM) (red). n = 3 biological replicates, p = 0.0156 (DMSO vs. IL-17A), p = 0.0198 (IL-17A vs. IL-17A and inhibitor), n = 3 independent experiments. (F) Schematic of proposed IL-17A/TRAF6/NFκB-mediated regulation of *Jmjd3*. Data were analyzed for variances, and 2-tailed Student's t tests for (A-B) and 1-way ANOVA tests for (C-E) were performed. Data are presented as the mean ± SEM.

2.4.3 Jmjd3 Directly Regulates Anti-Migratory and Inflammatory Genes in Wound Keratinocytes in Response to IL-17A and Direct Inhibition of Jmjd3 in Keratinocytes Improves Migration / Wound Closure Rate

JMJD3 is a histone demethylase that has specificity for the lysine 27 site on histone 3 site (H3K27), resulting in the opening of chromatin that renders promoter sites accessible for transcription factor binding, thus effectively increasing gene expression (69). To examine if IL-17A increases JMJD3-mediated H3K27 demethylation on specific gene promoters, we isolated keratinocytes, stimulated them with rIL-17A (40 ng/mL), and analyzed by chromatin immunoprecipitation (ChIP) for H3K27me3 methylation at gene promoters of anti-migratory (*Itga3, Timp1*) and inflammatory (*Ccl20, Cxcl1, Cxcl3,* and *Cxcl5*) genes. We found decreased H3K27me3 on the anti-migratory and inflammatory gene promoters in the IL-17A-stimulated keratinocytes compared to unstimulated controls (Figure 2-5A). Since there are other chromatin modifying enzymes (CMEs) that methylate the H3K27 site, we stimulated primary murine keratinocytes with rIL-17A (40 ng/mL) and treated them with a pharmacological inhibitor, GSK-J4 (1 μM), that specifically blocks JMJD3 demethylase activity (169). Treatment of IL-17A-stimulated keratinocytes with GSK-J4 resulted in both decreased gene (Figure 2-5B) and protein (Figures 2-5C, D) expression (*Itga3, Timp1, Ccl20, Cxcl1, Cxcl3, Cxcl5*) compared to keratinocytes stimulated with IL-17A alone. To address any potential off-target effects of GSK-J4, we treated keratinocytes with siRNA targeting *Jmjd3* and found decreased anti-migratory and inflammatory gene expression compared to non-targeting controls (Figure 2-5E).

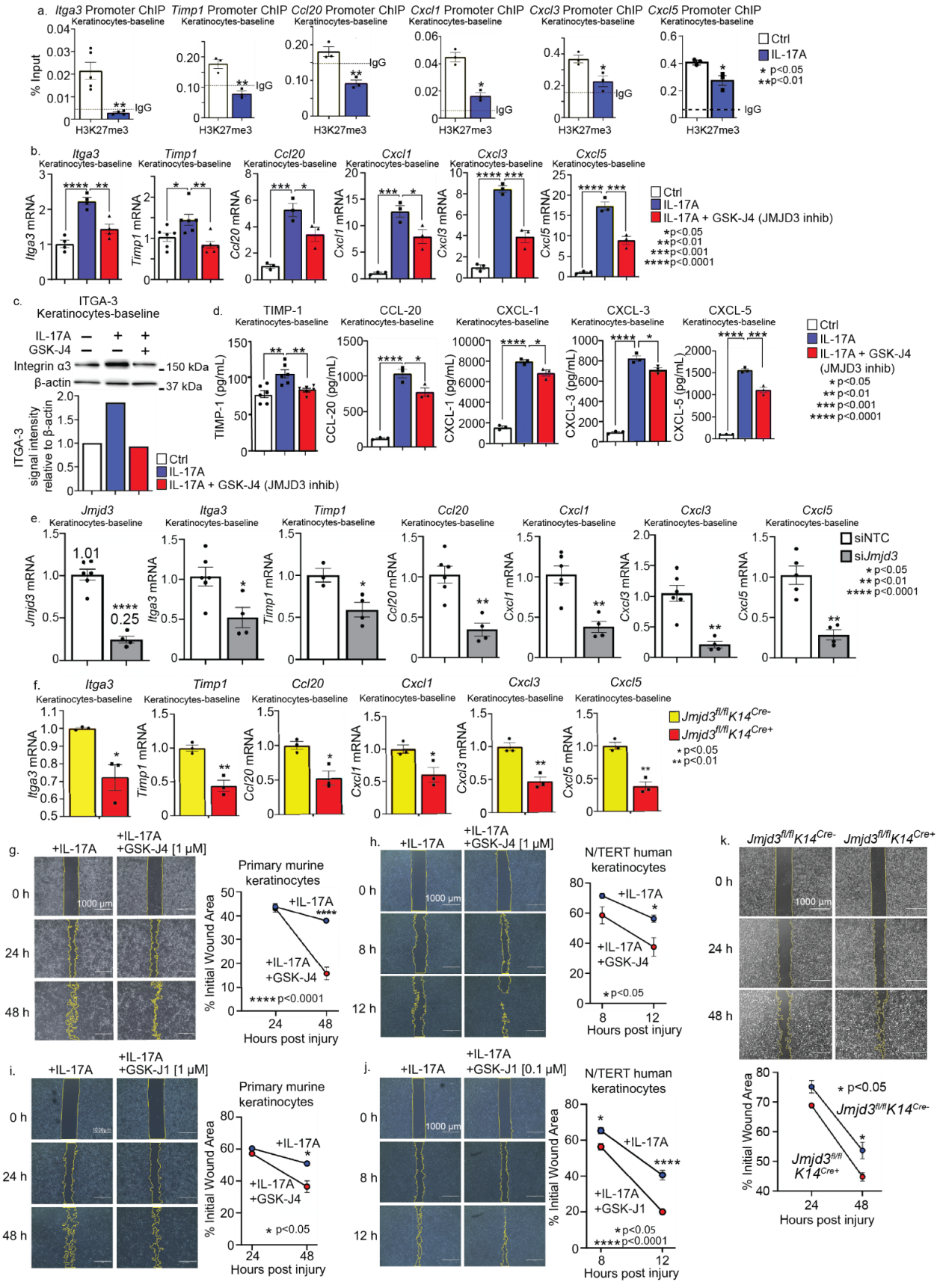

a. Itga3 Promoter ChIP Timp1 Promoter ChIP Ccl20 Promoter ChIP Cxcl1 Promoter ChIP Cxcl3 Promoter ChIP Cxcl5 Promoter ChIP
Keratinocytes-baseline
% Input
H3K27me3
IgG
Ctrl
IL-17A
* p<0.05
**p<0.01
b. Itga3 Timp1 Ccl20 Cxcl1 Cxcl3 Cxcl5
Keratinocytes-baseline
Itga3 mRNA
Timp1 mRNA
Ccl20 mRNA
Cxcl1 mRNA
Cxcl3 mRNA
Cxcl5 mRNA
Ctrl
IL-17A
IL-17A + GSK-J4 (JMJD3 inhib)
*p<0.05
**p<0.01
***p<0.001
****p<0.0001
c. ITGA-3
Keratinocytes-baseline
IL-17A
GSK-J4
Integrin α3
β-actin
150 kDa
37 kDa
ITGA-3 signal intensity relative to β-actin
Ctrl
IL-17A
IL-17A + GSK-J4 (JMJD3 inhib)
d. TIMP-1 CCL-20 CXCL-1 CXCL-3 CXCL-5
Keratinocytes-baseline
TIMP-1 (pg/mL)
CCL-20 (pg/mL)
CXCL-1 (pg/mL)
CXCL-3 (pg/mL)
CXCL-5 (pg/mL)
Ctrl
IL-17A
IL-17A + GSK-J4 (JMJD3 inhib)
* p<0.05
** p<0.01
*** p<0.001
**** p<0.0001
e. Jmjd3 Itga3 Timp1 Ccl20 Cxcl1 Cxcl3 Cxcl5
Keratinocytes-baseline
Jmjd3 mRNA
1.01
0.25
siNTC
siJmjd3
* p<0.05
** p<0.01
**** p<0.0001
f. Itga3 Timp1 Ccl20 Cxcl1 Cxcl3 Cxcl5
Keratinocytes-baseline
Jmjd3fl/flK14Cre-
Jmjd3fl/flK14Cre+
* p<0.05
** p<0.01
g. +IL-17A
+IL-17A +GSK-J4 [1 μM]
0 h
24 h
48 h
1000 μm
Primary murine keratinocytes
% Initial Wound Area
+IL-17A
+IL-17A +GSK-J4
**** p<0.0001
Hours post injury
h. +IL-17A
+IL-17A +GSK-J4 [1 μM]
0 h
8 h
12 h
1000 μm
N/TERT human keratinocytes
+IL-17A
+IL-17A +GSK-J4
* p<0.05
Hours post injury
k. Jmjd3fl/flK14Cre-
Jmjd3fl/flK14Cre+
0 h
24 h
48 h
1000 μm
* p<0.05
Jmjd3fl/flK14Cre-
Jmjd3fl/flK14Cre+
% Initial Wound Area
Hours post injury
i. +IL-17A
+IL-17A +GSK-J1 [1 μM]
0 h
24 h
48 h
Primary murine keratinocytes
% Initial Wound Area
+IL-17A
+IL-17A +GSK-J4
* p<0.05
Hours post injury
j. +IL-17A
+IL-17A +GSK-J1 [0.1 μM]
0 h
8 h
12 h
1000 μm
N/TERT human keratinocytes
% Initial Wound Area
+IL-17A
+IL-17A +GSK-J1
* p<0.05
**** p<0.0001
Hours post injury

Figure 2-5: *Jmjd3* directly regulates anti-migratory and inflammatory genes in wound keratinocytes in response to IL-17A and direct inhibition of *Jmjd3* in keratinocytes improves migration / wound closure rate

(A) ChIP analysis of H3K27me3 or IgG at indicated promoters in keratinocytes with (white) or without (blue) IL-17A stimulation. *Itga3:* $n = 5$ (unstimulated), $n = 4$ (IL-17A-stimulated) technical replicates, $p = 0.0034$, *Timp1*: $n = 3$ technical replicates, $p = 0.0046$, *Ccl20*: $n = 3$ technical replicates, $p = 0.0059$, *Cxcl1*: $n = 3$ technical replicates, $p = 0.0020$, *Cxcl3*: $n = 3$ technical replicates, $p = 0.0258$, *Cxcl5*: $n = 3$ technical replicates, $p = 0.0174$. $n = 3$ independent experiments. (B) qPCR analysis of keratinocytes treated with DMSO only (white), with IL-17A alone (blue), or with IL-17A and GSK-J4 (1 μM) (red). *Itga3*: $n = 4$ biological replicates, $p < 0.0001$ (DMSO vs. IL-17A), $p = 0.0017$ (IL-17A vs. IL-17A and inhibitor), *Timp1:* $n = 6$ biological replicates, $p < 0.0312$ (DMSO vs. IL-17A), $p = 0.0029$ (IL-17A vs. IL-17A and inhibitor), *Ccl20:* $n = 3$ biological replicates, $p = 0.0008$ (DMSO vs. IL-17A), $p = 0.0428$ (IL-17A vs. IL-17A and inhibitor), *Cxcl1*: $n = 3$ biological replicates, $p = 0.0003$ (DMSO vs. IL-17A), $p = 0.0294$ (IL-17A vs. IL-17A and inhibitor), *Cxcl3*: $n = 3$ biological replicates, $p < 0.0001$ (DMSO vs. IL-17A), $p = 0.0003$ (IL-17A vs. IL-17A and inhibitor), *Cxcl5*: $n = 3$ biological replicates, $p < 0.0001$ (DMSO vs. IL-17A), $p = 0.0007$ (IL-17A vs. IL-17A and inhibitor), $n = 3$ independent experiments. (C) Western blot of ITGA-3 expression in keratinocytes treated with DMSO only (white), with IL-17A alone (blue), or with IL-17A and GSK-J4 (red). Representative densitometry plot is shown. $n = 3$ independent experiments. (D) Protein quantification of lysates from keratinocytes treated with DMSO only (white), with IL-17A alone (blue), or with IL-17A and GSK-J4 (red). TIMP-1: $n = 6$ biological replicates, $p = 0.0012$ (DMSO vs. IL-17A), $p = 0.0068$ (IL-17A vs. IL-17A and inhibitor), CCL-20: $n = 3$ biological replicates, $p < 0.0001$ (DMSO vs. IL-17A), $p = 0.0199$ (IL-17A vs. IL-17A and inhibitor), CXCL-1: $n = 3$ biological replicates, $p < 0.0001$ (DMSO vs. IL-17A), $p = 0.0158$ (IL-17A vs. IL-17A and inhibitor), CXCL-3: $n = 3$ biological replicates, $p < 0.0001$ (DMSO vs. IL-17A), $p = 0.0167$ (IL-17A vs. IL-17A and inhibitor), CXCL-5: $n = 3$ biological replicates, $p < 0.0001$ (DMSO vs. IL-17A), $p = 0.0005$ (IL-17A vs. IL-17A and inhibitor), $n = 3$ independent experiments. (E) qPCR analysis of keratinocytes treated with a non-targeting control (siNTC) (white) or si*Jmjd3* (gray). *Jmjd3*: $n = 6$ (siNTC), $n = 4$ biological replicates (si*Jmjd3*), $p = 0.0192$, *Itga3:* $n = 6$ (siNTC), $n = 4$ biological replicates (si*Jmjd3*), $p = 0.0019$, *Timp1:* $n = 3$ (siNTC), $n = 4$ biological replicates (si*Jmjd3*), $p = 0.0205$, *Ccl20:* $n = 6$ (siNTC), $n = 4$ biological replicates (si*Jmjd3*), $p = 0.0015$, *Cxcl1:* $n = 6$ (siNTC), $n = 4$ biological replicates (si*Jmjd3*), $p = 0.0019$, *Cxcl3:* $n = 6$ (siNTC), $n = 4$ biological replicates (si*Jmjd3*), $p = 0.0011$, *Cxcl5:* $n = 6$ (siNTC), $n = 4$ biological replicates (si*Jmjd3*), $p = 0.0011$, $n = 3$ independent experiments. (F) qPCR analysis of $Jmjd3^{fl/fl}$ $K14^{cre+}$ (red) and $Jmjd3^{fl/fl}$ $K14^{cre-}$ (yellow) keratinocytes. $n = 3$ biological replicates, *Itga3*: $p = 0.0184$, *Timp1*: $p = 0.0044$, *Ccl20*: $p = 0.0160$, *Cxcl1*: $p = 0.0371$, *Cxcl3*: $p = 0.0042$. $n = 3$ independent experiments. (G – H) Scratch assays of primary murine ($n = 3$ biological replicates, $p < 0.0001$ (48 h)) and N/TERT ($n = 3$ biological replicates, $p = 0.0340$ (12 h)) keratinocytes treated with IL-17A alone (blue) or IL-17A and GSK-J4 (red). $n = 3$ independent experiments. (I – J) Scratch assays of primary murine ($n = 3$ biological replicates, $p = 0.0016$ (48 h)) and N/TERT ($n = 6$ biological replicates (IL-17A alone), $n = 4$ biological replicates (IL-17A and GSK-J1), $p = 0.0223$ (8 h), $p < 0.0001$ (12 h)) keratinocytes treated with IL-17A alone (blue) or IL-17A and GSK-J1 (red). $n = 3$ independent experiments. (K) Scratch assay of $Jmjd3^{fl/fl}$ $K14^{cre+}$ (red) and $Jmjd3^{fl/fl}$ $K14^{cre-}$ (blue) keratinocytes. $n = 3$ biological replicates, $p = 0.0198$ (48 h). $n = 3$ independent experiments. Data were analyzed for variances, and 2-tailed Student's *t* tests for (A), (E), (F) and 1-way ANOVA tests for (B), (D), (G-K) were performed. Data are presented as the mean ± SEM.

Next, we generated a keratinocyte-specific *Jmjd3*-deficient murine model ($Jmjd3^{fl/fl}$ $K14^{cre+}$) and isolated keratinocytes from $Jmjd3^{fl/fl}$ $K14^{cre+}$ and their littermate controls ($Jmjd3^{fl/fl}$ $K14^{cre-}$), stimulated them with rIL-17A (40 ng/mL), and examined changes in anti-migratory and inflammatory gene expression. In response to IL-17A stimulation, $Jmjd3^{fl/fl}$ $K14^{cre+}$ keratinocytes had decreased gene expression (*Itga3, Timp1, Ccl20, Cxcl1, Cxcl3, Cxcl5*) compared to their $Jmjd3^{fl/fl}$ $K14^{cre-}$ controls (Figure 2-5F). To specifically interrogate the role of JMJD3 on keratinocyte function, we performed a scratch assay of both murine and human keratinocytes

treated with or without GSK-J4 over a 48-hour or 12-hour period. With GSK-J4 treatment, murine keratinocytes displayed improved wound closure rates at 48 hours (Figure 2-5G), while human keratinocytes displayed improved wound closure rates at 12 hours compared to their untreated controls (Figure 2-5H), suggesting that inhibiting JMJD3 demethylase activity improves keratinocyte migration. Additionally, we repeated the scratch assay using an alternative pharmacological inhibitor called GSK-J1 to confirm the specificity of JMJD3-mediated migration defects. We demonstrated that GSK-J1 treatment resulted in improved migration rates in both murine and human keratinocytes (Figures 2-5I, J). To further assess changes in migration rates using our genetic model and control for off-target effects of pharmacological inhibitors, we performed a scratch wound assay of keratinocytes isolated from *Jmjd3*$^{fl/fl}$ *K14*$^{cre+}$ mice and littermate controls (*Jmjd3*$^{fl/fl}$ *K14*$^{cre-}$) over a 48-hour period. At 48 hours, *Jmjd3*$^{fl/fl}$ *K14*$^{cre+}$ keratinocytes displayed increased wound closure rates compared to controls (Figure 2-5K). To exclude the role of JMJD3 in keratinocyte proliferation, we conducted proliferation assays using keratinocytes isolated from *Jmjd3*$^{fl/fl}$ *K14*$^{cre+}$ mice and littermate controls (*Jmjd3*$^{fl/fl}$ *K14*$^{cre-}$). Proliferation-inhibited controls confirmed no change in proliferation (Figure 2-6A). Both *Jmjd3*$^{fl/fl}$ *K14*$^{cre-}$ and *Jmjd3*$^{fl/fl}$ *K14*$^{cre+}$ keratinocytes resulted in around a 2-fold increase in proliferation at 48 hours (Figure 2-6B), and the difference between the two groups was not significant, suggesting that the role of JMJD3 on keratinocyte proliferation is minimal. Together, these data indicate that JMJD3 impairs wound closure by upregulating anti-migratory and inflammatory gene expression in wound keratinocytes.

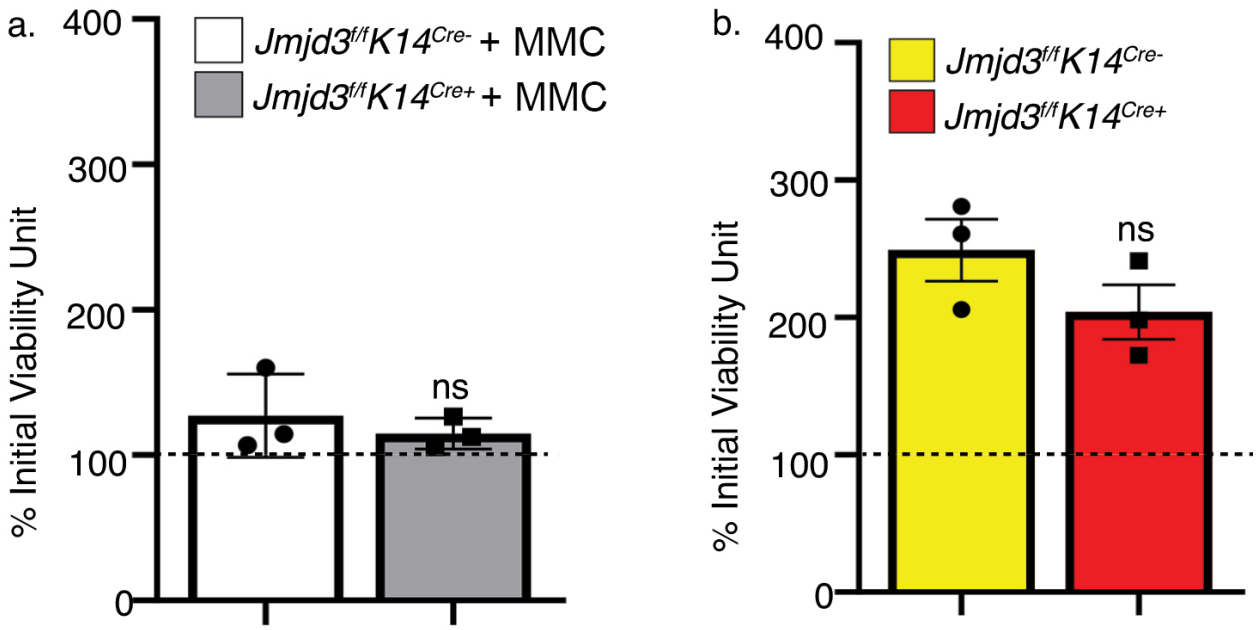


Figure 2-6: The role of JMJD3 on keratinocyte proliferation is minimal
(A) Proliferation assay of keratinocytes isolated from *Jmjd3*$^{fl/fl}$ *K14*$^{cre+}$ (gray) and their littermate controls (*Jmjd3*$^{fl/fl}$ *K14*$^{cre-}$) (white) treated with Mitomycin C. n = 3 biological replicates, p = 0.5284. (B) Proliferation assay of keratinocytes isolated from *Jmjd3*$^{fl/fl}$ *K14*$^{cre+}$ (red) and their littermate controls (*Jmjd3*$^{fl/fl}$ *K14*$^{cre-}$) (yellow). n = 3 biological replicates, p = 0.2085. n = 2 independent experiments. Dotted line represents 100% initial viability unit. Data were analyzed for variances, and 2-tailed Student's t tests were performed. Data are presented as mean ± SEM.

2.4.4 Human and Murine Diabetic Wounds Display Increased IL-17A Signaling, JMJD3, and Expression of Anti-Migratory / Inflammatory Genes in Wound Keratinocytes

Recent studies have identified that IL-17A is increased in diabetes (57, 115, 120-122, 170), hence, we analyzed our human bulk RNA-Seq dataset isolated from T2D and non-T2D patients for IL-17A signaling (69, 130, 171). We identified that there is increased IL-17A signaling in human T2D wounds compared to non-T2D controls (Figure 2-7A). Since these samples are not cell-specific and IL-17A signaling could be increased in many wound cell types, we sought to specifically examine diabetic wound keratinocytes for IL-17A signaling. Using a well-established murine model of T2D, *db/db* mice, which lack a functional leptin receptor (172), we wounded mice and isolated keratinocytes on day 5 as previously described (133) and performed bulk RNA-Seq. Analysis of bulk RNA-Seq of diabetic wound keratinocytes demonstrated increased

expression of IL-17A-induced genes in the diabetic wound keratinocytes compared to littermate controls (Figure 2-7B). To obtain kinetic and spatial data of IL-17A expression in diabetic wounds, we performed immunofluorescence (IF) staining for IL-17A, H3K27me3, and Keratin 14 in control and diabetic wounds collected at multiple timepoints (days 1, 3, 7) post-wounding (Figures 2-8A, B). We utilized a second model of diabetes, diet-induced obesity (DIO) mice, that were generated by feeding mice with a high fat diet (HFD) for 12 – 16 weeks to simulate a "prediabetic" state that is physiologically similar to humans (173). Mice were subjected to 6 mm punch biopsy wounds and collected at days 1, 3, and 7 post-wounding for histology, as we have previously described (7). We found that DIO wounds displayed elevated IL-17A at days 1, 3, 7 while control wounds only displayed elevated IL-17A at day 1. We observed that IL-17A was highly localized near the wound edge close to the epidermis.

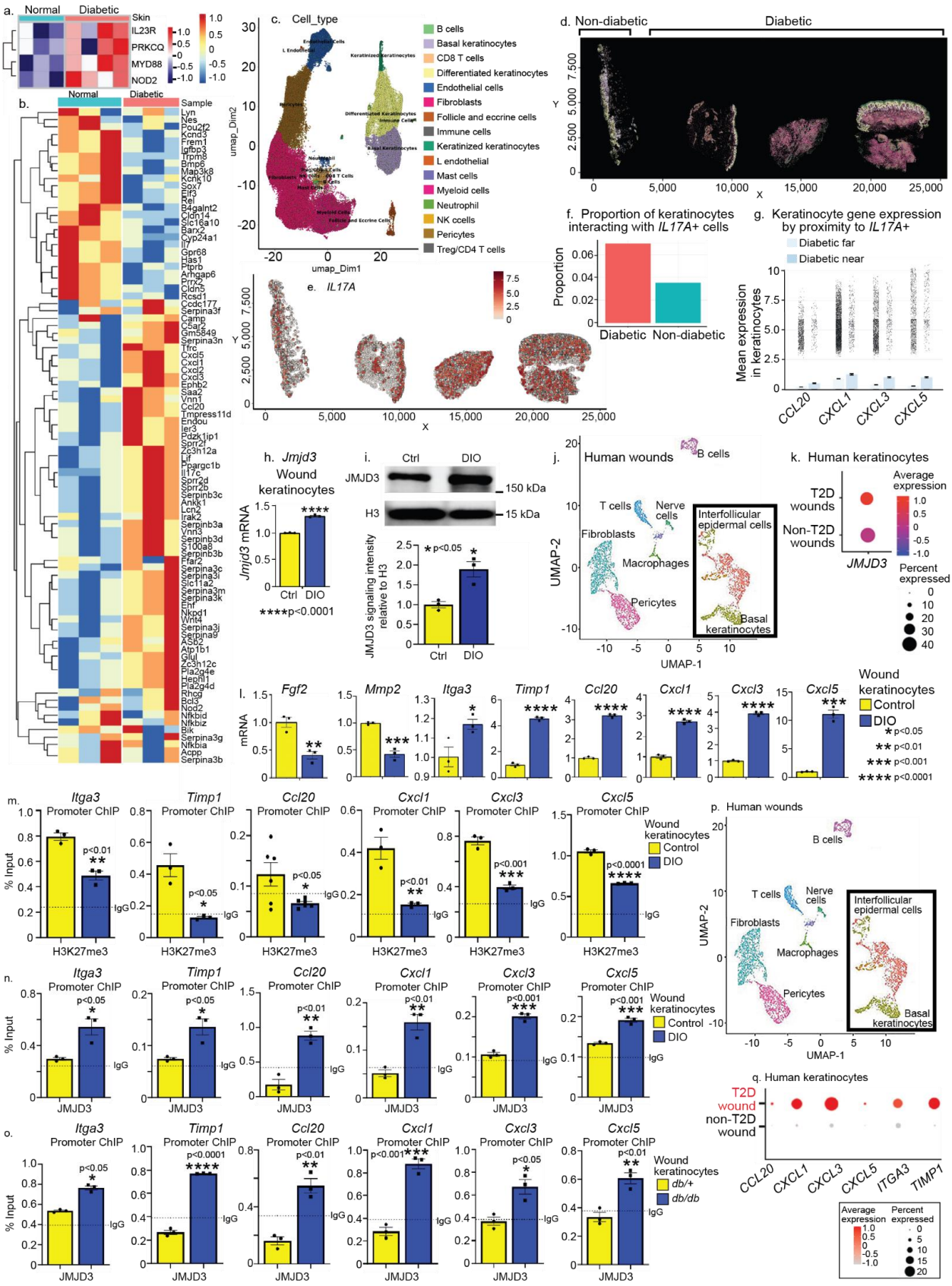

a.
Normal
Diabetic
Skin
IL23R
PRKCQ
MYD88
NOD2
b.
Sample
c. Cell_type
B cells
Basal keratinocytes
CD8 T cells
Differentiated keratinocytes
Endothelial cells
Fibroblasts
Follicle and eccrine cells
Immune cells
Keratinized keratinocytes
L endothelial
Mast cells
Myeloid cells
Neutrophil
NK ccells
Pericytes
Treg/CD4 T cells
umap_Dim1
umap_Dim2
d. Non-diabetic
Diabetic
e. IL17A
f. Proportion of keratinocytes interacting with IL17A+ cells
Proportion
Diabetic
Non-diabetic
g. Keratinocyte gene expression by proximity to IL17A+
Diabetic far
Diabetic near
Mean expression in keratinocytes
CCL20
CXCL1
CXCL3
CXCL5
h. Jmjd3
Wound keratinocytes
Jmjd3 mRNA
Ctrl
DIO
****p<0.0001
i.
JMJD3
H3
150 kDa
15 kDa
JMJD3 signaling intensity relative to H3
*p<0.05
j.
Human wounds
B cells
T cells
Nerve cells
Fibroblasts
Macrophages
Pericytes
Interfollicular epidermal cells
Basal keratinocytes
UMAP-1
UMAP-2
k. Human keratinocytes
T2D wounds
Non-T2D wounds
JMJD3
Average expression
Percent expressed
l.
Fgf2
Mmp2
Itga3
Timp1
Ccl20
Cxcl1
Cxcl3
Cxcl5
mRNA
Wound keratinocytes
Control
DIO
*p<0.05
**p<0.01
***p<0.001
****p<0.0001
m.
Promoter ChIP
% Input
IgG
H3K27me3
n.
JMJD3
o.
db/+
db/db
p. Human wounds
q. Human keratinocytes
T2D wound
non-T2D wound
ITGA3
TIMP1

Figure 2-7: Human and murine diabetic wounds display increased IL-17A signaling, JMJD3, and expression of anti-migratory / inflammatory genes in wound keratinocytes

(A) Human bulk RNA-seq heatmap of IL-17A pathway genes in T2D ($N = 4$) vs. non-T2D ($N = 3$) wounds. (B) Bulk RNA-seq heatmap of IL-17A-induced genes in keratinocytes from *db/db* ($n = 3$) vs. *db/+* wounds ($n = 3$). (C–E) Spatial scRNA-seq of T2D ($N = 3$) and control ($N = 1$) wounds: UMAP clustering (C), lineage annotation (D), and IL-17A expression (E). (F-G) Proximity analysis of keratinocytes near IL-17A$^+$ cells in T2D (pink) vs. non-T2D (teal) wounds, with differential expression of *CCL20, CXCL1, CXCL3, CXCL5* in keratinocytes near (light blue) vs. far (dark blue) from IL-17A$^+$ cells in T2D wounds (G). $n = 21734$ (diabetic far), $n = 1629$ (diabetic near) cells. (H-I) *Jmjd3* mRNA ($n = 3$ technical replicates, $p < 0.0001$, $n = 3$ independent experiments) (H) and JMJD3 protein ($n = 3$ technical replicates, $p = 0.0127$, $n = 3$ independent experiments) (I) in keratinocytes from control (yellow) vs DIO (blue) wounds. (J-K) scRNA-seq of T2D ($N = 10$) and control ($N = 10$) wounds: UMAP clustering (J) and *JMJD3* expression in keratinocyte subsets (K). (L) qPCR analysis of migration-related and inflammatory gene expression in keratinocytes from control (yellow) vs. DIO (blue) wounds. $n = 3$ technical replicates, *Fgf2*: $p = 0.0059$, *Mmp2*: $p = 0.0008$, *Itga3*: $p = 0.0430$, *Timp1*: $p < 0.0001$, *Ccl20*: $p < 0.0001$, *Cxcl1*: $p < 0.0001$, *Cxcl3*: $p < 0.0001$, *Cxcl5*: $p = 0.0002$. $n = 3$ independent experiments. (M) ChIP for H3K27me3 at indicated promoters in keratinocytes from control (yellow) vs. DIO (blue) wounds. *Itga3*: $n = 3$ technical replicates, $p = 0.0027$, *Timp1*: $n = 3$ technical replicates, $p = 0.0104$, *Ccl20*: $n = 6$ technical replicates, $p = 0.0347$, *Cxcl1*: $n = 3$ technical replicates, $p = 0.0072$, *Cxcl3*: $n = 3$ technical replicates, $p = 0.0005$, *Cxcl5*: $n = 3$ technical replicates, $p < 0.0001$. $n = 3$ independent experiments. (N) ChIP for JMJD3 at indicated promoters in keratinocytes from control (yellow) vs. DIO (blue) wounds. $n = 3$ technical replicates. *Itga3*: $p = 0.0170$, *Timp1*: $p = 0.0350$, *Ccl20*: $p = 0.0021$, *Cxcl1*: $p = 0.0037$, *Cxcl3*: $p = 0.0003$, *Cxcl5*: $p = 0.0005$. $n = 3$ independent experiments. (O) ChIP for JMJD3 at indicated promoters in keratinocytes from *db/+* (yellow) vs. *db/db* (blue) wounds. $n = 3$ technical replicates. *Itga3*: $p = 0.0407$, *Timp1*: $p < 0.0001$, *Ccl20*: $p = 0.0026$, *Cxcl1*: $p = 0.0004$, *Cxcl3*: $p = 0.0143$, *Cxcl5*: $p = 0.0060$. $n = 3$ independent experiments. (P–Q) scRNA-seq of T2D vs control wounds showing keratinocyte subsets (P) and expression of indicated genes (Q). Data were analyzed for variances, and 2-tailed Student's *t* tests for (H-I), (L-O) were performed. Data are presented as the mean ± SEM.

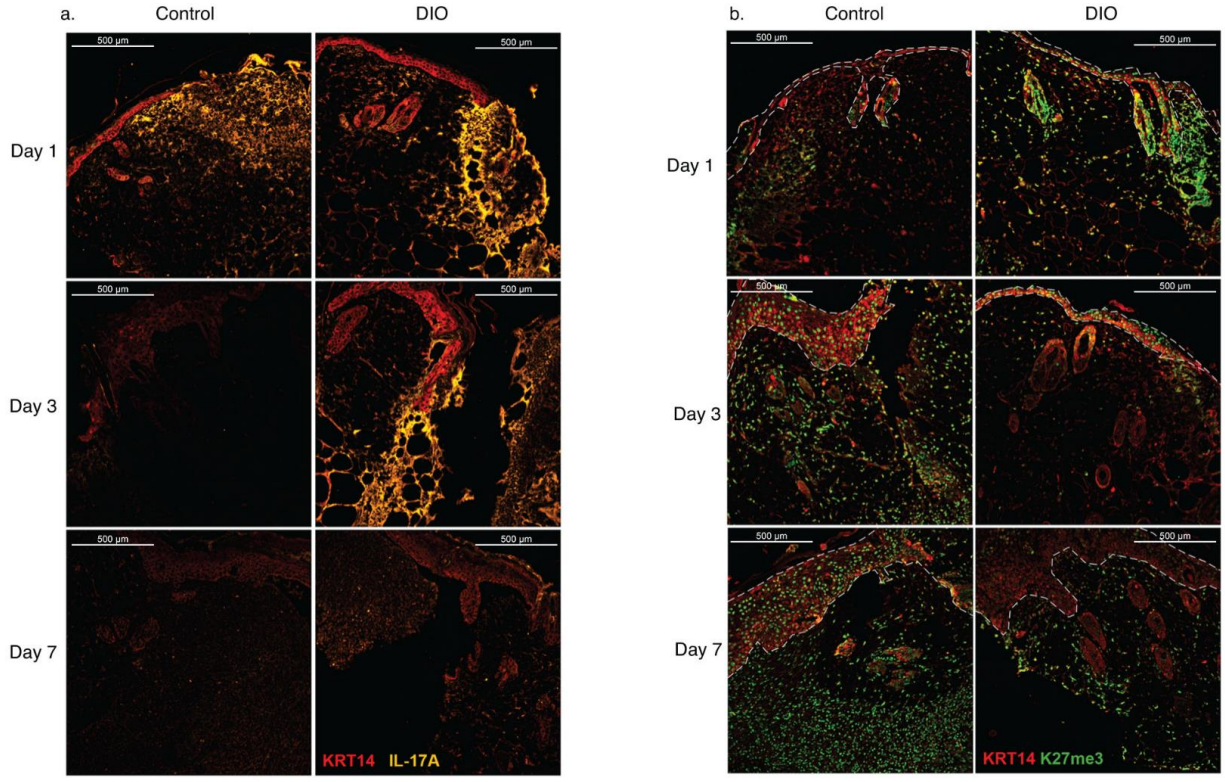


Figure 2-8: Spatial and kinetic data of IL-17A and K27me3 display increasing IL-17A and decreasing K27me3 levels in diabetic wounds throughout the course of wound healing

(A) Immunofluorescence imaging of IL-17A (yellow) and Keratin 14 (red)-stained wounds from control (n = 2 mice/timepoint) and DIO (n = 2 mice/timepoint) mice. (B) Immunofluorescence imaging of K27me3 (green) and Keratin 14 (red)-stained wounds from control (n = 2 mice/timepoint) and DIO (n = 2 mice/timepoint) mice. White dotted lines indicate the epidermal layer of the wound edge.

To identify potential sources of IL-17A in diabetic wounds, we analyzed our spatial RNA-seq dataset of wounds from T2D and non-T2D patients (Figure 2-7C). Cell clusters were annotated using lineage-specific markers to visualize the organization of distinct cell types (Figure 2-7D). We observed an increased number of IL-17A-expressing cells adjacent to keratinocytes in diabetic wounds (Figure 2-7E). Proximity-based interaction analysis further revealed a higher proportion of keratinocytes interacting with IL-17A-expressing cells in the diabetic setting (Figure 2-7F). In non-diabetic wounds, IL-17A-expressing cells were mainly restricted to the epidermis, whereas in diabetic wounds, they were more abundant and dispersed throughout the wound bed. To characterize the cellular sources of IL-17A, we subclustered IL-17A-expressing cells based on lineage markers and identified myeloid cells, $CD8^+$ T cells, neutrophils, NK cells, and $CD4^+$ T cells as the predominant producers (Figures 2-9A-C). Additionally, we found that keratinocytes located near IL-17A-expressing cells expressed higher levels of *CCL20, CXCL1*, *CXCL3*, and *CXCL5* (Figure 2-7G), suggesting a localized inflammatory response driven by IL-17A in diabetic wounds. Specifically, given that diabetic wound keratinocytes near $IL\text{-}17A^+$ cells exhibit increased expression of myeloid chemoattractants (*CXCL1, CXCL3,* and *CXCL5*) (Figure 2-7G), we used our spatial RNA-seq to classify immune cell types adjacent to keratinocytes in diabetic and non-diabetic wounds. Proximity analysis revealed a higher frequency of keratinocyte interactions with myeloid cells and neutrophils in diabetic wounds (Figures 2-9D, E), suggesting that keratinocyte-derived chemokines contribute to increased immune cell recruitment.

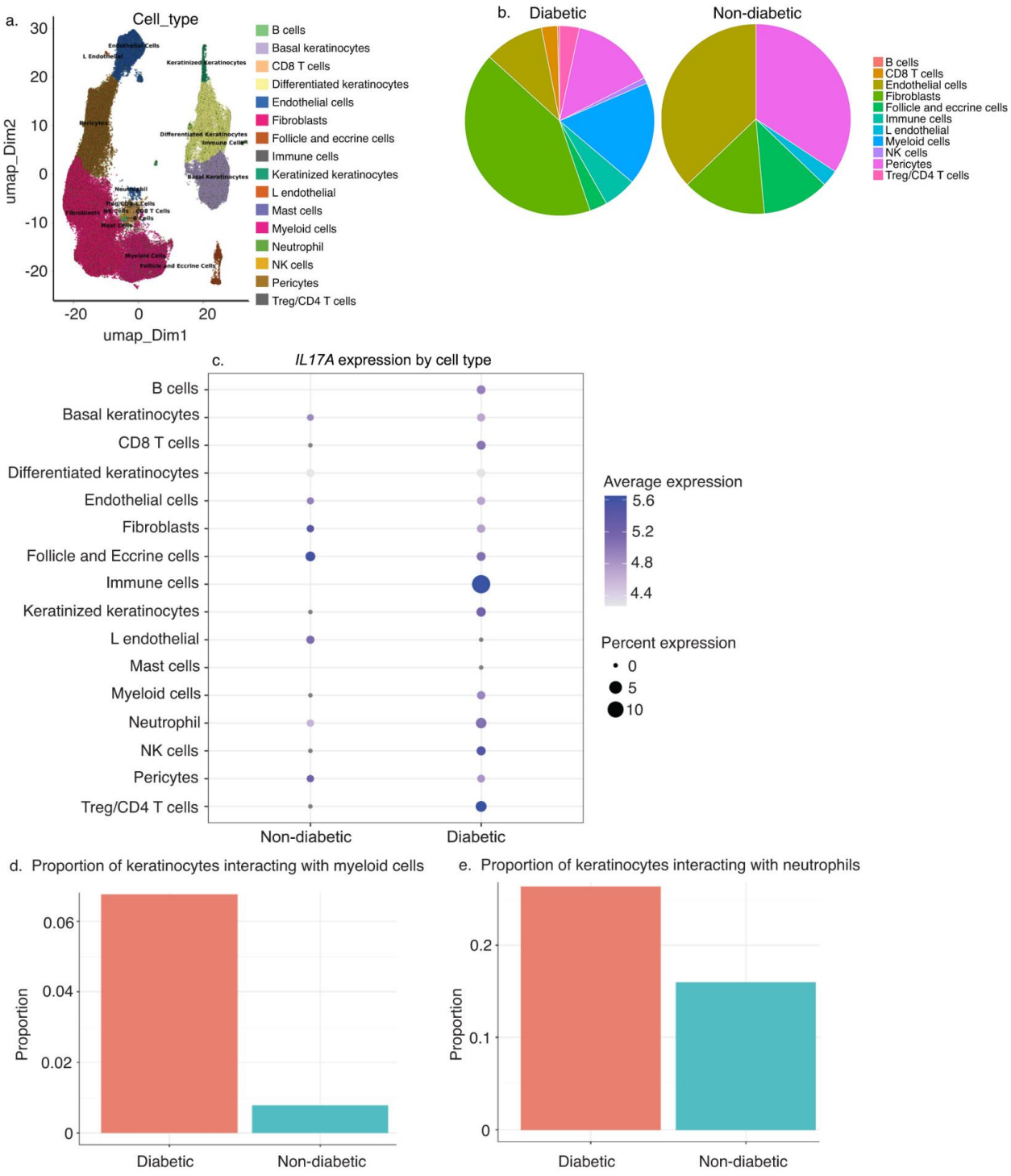


Figure 2-9: Spatial single cell RNA-sequencing analysis of keratinocyte-immune cell interactions in human diabetic wounds

(A) UMAP visualization of spatial scRNA-seq data of T2D (N = 3) and nondiabetic wound (N = 1) samples. (B) Composition of IL-17A-expressing cell types in diabetic and nondiabetic wounds. (C) Dot plot of IL-17A expression level by cell type. Dot size indicates proportion of cells within the group expressing *Il17a*, color indicates expression level. (D) Proximity-based interaction analysis of keratinocyte-myeloid cell interactions. (E) Proximity-based interaction analysis of keratinocyte-neutrophil interactions.

Since IL-17A is increased in diabetic wounds, and IL-17A signaling is increased in diabetic keratinocytes, we examined whether *Jmjd3* is elevated in diabetic murine wound keratinocytes. Mice were subjected to 6 mm punch biopsy wounds and wound keratinocytes were collected from control and DIO mice as we have previously described (21) on day 5, a timepoint when IL-17A production is significantly increased in mice (115). We observed increased expression of JMJD3 mRNA and protein in murine diabetic wound keratinocytes compared to their nondiabetic controls (Figure 2-7H, I), suggesting a link between elevated IL-17A levels in the diabetic wound environment and increased *Jmjd3* expression in keratinocytes. To assess the spatial and temporal dynamics of JMJD3 activity in relation to IL-17A expression during wound healing, we examined our IF staining of H3K27me3 and Keratin 14 in control and DIO wounds at days 1, 3, and 7 post-wounding. Due to JMJD3's nuclear localization, low abundance, and the lack of a reliable antibody, direct detection via immunohistochemistry or IF remains challenging. Instead, we used H3K27me3 as an indirect readout of JMJD3 activity. We observed increased colocalization of H3K27me3 with keratinocytes in control wounds at days 3 and 7, while DIO wounds showed decreased H3K27me3 signal in keratinocytes at day 7 (Figure 2-8B). These findings suggest enhanced H3K27 demethylation—and thus increased JMJD3 activity—in diabetic keratinocytes at later stages. Notably, this increase in JMJD3 activity coincides with increased IL-17A protein expression near keratinocytes (Figure 2-8A), supporting a mechanistic link between IL-17A signaling and JMJD3 activation.

In order to determine the translational relevance and keratinocyte-specificity of JMJD3 expression, we analyzed our scRNA-Seq dataset on wounds from T2D patients and non-T2D controls (21, 69, 76, 171). Cluster analysis was performed using uniform manifold approximation and projection (UMAP) as previously described (131); 10 cell clusters were identified in wounds

following injury. We identified 3 clusters of keratinocytes, including keratinized, differentiated, and basal keratinocytes (Figure 2-7J). We identified that *JMJD3* expression is increased in human T2D wound keratinocytes compared to non-T2D controls (Figure 2-7K).

Next, to confirm that downstream JMJD3 target genes are altered in diabetic wound keratinocytes, we collected wound keratinocytes from control and DIO mice and examined for anti-migratory and inflammatory genes. We found that expression of pro-migratory genes fibroblast growth factor 2 (*Fgf2*) and MMP-2 (*Mmp2*) was decreased, while expression of anti-migratory genes integrin alpha 3 (*Itga3*) and TIMP-1 (*Timp1*) was increased in diabetic wound keratinocytes (Figure 2-7L). Additionally, we found that expression of inflammatory genes (*Ccl20, Cxcl1, Cxcl3,* and *Cxcl5*) was increased in murine diabetic wound keratinocytes compared to controls (Figure 2-7L). We further confirmed increased expression of JMJD3-mediated anti-migratory (Integrin α3, TIMP-1) and inflammatory (CCL-20, CXCL-1, CXCL-3, CXCL-5) target genes in DIO wounds at the protein level via western blot or ELISA (Figures 2-10A-F).

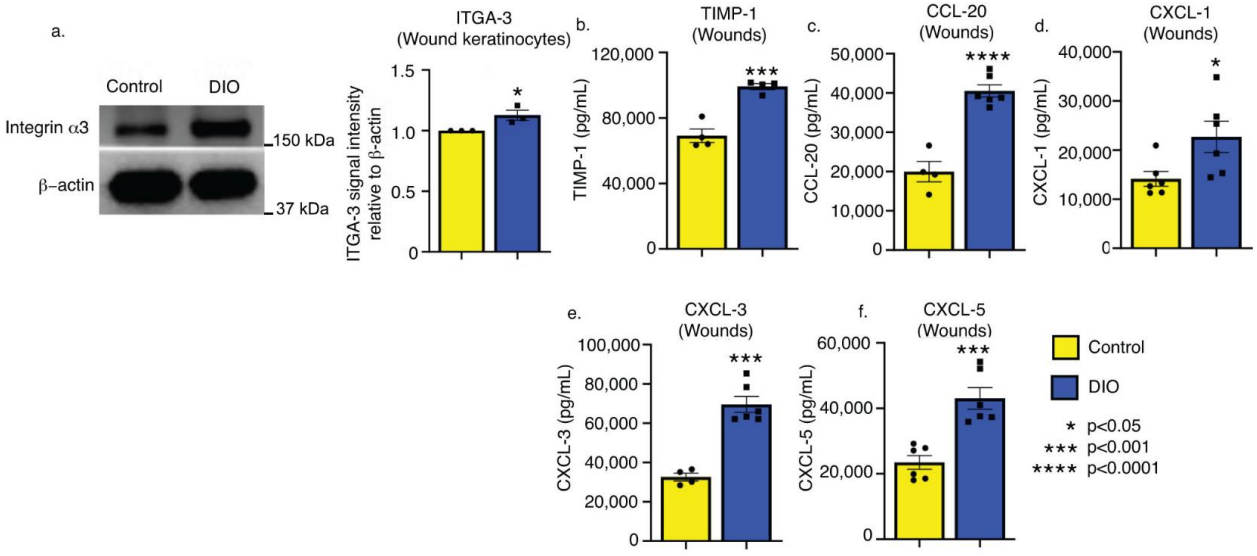


Figure 2-10: Expression of JMJD3-mediated target genes is increased at the protein level in diabetic wounds (A) Western blot of ITGA-3 in control (yellow) and DIO (blue) keratinocytes. $n = 3$ technical replicates, $p = 0.0378$. $n = 2$ independent experiments. Representative densitometry plot shown. (B-F) Protein quantification of lysates from control (yellow) and DIO (blue) wounds. TIMP-1: $n = 4$ biological replicates, $p = 0.0005$, CCL-20: $n = 4$ (control), $n = 6$ biological replicates (DIO), $p < 0.0001$, CXCL-1: $n = 6$ biological replicates, $p = 0.0357$, CXCL-3: $n = 4$ (control),

n = 6 biological replicates (DIO), p = 0.0001, CXCL-5: n = 6 biological replicates, p = 0.0005. n = 2 independent experiments. Data were analyzed for variances, and 2-tailed Student's t tests were performed. Data are presented as mean ± SEM.

To confirm that JMJD3 directly mediates H3K27me3 demethylase activity on anti-migratory and inflammatory gene promoters in diabetic wound keratinocytes, we performed ChIP studies analyzing K27 trimethylation and JMJD3 occupancy in wound keratinocytes isolated from DIO and *db/db* mice. K27me3 deposition on anti-migratory (*Itga3, Timp1*) and inflammatory (*Ccl20, Cxcl1, Cxcl3, Cxcl5*) gene promoters was significantly decreased in DIO wound keratinocytes compared to controls (Figure 2-7M). Additionally, we observed a significant increase in JMJD3 binding to these promoters in both DIO and *db/db* keratinocytes, further providing direct evidence for JMJD3-mediated K27me3 demethylation in diabetic wound keratinocytes (Figures 2-7N, O). As a translational corollary to our murine data, using our scRNA-Seq dataset, we identified that expression of anti-migratory genes *ITGA3* and *TIMP1* and inflammatory genes *CCL20, CXCL1, CXCL3,* and *CXCL5* was all increased in human T2D basal keratinocytes compared to their non-T2D controls (Figures 2-7P, Q). Altogether, these data suggest that increased IL-17A signaling in human and murine diabetic wounds drives the upregulation of JMJD3 and regulates downstream anti-migratory and inflammatory genes in diabetic wound keratinocytes, providing a potential mechanism for impaired wound repair in diabetic wounds.

2.4.5 Disruption of the IL-17A/JMJD3 Cascade in Diabetic Wound Keratinocytes Improves Wound Repair via Decreased Expression of Anti-Migratory / Inflammatory Genes

Since JMJD3 appears to be playing a pathologic role in diabetic keratinocytes, we first examined if pharmacological modulation of JMJD3 *in vivo* would result in improved healing in diabetes. We first utilized the genetic T2D murine model, *db/db* mice, created 6 mm punch biopsy

wounds, and administered daily injections of GSK-J4 (1 mg/kg) or vehicle only (DMSO) as we have previously described (131). We found that there is increased wound healing in *db/db* mice treated with local wound GSK-J4 injections at later timepoints, days 8 and 9, compared to their vehicle only controls (Figure 2-11). Representative images on day 9 are shown.

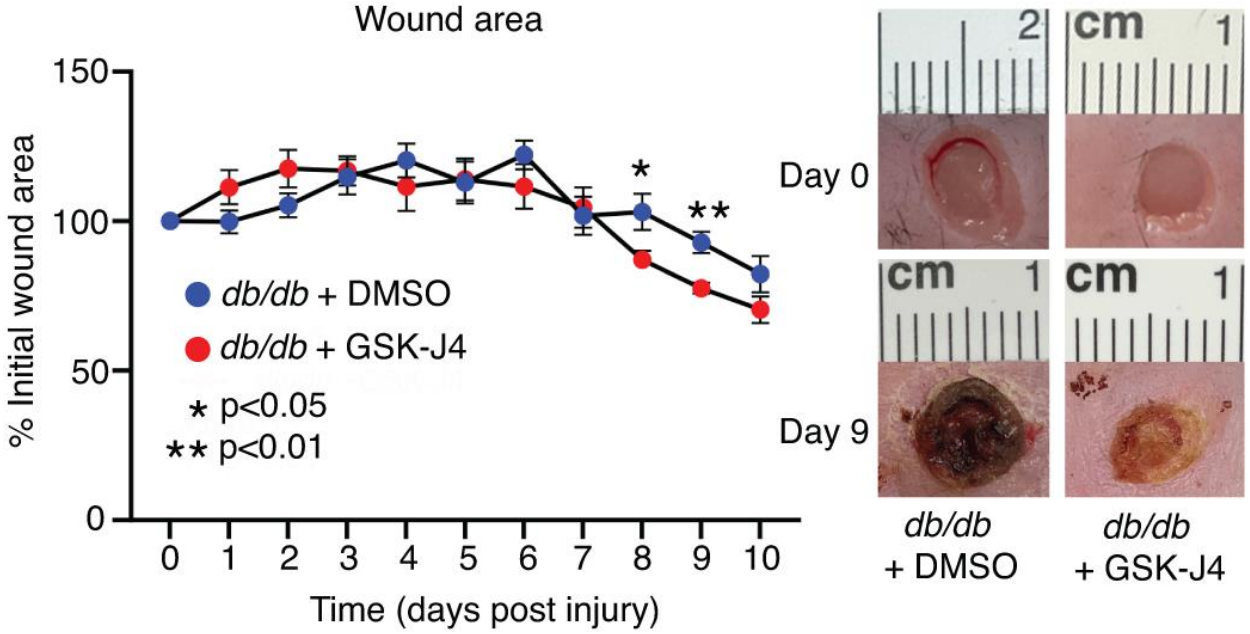


Figure 2-11: Pharmacological modulation of JMJD3 *in vivo* in diabetic murine model (*db/db*) results in improved wound healing

Wound closure in diabetic (*db/db*) mice subjected to daily subcutaneous GSK-J4 (1 mg/kg) (red) or vehicle only (DMSO) (blue) injections near the wound edge. $n = 6$ mice/group. Day 8: $p = 0.0378$, day 9: $p = 0.0036$. Data were analyzed for variances, and 2-tailed Student's t tests were performed. Data are presented as mean ± SEM.

To cell-specifically examine the effects of manipulating the IL-17A/JMJD3 axis in keratinocytes on wound healing, we utilized our mice with keratinocyte-specific IL-17A signaling deficiency (*Il17ra*$^{fl/fl}$ *K14*$^{cre+}$). We first determined whether these effects were specific to the diabetic context by analyzing wound healing in non-diabetic *Il17ra*$^{fl/fl}$ *K14*$^{cre+}$. Mice were subjected to 6 mm punch biopsy wound, and following injury, wound closure was monitored daily using NIH ImageJ software, and the epithelial gap was measured by histology, as we have previously described (7, 8, 12, 25, 46, 54). *Il17ra*$^{fl/fl}$ *K14*$^{cre+}$ mice did not show a significant

improvement in wound closure compared to their littermate controls (*Il17ra*$^{fl/fl}$ *K14*$^{cre-}$) (Figure 2-12).

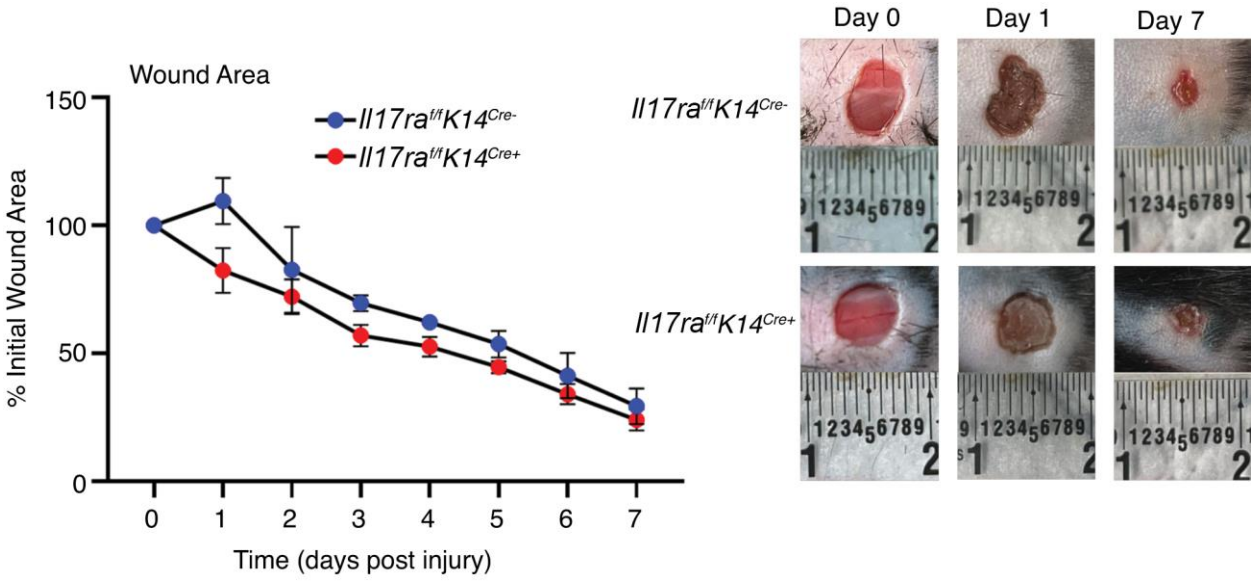


Figure 2-12: Keratinocyte-specific IL-17A signaling deficiency (*Il17ra*$^{fl/fl}$ *K14*$^{cre+}$) does not result in improved healing in the non-diabetic setting

Wound closure in non-diabetic *Il17ra*$^{fl/fl}$ *K14*$^{cre+}$ mice (red) (n = 5 mice) and their littermate controls (*Il17ra*$^{fl/fl}$ *K14*$^{cre-}$) (blue) (n = 4 mice). Data were analyzed for variances, and 2-tailed Student's t tests were performed. Data are presented as mean ± SEM.

Next, we examined if a reduction of IL-17A signaling in diabetic keratinocytes would result in decreased JMJD3 and improved healing in diabetes using the same model (*Il17ra*$^{fl/fl}$ *K14*$^{cre+}$) and inducing diabetes. *Il17ra*$^{fl/fl}$ *K14*$^{cre+}$ mice were fed a high fat diet (HFD) for 12 – 16 weeks to create a diet-induced obesity (DIO) model (57). Oral glucose tolerance test (OGTT) studies confirmed glucose intolerance in these mice. DIO *Il17ra*$^{fl/fl}$ *K14*$^{cre+}$ mice demonstrated improved wound closure rates compared to their littermate controls (DIO *Il17ra*$^{fl/fl}$ *K14*$^{cre-}$) (Figure 2-13A). Representative images from day 7 are shown. These findings indicate that excessive IL-17A signaling in diabetes, rather than IL-17A signaling under homeostatic conditions, drives impaired healing.

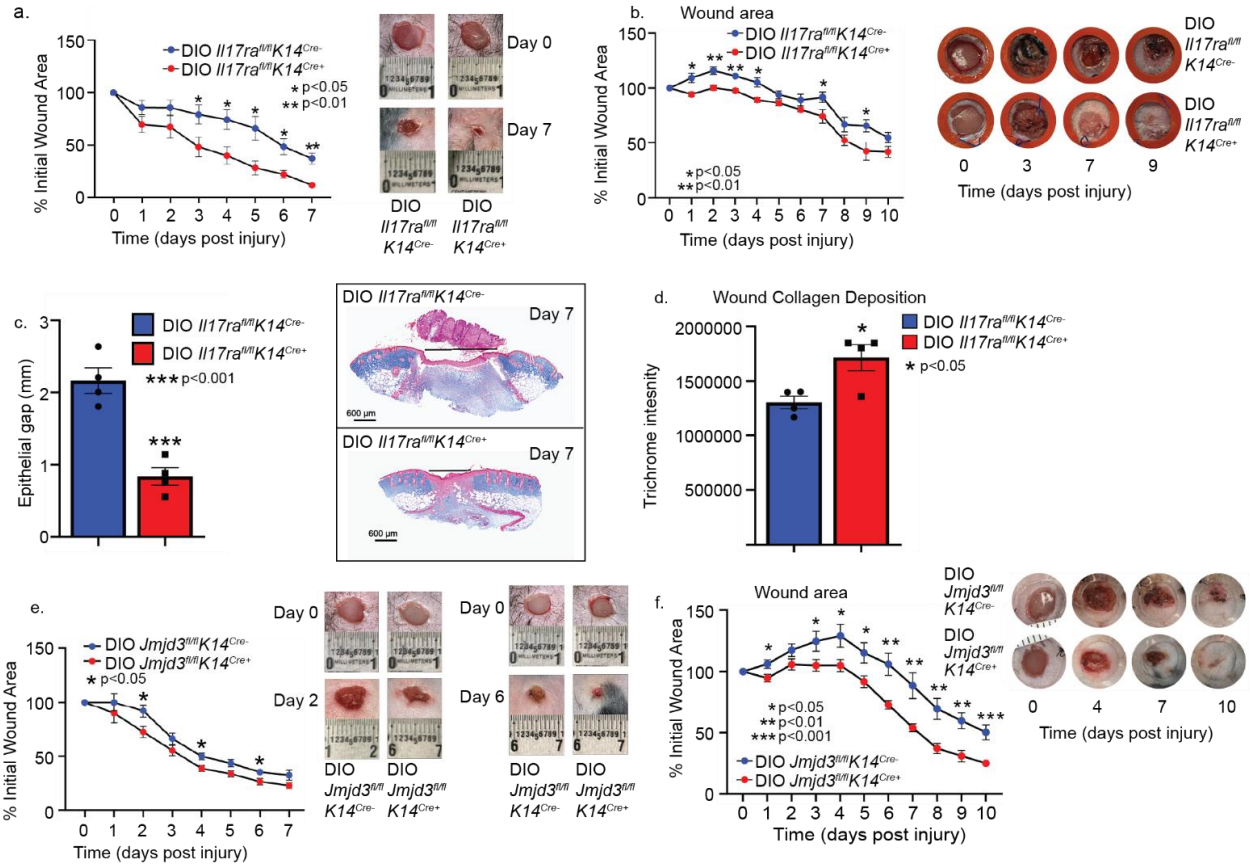

a.
% Initial Wound Area
DIO Il17ra^fl/fl K14^Cre-
DIO Il17ra^fl/fl K14^Cre+
* p<0.05
** p<0.01
Time (days post injury)
Day 0
Day 7
b.
Wound area
Time (days post injury)
0 3 7 9
c.
Epithelial gap (mm)
*** p<0.001
600 µm
d.
Wound Collagen Deposition
Trichrome intesnity
* p<0.05
e.
DIO Jmjd3^fl/fl K14^Cre-
DIO Jmjd3^fl/fl K14^Cre+
Day 2
Day 6
f.
Wound area
* p<0.05
** p<0.01
*** p<0.001
0 4 7 10
g.
Epithelial gap (mm)
** p<0.01
h.
Wound Collagen Deposition
Trichrome intensity
i.
Itga3 (Wound keratinocytes)
Timp1 (Wound keratinocytes)
Ccl20 (Wound keratinocytes)
Itga3 mRNA
Timp1 mRNA
Ccl20 mRNA
**** p<0.0001
Cxcl1 (Wound keratinocytes)
Cxcl3 (Wound keratinocytes)
Cxcl5 (Wound keratinocytes)
Cxcl1 mRNA
Cxcl3 mRNA
Cxcl5 mRNA

Figure 2-13: Disruption of the IL-17A/JMJD3 cascade in diabetic wound keratinocytes improves wound repair via decreased expression of anti-migratory / inflammatory genes

(A) Non-splinted wound closure in DIO *Il17ra*$^{fl/fl}$ *K14*$^{cre+}$ (red) (n = 4 mice) and littermate controls (blue) (n = 6 mice). Day 3: p = 0.0497, day 4: p = 0.0336, day 5: p = 0.0358, day 6: p = 0.0276, day 7: p = 0.0056. n = 2 independent experiments. (B) Splinted wound closure in DIO *Il17ra*$^{fl/fl}$ *K14*$^{cre+}$ (red) (n = 6 mice) and littermate controls (blue) (n = 9 mice). Day 1: p = 0.0155, day 2: p = 0.0048, day 3: p = 0.0042, day 4: p = 0.0118, day 7: p = 0.0422, day 9: p = 0.0295. (C-D) Day 7 wound diameter (C) and trichrome staining for collagen deposition (D). DIO *Il17ra*$^{fl/fl}$ *K14*$^{cre+}$ (red) (n = 4 mice) and littermate controls (blue) (n = 4 mice). Epithelial gap: p =0.0008, collagen: p = 0.0211. (E) Non-splinted wound closure in DIO *Jmjd3*$^{fl/fl}$ *K14*$^{cre+}$ (red) (n = 5 mice) and littermate controls (blue) (n = 5 mice). Day 2: p = 0.0336, day 4: p = 0.0267, day 6: p = 0.0419. n = 2 independent experiments. (F) Splinted wound closure in DIO *Jmjd3*$^{fl/fl}$ *K14*$^{cre+}$ (red) (n = 10 mice) and littermate controls (blue) (n = 8 mice). Day 1: p = 0.0225, day 3: p = 0.0431, day 4: p = 0.0272, day 5: p = 0.0202, day 6: p = 0.0019, day 7: p = 0.0031, day 8: p = 0.0023, day 9: p = 0.0020, day 10: p = 0.0007. (G-H) Day 6 wound diameter (G) and trichrome staining for collagen deposition (H). DIO *Jmjd3*$^{fl/fl}$ *K14*$^{cre+}$ (red) (n = 4 mice) and littermate controls (blue) (n = 4 mice). Epithelial gap: p =0.0031, collagen: p = 0.0257. (I) qPCR of anti-migratory and inflammatory genes in wound keratinocytes from *Jmjd3*$^{fl/fl}$ *K14*$^{cre+}$ (red) (n = 3 technical replicates) vs. littermate controls (blue) (n = 3 technical replicates). *Itga3*: p = 0.0004, *Timp1*: p = 0.0010, *Ccl20*: p < 0.0001, *Cxcl1*: p < 0.0001, *Cxcl3*: p < 0.0001, *Cxcl5*: p = 0.0233. n = 2 independent experiments. Data were analyzed for variances, and 2-tailed Student's t tests for (A-I) were performed. Data are presented as the mean ± SEM.

To further evaluate the contribution of wound contraction in this acute (non-splinted) healing model, we performed histomorphometric analyses of wounds from DIO *Il17ra*$^{fl/fl}$ *K14*$^{cre+}$ mice. To assess the involvement of myofibroblasts, the key mediators of contraction, we stained wound sections for alpha smooth muscle actin (αSMA). DIO *Il17ra*$^{fl/fl}$ *K14*$^{cre+}$ mice exhibited minimal improvement in re-epithelialization (Figure 2-14A) but significantly greater wound contraction (Figures 2-14B, C) and earlier αSMA^{+} myofibroblast transition (Figures 2-14D, E) compared to controls (DIO *Il17ra*$^{fl/fl}$ *K14*$^{cre-}$).

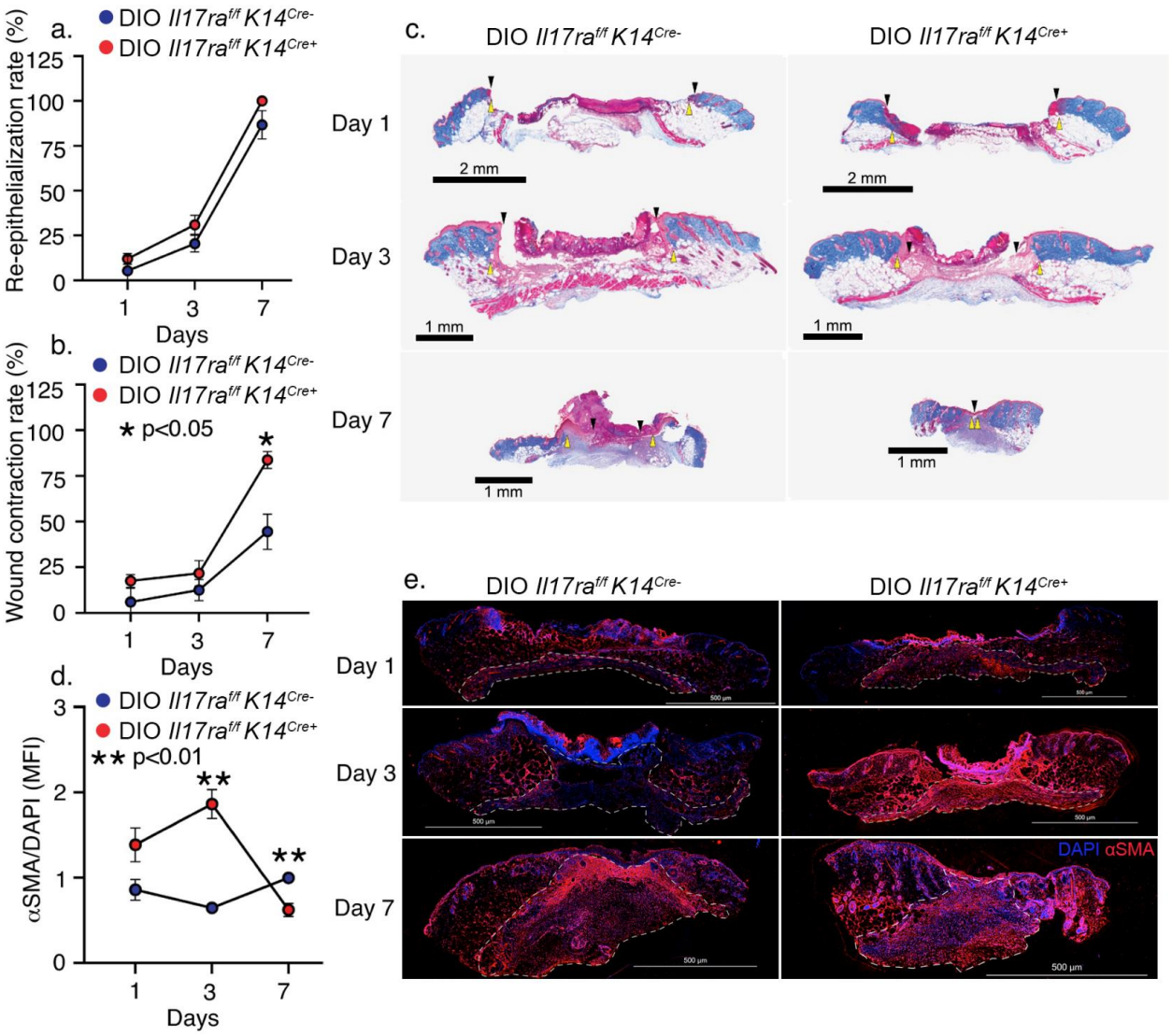


Figure 2-14: Histomorphometric analysis of wound contraction and myofibroblast transition in DIO *Il17ra*$^{fl/fl}$ *K14*$^{cre+}$ mice

(A) Re-epithelialization rate of DIO *Il17ra*$^{fl/fl}$ *K14*$^{cre+}$ mice (red) and littermate control (DIO *Il17ra*$^{fl/fl}$ *K14*$^{cre-}$) (blue) wounds. DIO *Il17ra*$^{fl/fl}$ *K14*$^{cre-}$: $n = 3$ mice (day 1), $n = 4$ mice (day 3), $n = 4$ mice (day 7). DIO *Il17ra*$^{fl/fl}$ *K14*$^{cre+}$: $n = 2$ mice (day 1), $n = 3$ mice (day 3), $n = 4$ mice (day 7). (B) Wound contraction rate of DIO *Il17ra*$^{fl/fl}$ *K14*$^{cre+}$ mice (red) and littermate control (DIO *Il17ra*$^{fl/fl}$ *K14*$^{cre-}$) (blue) wounds. DIO *Il17ra*$^{fl/fl}$ *K14*$^{cre-}$: $n = 3$ mice (day 1), $n = 4$ mice (day 3), $n = 4$ mice (day 7). DIO *Il17ra*$^{fl/fl}$ *K14*$^{cre+}$: $n = 2$ mice (day 1), $n = 3$ mice (day 3), $n = 4$ mice (day 7). Day 7: $p = 0.0103$. (C) Representative trichrome stained images with arrows marking epithelial tongue edges (black) and intact dermis edges (yellow). (D) αSMA / DAPI ratios of DIO *Il17ra*$^{fl/fl}$ *K14*$^{cre+}$ mice (red) and littermate control (DIO *Il17ra*$^{fl/fl}$ *K14*$^{cre-}$) (blue) wounds. DIO *Il17ra*$^{fl/fl}$ *K14*$^{cre-}$: $n = 3$ mice (day 1), $n = 3$ mice (day 3), $n = 3$ mice (day 7). DIO *Il17ra*$^{fl/fl}$ *K14*$^{cre+}$: $n = 2$ mice (day 1), $n = 3$ mice (day 3), $n = 3$ mice (day 7). Day 3: $p = 0.0021$, day 7: $p = 0.0096$. (E) Representative αSMA (red) and DAPI (blue) stained immunofluorescence images. Data were analyzed for variances, and 2-tailed Student's *t* tests were performed. Data are presented as mean ± SEM.

To specifically assess re-epithelialization independent of contraction, we performed a well-established model of chronic (splinted) wound healing of DIO *Il17ra*$^{fl/fl}$ *K14*$^{cre+}$ mice for 10 days as we have previously described (21). The chronic (splinted) wound model also displayed significantly improved wound healing in the IL-17A signaling deficient mice on days 1, 2, 3, 4, 7, 9 (Figure 2-13B). Representative images from days 3, 7, and 9 are shown, and decreased epithelial gap by histology from day 7 are shown (Figure 2-13C). Histologically, DIO *Il17ra*$^{fl/fl}$ *K14*$^{cre+}$ wounds harvested on day 7 post injury also exhibited improved wound healing and increased wound collagen deposition compared to DIO *Il17ra*$^{fl/fl}$ *K14*$^{cre-}$ mice (Figure 2-13D). Further, we performed single cell RNA-sequencing in wounds from keratinocyte-specific IL-17RA-deficient mice (*Il17ra*$^{fl/fl}$ *K14*$^{cre+}$) and wildtype (WT) controls to examine alterations in keratinocyte function and other cell types due to deletion of IL-17A signaling in keratinocytes. We first confirmed that *Jmjd3* expression was decreased in *Il17ra*$^{fl/fl}$ *K14*$^{cre+}$ keratinocytes compared to their controls (Figures 2-15A, B). To further validate that JMJD3 is regulated via an IL-17A pathway in our model, we examined expression of our JMJD3-mediated target genes in wound keratinocytes. Expression of inflammatory target genes *Cxcl3*, *Cxcl1*, and *Ccl20* was decreased in *Il17ra*$^{fl/fl}$ *K14*$^{cre+}$ keratinocytes compared to their controls (Figure 2-15C). Expression of JMJD3-mediated anti-migratory gene *Itga3* was decreased while expression of pro-migratory *Mmp9* that is regulated by *Timp1* was increased in *Il17ra*$^{fl/fl}$ *K14*$^{cre+}$ keratinocytes compared to their controls, suggesting improved migratory gene profile in the keratinocytes lacking IL-17A signaling (Figure 2-15C).

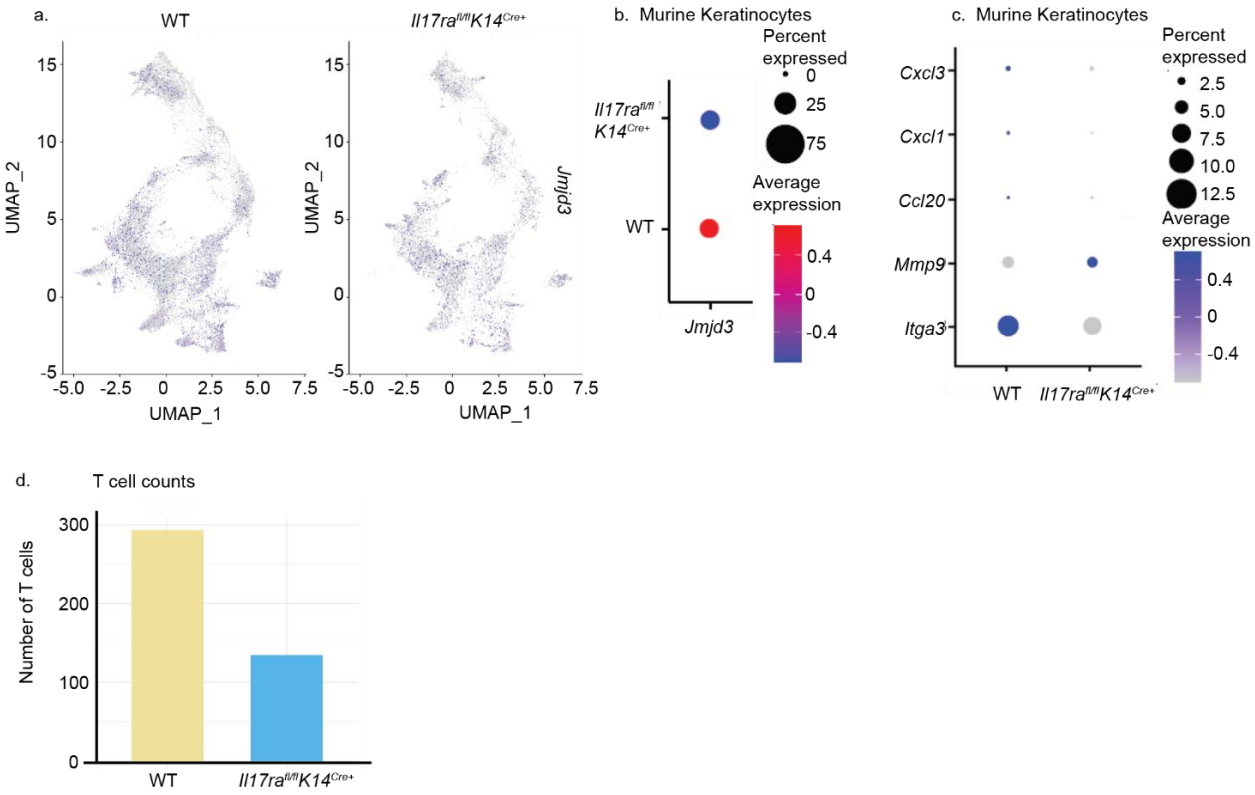


Figure 2-15: Single cell RNA-sequencing of mice with a keratinocyte-specific deletion of IL-17A signaling (*Il17ra*$^{fl/fl}$ *K14*$^{cre+}$) demonstrate decreased anti-migratory and inflammatory gene expression in wound keratinocytes and decreased T cell infiltration

(A) UMAP visualization of scRNA-seq data from wounds *Il17ra*$^{fl/fl}$ *K14*$^{cre+}$ (n = 4 mice) and control (WT) (n = 4) mice showing keratinocytes and *Jmjd3* expression per cell. (B) Dot plot of *Jmjd3* expression within keratinocyte populations. (C) Dot plot of *Cxcl3, Cxcl1, Ccl20, Mmp9, Itga3* expression within keratinocyte populations. (D) T cells identified using lineage specific cell markers; counts quantified in *Il17ra*$^{fl/fl}$ *K14*$^{cre+}$ and WT samples.

Next, we examined whether loss of JMJD3 in diabetic wound keratinocytes improves diabetic wound repair by altering migratory function. We used our murine model with a keratinocyte-specific deletion of JMJD3 (DIO *Jmjd3*$^{fl/fl}$ *K14*$^{cre+}$) and their littermate controls (DIO *Jmjd3*$^{fl/fl}$ *K14*$^{cre-}$), placed them on a HFD for 12 – 16 weeks, confirmed glucose intolerance, and created 6 mm punch biopsy wounds. Following injury, wound closure was monitored daily, and the epithelial gap was measured by histology. DIO *Jmjd3*$^{fl/fl}$ *K14*$^{cre+}$ mice demonstrated significantly improved wound healing compared to their littermate controls on days 2, 4, 6 (Figure 2-13E). Representative images from days 2 and 6 are shown. We performed the chronic (splinted) wound healing model with these mice and observed an identical increase in wound closure rates

on days 1, 3, 4, 5, 6, 7, 8, 9, and 10 (Figure 2-13F). Representative images from days 4, 7, and 10 are shown, and decreased epithelial gap by histology from day 6 are shown (Figure 2-13G). Histologically, DIO *Jmjd3*$^{fl/fl}$ *K14*$^{cre+}$ wounds harvested on day 6 post injury exhibited improved wound healing and increased wound collagen deposition compared to DIO *Jmjd3*$^{fl/fl}$ *K14*$^{cre-}$ (Figure 2-13H). Additionally, we harvested wound keratinocytes from these mice on day 6 and examined anti-migratory and inflammatory gene expression. We found that DIO *Jmjd3*$^{fl/fl}$ *K14*$^{cre+}$ keratinocytes displayed decreased *Itga3, Timp1, Ccl20, Cxcl1, Cxcl3,* and *Cxcl5* (Figure 2-13I), suggesting that *Jmjd3*-deficiency downregulates anti-migratory and inflammatory gene expression in wound keratinocytes and improves diabetic wound repair.

Since keratinocyte crosstalk with other wound-resident cells is essential for coordinated tissue repair, we examined how deletion of IL-17A signaling and JMJD3 in keratinocytes affects other cell populations involved in wound healing. We characterized T cells, specifically T_H17 cells, that are recruited in response to CCL-20 as well as neutrophils that are recruited in response to CXCL-1, CXCL-3, and CXCL-5. Through our scRNA-Seq of *Il17ra*$^{fl/fl}$ *K14*$^{cre+}$ and control wounds, we first confirmed that deletion of IL-17A signaling in keratinocytes leads to decreased overall T cell counts (Figure 2-15D). Next, we performed flow cytometric analysis of wounds from our DIO *Il17ra*$^{fl/fl}$ *K14*$^{cre+}$ and DIO *Jmjd3*$^{fl/fl}$ *K14*$^{cre+}$ mice to analyze T_H17 cell and neutrophil numbers. We observed a decreased percentage of T_H17 cells within the $CD4^+$ T cell population in DIO *Il17ra*$^{fl/fl}$ *K14*$^{cre+}$ and DIO *Jmjd3*$^{fl/fl}$ *K14*$^{cre+}$ wounds and a decreased percentage of $Ly6G^+$ neutrophils within the $CD45^+$ immune cell population (Figures 2-16A-D). We further examined T cell phenotypes by sorting $CD4^+$ T cells ($CD11b^-$, $CD45R^-$, $Ter119^-$, $CD8a^-$, $CD49b^-$, $CD19^-$, $CD11c^-$, $TCRgd^-$, $CD24^-$, $CD4^+$) from *Il17ra*$^{fl/fl}$ *K14*$^{cre+}$ and *Jmjd3*$^{fl/fl}$ *K14*$^{cre+}$ wounds and analyzing expression of inflammatory (*Tnf, Il17a*) and reparative (*Il10*) genes. T cells from both *Il17ra*$^{fl/fl}$

K14^{cre+} and *Jmjd3*$^{fl/fl}$ *K14*$^{cre+}$ displayed decreased *Tnf* and increased *Il10*, potentially suggesting increased reparative T regulatory cell phenotypes (Figures 2-16E, F). Additionally, *Jmjd3*$^{fl/fl}$ *K14*$^{cre+}$ T cells displayed decreased *Il17a* (Figure 2-16F), corresponding with the decreased number of T_H17 cells (Figure 2-16D). Next, to examine macrophage phenotypes in these mice, we sorted macrophages (CD3$^-$, CD19$^-$, Ly6G$^-$, CD11b$^+$) from *Il17ra*$^{fl/fl}$ *K14*$^{cre+}$ and *Jmjd3*$^{fl/fl}$ *K14*$^{cre+}$ wounds and analyzed expression of inflammatory (*Il1b, Il6, Tnf, Nos2*) genes (Figures 2-16G, H). We found that *Il17ra*$^{fl/fl}$ *K14*$^{cre+}$ macrophages expressed decreased inflammatory *Il1b, Tnf, Nos2* expression compared to their littermate (*Il17ra*$^{fl/fl}$ *K14*$^{cre-}$) controls (Figure 2-16G). *Jmjd3*$^{fl/fl}$ *K14*$^{cre+}$ macrophages expressed decreased inflammatory *Il1b, Il6, Tnf, Nos2* expression compared to their littermate (*Jmjd3*$^{fl/fl}$ *K14*$^{cre-}$) controls (Figure 2-16H). Lastly, given the importance of keratinocyte-fibroblast crosstalk in regulating fibroblast functions such as collagen deposition and differentiation into reparative myofibroblasts, we assessed fibroblast function in these mice. Myofibroblasts are essential for wound contraction, and previous work from our group and others has shown that their transition is impaired in diabetic wounds (174). We sorted wound fibroblasts (CD45$^-$, CD31$^-$, EpCAM$^-$, TER119$^-$, Tie2$^-$) from *Il17ra*$^{fl/fl}$ *K14*$^{cre+}$ and *Jmjd3*$^{fl/fl}$ *K14*$^{cre+}$ mice and analyzed expression of collagen production genes (*Col1a1, Cald1)* and myofibroblast genes (*Myl9, Acta*). We found increased *Col1a1* and *Cald1* in *Il17ra*$^{fl/fl}$ *K14*$^{cre+}$ fibroblasts and increased *Myl9* and *Acta* in *Jmjd3*$^{fl/fl}$ *K14*$^{cre+}$ fibroblasts (Figures 2-16I, J). Additionally, through our single cell RNA-sequencing analysis of wounds from *Il17ra*$^{fl/fl}$ *K14*$^{cre+}$, we identified that myofibroblast gene *Acta* expression was increased in *Il17ra*$^{fl/fl}$ *K14*$^{cre+}$ fibroblasts compared to their controls (Figures 2-17A, B), suggesting increased reparative myofibroblast transition. Collectively, these findings demonstrate that keratinocyte-specific targeting of JMJD3 in diabetic wounds may be a viable therapeutic strategy to improve keratinocyte migration and decrease inflammation, thereby

limiting excessive recruitment of pathologic cell types and promoting a reparative landscape in diabetic wounds.

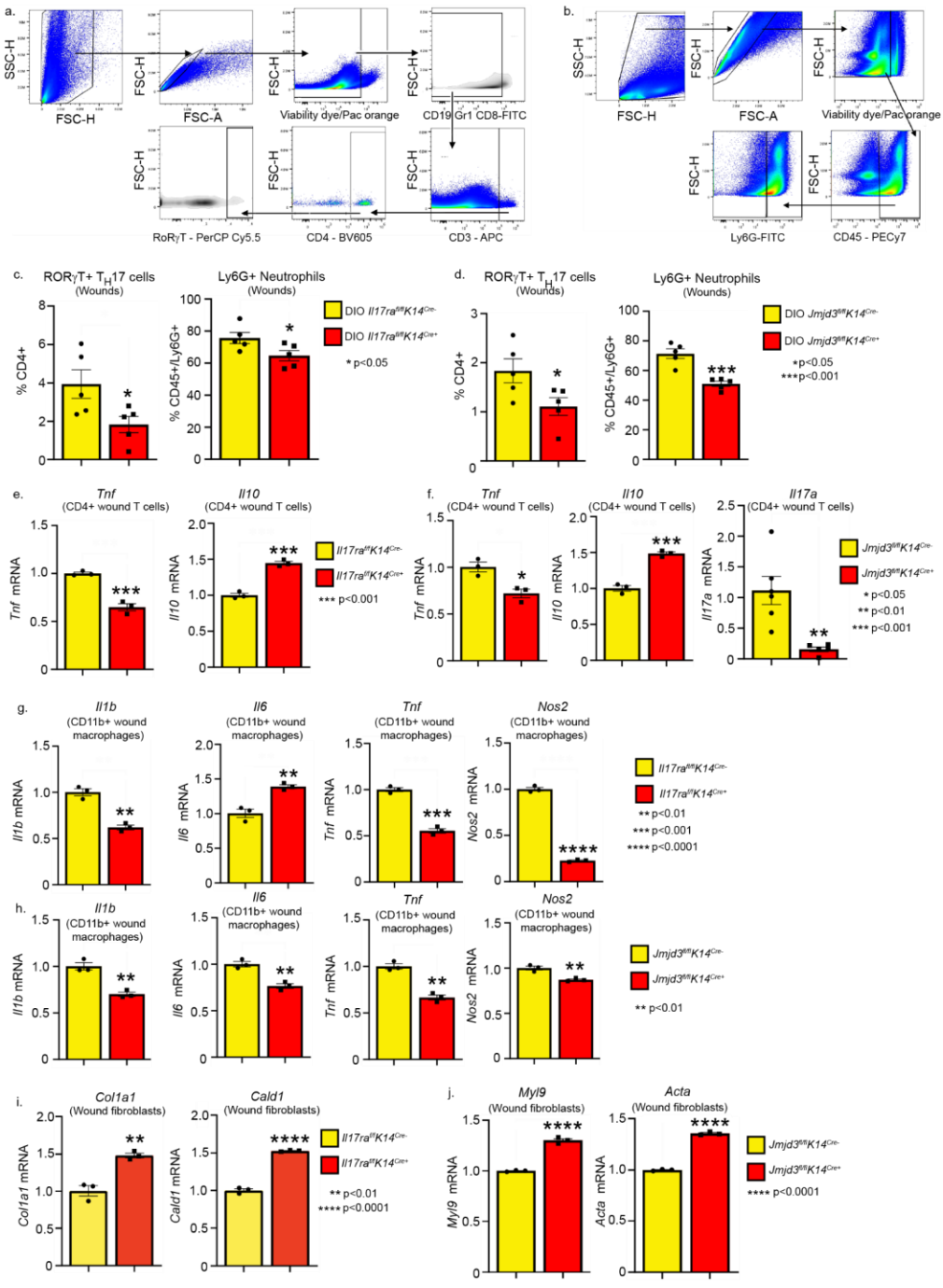


Figure 2-16: Keratinocyte-specific deletions of IL-17A signaling or JMJD3 result in increased reparative immune and fibroblast phenotypes in wounds

(A) Flow gating strategy for T_H17 cells (Live/CD19$^-$Gr1$^-$CD8$^-$/CD3$^+$/CD4$^+$/RORγT$^+$). (B) Flow gating strategy for neutrophils (Live/CD45$^+$/Ly6G$^+$). (C) Flow cytometry analysis of wound T_H17 cells and neutrophils from DIO *Il17ra*$^{fl/fl}$ *K14*$^{cre+}$ mice (red) (n = 5 mice) and littermate controls (yellow) (n = 5 mice). T_H17 cells: p = 0.0393,

Neutrophils: $p = 0.0489$. $n = 2$ independent experiments. (D) Flow cytometry analysis of wound T_H17 cells and neutrophils from DIO *Jmjd3*$^{fl/fl}$ *K14*$^{cre+}$ mice (red) ($n = 5$ mice) and littermate controls (yellow) ($n = 5$ mice). T_H17 cells: $p = 0.0444$, Neutrophils: $p = 0.0006$. $n = 2$ independent experiments. (E) qPCR analysis of CD4$^+$ T cells sorted from *Il17ra*$^{fl/fl}$ *K14*$^{cre+}$ (red) and control (*Il17ra*$^{fl/fl}$ *K14*$^{cre-}$) (yellow) wounds. $n = 3$ technical replicates. *Tnf*: $p = 0.0010$, *Il10*: $p = 0.0003$. $n = 2$ independent experiments. (F) qPCR analysis of CD4$^+$ T cells sorted from *Jmjd3*$^{fl/fl}$ *K14*$^{cre+}$ (red) and control (*Jmjd3*$^{fl/fl}$ *K14*$^{cre-}$) (yellow) wounds. *Tnf*: $n = 3$ technical replicates, $p = 0.0157$, *Il10*: 3 biological replicates, $p = 0.0005$, *Il17a*: $n = 6$ (cre-), $n = 5$ technical replicates (cre+), $p = 0.0044$. $n = 2$ independent experiments. (G) qPCR analysis of CD11b$^+$ macrophages sorted from *Il17ra*$^{fl/fl}$ *K14*$^{cre+}$ (red) and control (*Il17ra*$^{fl/fl}$ *K14*$^{cre-}$) (yellow) wounds. $n = 3$ technical replicates. *Il1b*: $p = 0.0012$, *Il6*: $p = 0.0044$, *Tnf*: $p = 0.0002$, *Nos2*: $p < 0.0001$. $n = 2$ independent experiments. (H) qPCR analysis of CD11b$^+$ macrophages sorted from *Jmjd3*$^{fl/fl}$ *K14*$^{cre+}$ (red) and control (*Jmjd3*$^{fl/fl}$ *K14*$^{cre-}$) (yellow) wounds. $n = 3$ technical replicates. *Il1b*: $p = 0.0028$, *Il6*: $p = 0.0034$, *Tnf*: $p = 0.0011$, *Nos2*: $p = 0.0054$. $n = 2$ independent experiments. (I) qPCR analysis of fibroblasts sorted from *Il17ra*$^{fl/fl}$ *K14*$^{cre+}$ (red) and control (*Il17ra*$^{fl/fl}$ *K14*$^{cre-}$) (yellow) wounds. $n = 3$ technical replicates. *Col1a1*: $p = 0.0035$, *Cald1*: $p < 0.0001$. $n = 3$ independent experiments. (J) qPCR analysis of fibroblasts sorted from *Jmjd3*$^{fl/fl}$ *K14*$^{cre+}$ (red) and control (*Jmjd3*$^{fl/fl}$ *K14*$^{cre-}$) (yellow) wounds. $n = 3$ technical replicates. *Myl9*: $p < 0.0001$, *Acta*: $p < 0.0001$. $n = 2$ independent experiments. Data were analyzed for variances, and 2-tailed Student's *t* tests were performed for (C-J). Data are presented as mean ± SEM.

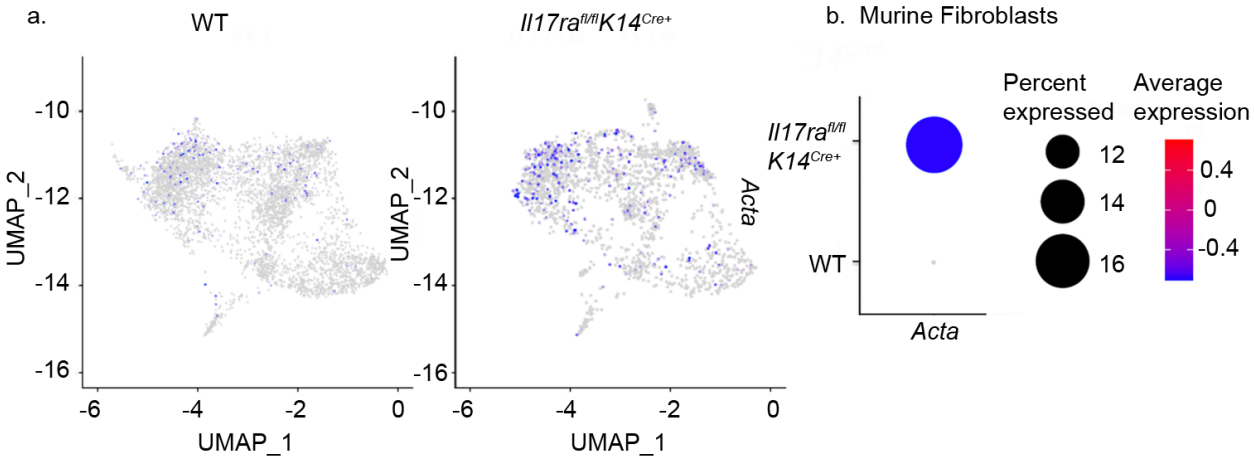


Figure 2-17: Single cell RNA-sequencing of mice with a keratinocyte-specific deletion of IL-17A signaling (*Il17ra*$^{fl/fl}$ *K14*$^{cre+}$) demonstrate increased myofibroblast transition in wound fibroblasts
(A) UMAP visualization of scRNA-seq data showing fibroblasts and *Acta* expression per cell. (B) Dot plot of *Acta* expression within fibroblast populations.

2.5 Discussion

Recent work has identified that increased inflammatory signals in the diabetic wound environment contribute to the reprogramming of critical immune and reparative cell types (115, 175, 176). Prior work done by our lab highlights that the functions of diabetic wound cells, including keratinocytes, are significantly altered leading to delayed wound re-epithelialization (21, 76). Additionally, our lab has identified that IL-17A is linked to increased T_H17 cell differentiation

in wound tissues (115). While IL-17A is essential for normal keratinocyte function, the downstream IL-17A signaling pathway in wound keratinocytes and the impact of excessive IL-17A levels on diabetic wound keratinocytes have not been studied. In this study, we found that high levels of IL-17A impair keratinocyte migration and induce an impaired keratinocyte phenotype by altering the expression of anti-migratory (*Itga3, Timp1*) and inflammatory (*Ccl20, Cxcl1, Cxcl3, Cxcl5*) genes, as summarized in our working model (Figure 2-18). Upregulation of *Itga3* and *Timp1* may impair keratinocyte migration by enhancing adhesion (154-157) and limiting matrix remodeling (160), while increased inflammatory chemokine expression promotes immune cell recruitment (123, 163), contributing to a pro-inflammatory wound environment and delayed healing. We further identified that JMJD3, a histone demethylase, is upregulated in response to IL-17A via a TRAF6/NFκB pathway downstream of the IL-17A receptor and results in a decrease in H3K27 trimethylation on the promoter(s) of anti-migratory and inflammatory genes (i.e., *Itga3, Timp1, Ccl20, Cxcl1, Cxcl3,* and *Cxcl5*). Importantly, treatment of IL-17A-stimulated keratinocytes with a JMJD3-specific inhibitor reduced both anti-migratory and inflammatory gene expression and protein levels. Our human bulk RNA-Seq and spatial scRNA-Seq analyses revealed increased IL-17A signaling and IL-17A-expressing cells in diabetic wounds, corresponding with our human single cell RNA-Seq data demonstrating elevated expression of JMJD3 and associated anti-migratory (*Itga3, Timp1*) and inflammatory (*Ccl20, Cxcl1, Cxcl3, Cxcl5*) genes in diabetic wound keratinocytes. Finally, using our diabetic murine models with keratinocyte-specific deficiencies in IL-17A signaling or JMJD3 (DIO $Il17ra^{fl/fl}$ $K14^{cre+}$ and DIO $Jmjd3^{fl/fl}$ $K14^{cre+}$), we found that loss of IL-17A signaling or JMJD3 in keratinocytes improved diabetic wound repair. Taken together, these findings suggest that the manipulation of the IL-17A/TRAF6/JMJD3 pathway in keratinocytes could be therapeutically manipulated to improve diabetic wound repair.

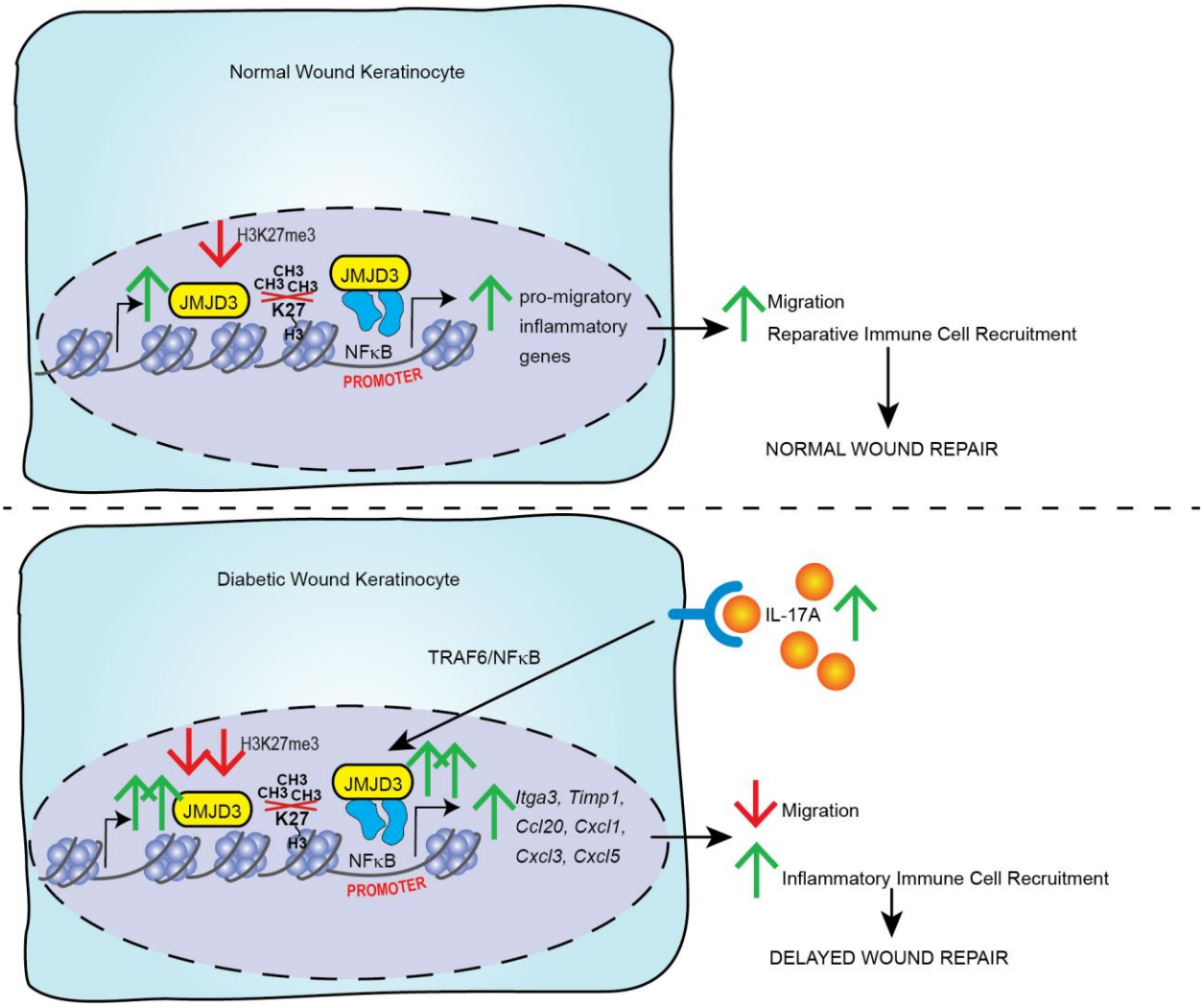


Figure 2-18: Schematic of IL-17A-mediated JMJD3 regulation of keratinocyte functions in normal and diabetic wound keratinocytes

(Top) In normal wounds, keratinocytes receive balanced environmental cues that support regulated JMJD3 activity, allowing appropriate H3K27me3 demethylation and expression of pro-migratory and inflammatory genes, promoting keratinocyte migration and timely recruitment of reparative immune cells. (Bottom) In diabetic wounds, elevated IL-17A engages the IL-17 receptor and signals through the TRAF6/NFκB pathway to drive increased JMJD3 expression, resulting in excessive H3K27me3 demethylation and increased expression of *Itga3*, *Timp1*, *Ccl20*, *Cxcl1*, *Cxcl3*, and *Cxcl5*. This cascade contributes to decreased keratinocyte migration, increased inflammatory immune cell recruitment, and impaired diabetic wound healing.

Although it has been previously identified that JMJD3 is relevant in keratinocytes following injury (70), the exact upstream regulation and the downstream genes that JMJD3 regulates were previously not explored. In this regard, our single cell RNA-Seq data from human wounds also supports JMJD3 as an upregulated enzyme in keratinocytes following injury, as it

was highly expressed in keratinocytes compared to other cell types. Our findings also indicate that primary keratinocytes isolated from our murine model with a keratinocyte-specific *Jmjd3*-deficiency exhibited improved migration rates. This contrasts with an existing scratch migration study, which shows worse gap closure in HaCaT keratinocyte cell lines where JMJD3 was inhibited via siRNA (70). However, our studies utilized primary keratinocytes which are known to behave differently from commercial cell lines, and we employed genetic deletion rather than siRNA treatment which could result in a compensatory increase in the expression of other genes involved in wound healing, potentially explaining these observed differences. Additionally, these mice displayed increased wound repair rates *in vivo* in the diabetic setting, suggesting that a fine balance of *Jmjd3* expression may be needed for proper keratinocyte function in tissue repair processes.

Our study demonstrates that the increased expression of JMJD3 in diabetic wound keratinocytes is induced via an IL-17A-mediated mechanism. While the role of IL-17A in the pathogenesis of other chronic inflammatory skin diseases (i.e., psoriasis, lupus) is well characterized, its involvement in diabetic wound healing has not been previously explored. IL-17A-mediated induction of TRAF6 has been shown to result in downstream activation of canonical NFκB pathways in keratinocytes (165). A previous study showed that NFκB can bind to the *Jmjd3* promoter, regulating its expression in macrophages under chronic inflammation (177). Further, through the use of keratinocyte-specific murine models and pharmacological approaches, we provide evidence linking the IL-17A/TRAF6/NFκB axis to epigenetic CMEs (i.e., JMJD3) for the first time. Thus, our studies find that the NFκB/JMJD3 axis is conserved in wound keratinocytes and identify IL-17A as an upstream regulator of this pathway in diabetic wounds. Although other sources of NFκB-mediated JMJD3 regulation in diabetic keratinocytes (i.e., PRRs, TLRs, TNF-α

receptor, and IL-1β receptor) (178) may exist, our data suggest that IL-17A is a significant driver, particularly given its established role in regulating keratinocyte migration and inflammatory responses (123, 162, 179).

We identified that the IL-17A/JMJD3 axis increases keratinocyte production of inflammatory chemokines, including *Cxcl1, Cxcl3,* and *Cxcl5,* which are known, amongst other functions, to promote neutrophil infiltration (180). This is highly relevant as diabetic wounds are characterized by an increased neutrophil population (181), although precise mechanisms remain unknown. In diabetic wounds, these neutrophils persist into the late stages of wound healing, contributing to prolonged inflammation. While IL-17A is known to directly promote neutrophil-induced inflammation (182), the additional production of neutrophil chemoattractants by keratinocytes may further elevate neutrophil levels, particularly during the late phases of re-epithelialization. Our flow cytometric analysis revealed decreased neutrophils in diabetic wounds from mice with keratinocyte-specific deletion of IL-17A signaling or JMJD3, indicating that the IL-17A/JMJD3 axis may drive the excessive neutrophil recruitment observed in diabetic wounds. Additionally, we observed that IL-17A/JMJD3 upregulates *Ccl20* in keratinocytes, which recruits $CCR6^+$ T_H17 cells (123). Consistently, keratinocyte-specific deletion of IL-17A signaling or JMJD3 resulted in decreased T_H17 cells, suggesting a potential positive feedback loop that further increases IL-17A levels in diabetic wounds. While this study focuses on the role of IL-17A in keratinocyte function, we acknowledge that IL-17A also directly regulates other cell types involved in wound healing. Notably, fibroblast function is significantly altered in diabetic wounds, leading to dysfunctional epithelialization (174). Diabetic wound fibroblasts are known to exhibit impaired transition into reparative myofibroblasts (174, 183). Under normal conditions, IL-17A enhances fibroblast survival and proliferation and promotes a profibrotic phenotype (184);

however, the impact of elevated IL-17A levels, as observed in diabetic wounds, on fibroblast dysfunction has not been explored. Therefore, additional studies investigating how abnormal IL-17A levels in tissues affect other cells within the wound environment would enhance our knowledge of the complex interplay in wound tissue environments.

While our study provides strong evidence for a keratinocyte-intrinsic IL-17A/JMJD3 axis contributing to impaired wound healing in diabetes, there are limitations that warrant further exploration. The use of mouse models, though well-established for studying wound healing mechanisms, may not fully recapitulate the complexity of human diabetic wounds. To help bridge this gap, we performed spatial RNA-sequencing on human diabetic and non-diabetic wound tissue, which allowed us to identify IL-17A-expressing immune populations and their spatial proximity to keratinocytes. Interestingly, we identified myeloid cells, $CD8^+$ T cells, neutrophils, and NK cells as prominent sources of IL-17A in diabetic wounds, highlighting less conventional producers beyond the well-established IL-17A-producing cell populations (i.e., $ROR\gamma T^+$ T_H17 and γδ T cells). Thus, this human dataset offers initial insights into a broader range of cellular sources contributing to elevated IL-17A levels. Nonetheless, further validation of this pathway and its upstream regulators in larger human cohorts will be critical to confirm its translational relevance.

Moreover, while our study identifies IL-17A-producing immune cells in diabetic wounds, we did not directly investigate the upstream factors driving increased IL-17A expression. Chronic inflammation, metabolic dysfunction, and microbial persistence in the diabetic wound environment have been implicated as potential contributors that may skew immune cell phenotypes toward IL-17A production (56, 57, 175). For example, dysregulated IL-17A expression has been shown to exacerbate inflammatory responses and alter the wound microbiome (123), while the diabetic microbiome itself may be more pathogenic, further promoting IL-17A-

driven inflammation (57). These factors likely contribute to a sustained pro-inflammatory milieu in diabetic wounds, and future studies will be necessary to define how these upstream cues influence IL-17A regulation in this context.

To conclude, our study highlights the role of the IL-17A/JMJD3 axis in diabetic keratinocytes, contributing to the dysregulated wound healing observed in diabetic tissue and identifies several promising therapeutic targets. While epigenetic regulation in non-immune cells remains underexplored, emerging evidence suggests that targeting these cells could offer therapeutic approaches (21, 185). While global inhibition of IL-17A likely disrupts essential functions in keratinocytes and other cell types, future therapies should involve cell-specific targeting to minimize off-target effects. In this regard, selective targeting of JMJD3 or its binding partners in keratinocytes may offer promise for restoring healing in diabetic patients.

Chapter 3 – Histone Methyltransferase SETDB2 Modulates Keratinocyte Inflammatory Cytokine Production in Diabetic Wounds by an IFNβ/JAK/STAT Mechanism

3.1 Abstract

Chronic, nonhealing wounds in patients with type 2 diabetes (T2D) are marked by dysregulated inflammation, and growing evidence suggests that impaired keratinocyte-mediated inflammatory responses contribute to this impaired repair. Work by our group and others has identified that wound cell phenotypes are controlled by CMEs, however epigenetic regulation of keratinocyte phenotypes has been largely unexplored in wound repair. Further, Type I interferons (i.e., IFNβ) are known regulators of keratinocyte-mediated inflammation, yet their role in diabetic wounds is undefined. Through unbiased transcriptomic analyses in both murine models of diabetes and human T2D wound keratinocytes, we identified the repressive chromatin modifier SETDB2 is decreased in the diabetic setting. Loss of SETDB2 was associated with increased expression of proinflammatory cytokines, consistent with reduced H3K9me3 deposition at inflammatory gene promoters. In contrast, IFNβ stimulation restored SETDB2 expression and suppressed inflammatory cytokines in keratinocytes through a JAK/STAT1-dependent mechanism. Importantly, increasing IFNβ-SETDB2 signaling *in vivo* improved wound healing and decreased

Portions of this chapter have been submitted for publication:

Moon JY, Joshi AD, Estor AL, Shadiow J, Wolf SJ, Mangum KD, Bauer TM, Hughes LD, Reyes-Arbujas J, Stark A, Rocco S, Saldana de Jimenez G, Nelapudi M, Li Q, Zhang H, Bogle R, Davis FM, Obi AT, Moore BB, Tsoi LC, Gudjonsson JE, Gallagher KA. Histone methyltransferase SETDB2 modulates keratinocyte inflammatory cytokine production in diabetic wounds in an IFNβ/JAK/STAT1 mechanism.

keratinocyte inflammatory profiles in diabetic mice. Together, these findings reveal SETDB2 as a key interferon-responsive epigenetic regulator that restrains keratinocyte inflammation and suggest that targeting the IFNβ-SETDB2 axis may represent a promising therapeutic strategy to improve diabetic wound repair.

3.2 Introduction

Cutaneous wound healing proceeds through overlapping stages of coagulation, inflammation, proliferation, and remodeling. Although many structural and immune cells participate in these processes, keratinocytes play central roles across multiple phases. During early healing, keratinocytes detect injury signals and serve as initiators of inflammation by producing cytokines and chemokines that recruit and activate immune cells at the wound site (19, 20, 100, 108, 186-188). As repair progresses, keratinocytes proliferate, migrate to close the epithelial gap, and eventually differentiate to restore the barrier (31, 108, 109). Dysregulation of any of these keratinocyte functions—including aberrant inflammatory signaling—can impair wound closure (189). An impaired inflammatory response is a hallmark of non-healing diabetic wounds and keratinocyte dysfunction has been found to contribute to this altered inflammation in diabetic wounds. The mechanisms responsible for the altered keratinocyte phenotype in type 2 diabetic (T2D) wounds have not been explored.

Epigenetic mechanisms help shape keratinocyte phenotypes by modulating chromatin accessibility and gene expression programs (15, 68, 126). Histone modifications—including methylation, acetylation, and phosphorylation—regulate transcription by altering the availability of promoter regions (126, 190). Trimethylation of histone H3 at lysine 9 (H3K9me3) is a well-established repressive mark associated with transcriptional silencing (68, 191-193). The histone methyltransferase SETDB2, which deposits H3K9me3, has been linked to inflammatory cytokine

gene expression in immune cells, yet its' role in structural cells such as keratinocytes, and the upstream signals that regulate its' expression during wound repair, remain poorly understood.

Type I interferons (T1IFNs) are key modulators of keratinocyte immune responses and signal through the JAK/STAT pathway to induce transcriptional programs essential for antiviral and inflammatory regulation (194, 195). JAK/STAT signaling in keratinocytes has been implicated in inflammatory skin diseases such as lupus, psoriasis, and atopic dermatitis (196-199), yet its function in diabetic wound keratinocytes is largely unexplored. Importantly, IFNβ and other JAK/STAT activators are decreased in diabetic wounds (15, 21), raising the possibility that impaired T1IFN signaling may contribute to dysregulated keratinocyte inflammation through loss of epigenetic control.

Here, we identify keratinocyte-mediated inflammation as a key contributor to impaired healing in diabetic wounds and define a central role for the type I interferon–regulated chromatin modifier SETDB2 in this process. Using an unbiased PCR array, we first identified SETDB2 as a markedly upregulated repressive CME in keratinocytes stimulated with IFNβ. IFNβ treatment reduced inflammatory cytokines (*Tnf*, *Il1b*, *Il23a*) in keratinocytes, whereas keratinocyte-specific *Setdb2* deficiency resulted in increased inflammatory gene and protein expression and impaired wound closure. To interrogate upstream regulation, both pharmacologic JAK inhibition (tofacitinib) and genetic loss of IFNAR or STAT1 reduced *Setdb2* expression, supporting regulation of SETDB2 via the IFNβ/JAK/STAT axis. Human scRNA-seq data further revealed that SETDB2 is increased in inflammatory keratinocyte subsets, suggesting a conserved role in modulating keratinocyte inflammatory states. In diabetic murine models, DIO and *db/db* keratinocytes exhibited decreased *Setdb2* expression, reduced H3K9me3 at inflammatory gene promoters, and heightened inflammatory cytokine production, alongside dampened

IFN/JAK/STAT signaling identified by bulk RNA-seq. Finally, restoring IFNβ signaling in diabetic mice via subcutaneous IFNβ treatment increased SETDB2 in keratinocytes, decreased keratinocyte inflammatory profiles, and improved wound healing. Collectively, these findings reveal that keratinocyte inflammation in diabetes is driven in part by loss of IFNβ-mediated SETDB2 activity and that therapeutically enhancing this pathway in keratinocytes may improve tissue repair in diabetic wounds.

3.3 Materials and Methods

3.3.1 Study Approval

All experiments using human samples were approved by the IRB at the University of Michigan (IRB#: HUM00098915) and were conducted in accordance with the principles in the Declaration of Helsinki. All mice used were on a C57BL/6 background. We used 2 diabetic models, diet-induced obesity (DIO) and *db/db,* which were used in acute and/or chronic wound models. DIO mice were generated by feeding mice with a high fat diet (HFD) for 12 – 16 weeks to simulate a "prediabetic" state that is physiologically similar to humans; mice were used at 20 weeks of age or older. Female C57BL/6J mice do not develop glucose intolerance/insulin resistance metabolic syndrome or "prediabetes" on a high-fat diet; therefore, they cannot be used in this T2D model. For *db/db* mice, both male and female mice were used in experiments starting at 7 weeks of age. Mice were housed at the University of Michigan Biomedical Sciences and Research Building in the Unit for Laboratory and Animal Medicine (ULAM) - a pathogen free animal facility. Mouse experiments were conducted with approval from our Institutional Animal Care and Use Committee (IACUC; Protocol no. PRO00011559) and all regulatory and safety standards were strictly adhered to.

3.3.2 Mice

All mice were housed at University of Michigan animal facilities. C57BL/6J, *db/db* [RRID:IMSR_JAX:000697], *K14*$^{cre+}$ [RRID:IMSR_JAX:018964], and *Stat1*$^{-/-}$ [RRID:IMSR_JAX:012606] mice were purchased from The Jackson Laboratory at 6 - 7 weeks of age and maintained in breeding pairs in Unit for Laboratory Animal Medicine (ULAM) facilities. *Ifnar*$^{-/-}$ mice on a C57BL/6J background were a gift from B. Moore (University of Michigan). *Setdb2*$^{fl/fl}$ were created as previously published by our lab (129). *Setdb2*$^{f/f}$ mice were then bred with *K14*$^{cre+}$ mice from the Jackson Laboratory to obtain mice deficient in Setdb2 in keratinocytes. Genotyping of floxed-cre mice was performed regularly after birth with custom primers. Floxed-cre mice were genotyped regularly after birth with custom primers. All mice were housed on a 14-hour light/10-hour dark cycle with free access to food, water, and bedding (Andersons Lab Bedding Bed-o'Cobs combination) at ambient temperatures of 65-75°F (18-23°C) and 40-60% humidity.

3.3.3 Wound-Healing Assessment

Mice were anesthetized with isoflurane using a vaporizer with the station flowmeter set at 2.0 liters per minute (LPM). Mice were depleted of hair on their dorsum via Veet (Reckitt Benckiser), and two 6 mm punch biopsy wounds were created per mouse (130). In IFNβ injection experiments, 0.25 μg rIFNβ (R&D Systems, Catalog 8234-MB-010/CF) or PBS control injection was performed s.c. at 2 points along the wound edge, as described previously by our group (21, 130). An iPad camera (8-megapixel) was used to take digital photographs daily. The wound surface area was calculated using ImageJ software (NIH) and was expressed as percentage of original wound size/time. The wounds were collected at the indicated time points and immediately snap-frozen and placed at –80°C for RNA isolation, prepared for keratinocyte isolation or placed

in formalin for histology. For wound keratinocyte isolation experiments, 6 mm wound biopsies were obtained, encompassing a 2 mm margin around the wound.

3.3.4 Primary Keratinocyte Isolation

Primary keratinocytes were isolated from the tails or wounds of mice (133). First, skin from tails and wounds was incubated in 1% trypsin for 1.5 hours and 2 hours, respectively, at 37°C. Following incubation, the epidermis from tails and wounds was peeled off, and epidermal cells (containing primarily keratinocytes) were agitated off into high-calcium (HiCa) medium (8% nonmixed FBS in EpiLife, with 60 μM Ca^{2+} (Gibco)). Next, primary keratinocytes from the tail were cultured in low-calcium (LoCa) medium (8% mixed FBS in EpiLife, with 60 μM Ca^{2+} (Gibco), at 0.05 mM final Ca^{2+} concentration) for 1 - 2 days at 37°C. Following isolation of primary keratinocytes (tail) and wounds, cells were harvested for RNA or fixed in 1% paraformaldehyde for ChIP.

3.3.5 RNA Extraction

Total RNA extraction was performed with TRIzol (Invitrogen) using manufacturer's directions. RNA was extracted using chloroform, isopropanol and ethanol. Superscript III Reverse transcriptase (ThermoFisher Scientific) kits were used to synthesize cDNA from extracted RNA. cDNA primers for *Setdb2* (Mm01318752), *Il1b* (Mm00434228), *Tnf* (Mm00443258), *Il23a* (Mm00518984), and 18s (no. 4318839) were purchased from Applied Biosciences. RT-PCR was conducted with 2x Taqman Fast PCR mix and run on a 7500 Real-Time PCR system (Applied Biosciences), and data was then reviewed in a relative quantification analysis to the 18s ribosomal RNA. All samples were assayed in triplicate. Data was then compiled in Excel (Microsoft) and presented using Prism software (GraphPad version 10.2.2).

3.3.6 PCR Array Analysis

Keratinocytes were isolated from tails of C57BL/6 mice, cultured, and stimulated with rIFNβ (20 U/mL) for 8 hours. RNA was isolated and DNase digested using the RNAeasy mini kit, and reverse transcription was performed using the RT^2 first strand kit (QIAGEN). Gene expression was analyzed using PCR array PAMM-085Z (Qiagen), which includes PCR primers for 84 chromatin-modifying enzymes. Data were analyzed using the PCR Array Data Analysis Web Portal.

3.3.7 Murine Bulk RNA Sequencing Analysis

Keratinocytes were isolated from day 5 wounds from *db/+* and *db/db* mice. RNA isolation was performed using a RNeasy Kit (Qiagen) with DNase digestion. Library construction and analysis of reads was performed as described previously (56). Briefly, reads were trimmed using Trimmomatic and mapped using HiSAT2 (137, 138). Read counts were performed using the feature-counts option from the subRead package followed by the elimination of low reads, normalization and differential gene expression using edgeR (139, 140). Differential expression was performed on mapped reads using the taqwise dispersion algorithm in edgeR.

3.3.8 Chromatin Immunoprecipitation Assay

Chromatin immunoprecipitation assay was performed as described previously using a kit purchased from Abcam (ab500) (141). Briefly, following *ex vivo* studies, keratinocytes were cross linked in 1% formaldehyde for 10 min at RT and pellets stored at -80°C until analyzed. Following manufacturer's instructions, cells were lysed for 10 min on ice in an SDS-containing lysis buffer (Abcam), supplemented with a protease inhibitor cocktail (Abcam), sonicated to generate 100-300 base pair fragments. Five percent of the total chromatin volume was put aside for the input control. The rest of the chromatin was subsequently incubated with antibodies against trimethylated H3K9

(Active Motif, Cat# 61013) at 1 µg/sample, or rabbit polyclonal IgG (Diagenode, Cat# C15410206) at 1 µg/sample overnight at 4°C. This was followed by addition of Protein A sepharose beads (Abcam) for 1 hour at 4°C. The pellet was washed, and a DNA purifying slurry (Abcam) was added. The eluates were reverse cross linked for 10 min at 98°C, followed by a proteinase K digestion for 30 min at 55°C and 10 min at 98°C. Precipitated DNA was analyzed by quantitative real time PCR on a Taqman 7500 sequence detection system. The following primers were used to amplify DNA in samples: *Il1b*: (forward) 5' ACCTTTGTTCCGCACATCCT 3' and (reverse) 5' GGCATTATTTCCCCCTGGACA 3', *Tnf*: (forward) 5' TCCTGATTGGCCCCAGATTG 3' and (reverse) 5' TAGTGGCCCTACACCTCTGT 3', *Il23a*: (forward) 5' TCACCTCTAGTTCCTCCCTG 3' and (reverse) 5' ACAAGTTCTCAATGGGGGTC 3'

3.3.9 Enzyme Linked Immunosorbent Assay (ELISA)

Keratinocytes were isolated, cultured, scratched, and stimulated in culture for 24 or 48 hours in low-calcium (LoCa) medium. After stimulation, cell free supernatant was collected and analyzed by the University of Michigan Immune Monitoring Shared Resource Core for TNF-α, IL-1β, and IL-23.

3.3.10 Western Blot

Cell suspensions were lysed in radioimmunoprecipitation assay (RIPA) buffer (Sigma) and standardized for protein concentrations using a Bradford protein assay (BioRad) to generate a standard curve. Equal amounts of protein were then loaded onto to 4 to 12% sodium dodecyl sulfate gel electrophoresis under reducing conditions. Protein bands were then transferred to nitrocellulose membranes and probed with primary antibody anti-mouse SETDB2 (Cat# PA5-110357, Invitrogen, 1:1000), anti-mouse beta actin (Cat# A5316-100UL, Sigma Aldrich, 1:1000)

at 4 °C for 24 hr. All primary antibodies were diluted 1:1000 in 1% BSA in 0.1% Tween Tris-buffered saline (TBS-T) solution. Nitrocellulose membranes were then washed and incubated with horseradish peroxidase−labeled secondary antibody (Cell Signaling) for 1 hr at room temperature and visualized with chemiluminescence (Thermo Fisher Scientific). Blot images were analyzed using NIH ImageJ software to obtain sample densitometry readings normalized to beta actin.

3.3.11 Histology

Tissues were harvested from mice and fixed in 10% formalin for 24 hours then stored in 70% ethanol. Specimens were embedded in paraffin and sectioned onto microscope slides. After deparaffinization, murine tissue slides were stained with Masson's trichrome stain, as previously described (132). Images were taken using a Zeiss Axioskop 2 microscope. Trichrome staining intensity was calculated using ImageJ software.

3.3.12 Human Wound Isolation

All experiments using human samples were approved by the IRB at the University of Michigan and were conducted in accordance with the principles in the Declaration of Helsinki. Written informed consent was obtained from all subjects involved in human studies. Human subject data is de-identified and these patients are not followed after the sample is collected. Per our IRB, at initial sample collection, we obtain information on age, sex, and diabetes status. For the scRNA-Seq cohort, biopsies from human diabetic wounds versus normal skin samples were collected. Within the diabetic patient samples for scRNA-Seq, the average age was 60 years, with all patients having diabetes, hypertension, hyperlipidemia, and coronary artery disease. Within the nondiabetic patient samples, the average age was 70 years, with 50% of patients having hypertension, hyperlipidemia, and coronary artery disease. Wounds were obtained from the lateral edge of wound specimens using an 8 mm punch biopsy tool and processed for RNA extraction and

sequencing as described for the murine wounds, and the material was fully consumed during analysis. RNA with RNA integrity number scores of greater than 8 were used, and all values were done with comparison to 28S/18S ratios and other housekeeping genes.

3.3.13 Human ScRNA-Seq Analysis

Single-cell suspensions for scRNA-Seq were generated as follows. Wound tissue from diabetic and non-diabetic patients was collected by punch biopsy and immediately processed. Samples were incubated overnight at 4°C in 0.4% Dispase (Life Technologies, Thermo Fisher Scientific) prepared in HBSS (Gibco, Thermo Fisher Scientific). The epidermal and dermal layers were then separated. The epidermis was enzymatically digested with 0.25% Trypsin-EDTA (Gibco, Thermo Fisher Scientific) containing 10 U/mL DNase I (Thermo Fisher Scientific) for 1 hour at 37°C, followed by quenching with FBS (Atlanta Biologicals) and filtration through a 70 μm strainer. Dermal tissue was finely minced and digested in 0.2% Collagenase II (Life Technologies, Thermo Fisher Scientific) and 0.2% Collagenase V (MilliporeSigma) for 1.5 hours at 37°C, then passed through a 70 μm strainer. Epidermal and dermal cells were combined in a 1:1 ratio and submitted to the University of Michigan Advanced Genomics Core for scRNA-Seq library generation on the 10x Genomics Chromium platform. Libraries were sequenced on the Illumina NovaSeq 6000 to produce 151 bp paired-end reads. Read trimming and quality control followed standard pipelines (142, 143). Processed reads were aligned to the human reference genome (GRCh37) using STAR (144). Gene-level counts were obtained with HTSeq (145) and normalized using DESeq2 (146), which was also used for differential expression testing with negative binomial models. To expand control sample representation, additional skin biopsy data from our prior study (147) were incorporated. ScRNA-seq data have been deposited in the Gene Expression Omnibus under accession number GSE154557. For scRNA-Seq processing, Cell

Ranger (10x Genomics) was used for alignment, quality filtering, and quantification. Subsequent normalization, data integration, and clustering were carried out in Seurat (148).

3.3.14 Statistics

GraphPad Prism software (RRID:SCR_002798) version 10.2.2 was used to analyze the data. Data were analyzed for normal distribution and then statistical significance between multiple groups was determined using a one-way analysis of variance test followed by Newman-Keuls post hoc test. For all single group comparisons, if data passed normality test, we used a two-tailed Student's t test. Otherwise, data were analyzed using the Mann–Whitney *U*-test. All data are representative of at least two independent experiments as detailed in the figure legends. A P value of less than or equal to 0.05 was significant. Values smaller than 0.0001 are reported as $P < 0.0001$.

3.3.15 Data Availability

Source data are provided with this paper. All sequencing data generated in this study have been deposited in the Gene Omnibus (GEO) or Zenodo repositories. The human scRNA-sequencing data have been deposited under accession code GSE154557 [https://www.ncbi.nlm.nih.gov/geo/query/acc.cgi?acc=GSE154557]. The mouse bulk RNA-sequencing data of *db/+* and *db/db* wounds are available at [https://doi.org/10.5281/zenodo.17508179].

3.4 Results

3.4.1 IFNβ Decreases Inflammatory Cytokine Gene Expression via Setdb2 in Keratinocytes

Precise regulation of inflammation is essential for proper wound repair. Under normal conditions, inflammation initiates early after injury and resolves as healing progresses. In contrast, T2D wounds exhibit prolonged, unresolved inflammation that impairs tissue repair. Type I

interferons are produced by tissue-resident cells following skin injury and contribute to keratinocyte growth, differentiation, and immune regulation (21, 200). However, the specific role of IFNβ in controlling keratinocyte inflammatory responses and cell phenotype, particularly in the context of diabetic wound healing, remains poorly understood.

To identify epigenetic regulators responsive to IFNβ signaling in wound keratinocytes, we performed an unbiased PCR array of chromatin-modifying enzymes (CME) that are relevant in wound repair (Figure 3-1A). We isolated and cultured basal keratinocytes from C57BL/6 mice as we have previously described (133), stimulated them with or without recombinant mouse IFNβ (rIFNβ) (20 U/mL) and performed a 96-well epigenetic super array (15, 76, 115, 164). Among the upregulated candidates, the histone methyltransferase SETDB2 emerged as a potentially important CME, given it is relevant in wound repair (15, 201). Next, to confirm our super array results, we examined *Setdb2* expression via qPCR in rIFNβ-stimulated keratinocytes isolated from C57BL/6 mice and found that IFNβ significantly increases expression of *Setdb2* (Figure 3-1B). SETDB2 deposits the repressive H3K9me3 modification at target gene promoters, thereby reducing gene transcription (Figure 3-1C). We then assessed whether IFNβ enhances SETDB2-mediated repression at inflammatory gene promoters, by performing chromatin immunoprecipitation (ChIP) on keratinocytes isolated from C57BL/6 mice and stimulated with IFNβ (rIFNβ) (20 U/mL) for 8 hours. ChIP analysis of SETDB2-mediated H3K9me3 showed that IFNβ stimulation increased H3K9me3 enrichment at *Il1b*, *Tnf*, and *Il23a* promoters (Figure 3-1D), corresponding with decreased expression of these cytokines in wound keratinocytes (Figure 3-1E). These data support an IFNβ/SETDB2/H3K9me3 axis that limits keratinocyte inflammatory responses.

Next, to examine the relevance of *Setdb2* in keratinocytes in wound healing *in vivo*, we used our murine model with a keratinocyte-specific *Setdb2* deficiency ($Setdb2^{fl/fl}$ $K14^{cre+}$). Mice

were subjected to 6 mm punch biopsy wounds, and following injury, wound closure was monitored daily using NIH ImageJ software, as we have previously described (15, 21, 76, 115, 130, 164). We found that there was a decrease in closure rates during earlier time points in mice with the *Setdb2* deficiency (*Setdb2*$^{fl/fl}$ *K14*$^{cre+}$), (Figure 3-1F). Since inflammation peaks during the early phase of healing, these findings suggest that *Setdb2* may act to fine-tune the early inflammatory response, preventing excessive inflammation that can hinder proper wound closure. We confirmed that *Setdb2* expression was significantly decreased in wound keratinocytes isolated from *Setdb2*$^{fl/fl}$ *K14*$^{cre+}$ (Figure 3-2). To examine the effects of genetic deletion of *Setdb2* on inflammatory cytokine expression in keratinocytes, we also assessed *Il1b, Tnf,* and *Il23a* expression in *Setdb2*$^{fl/fl}$ *K14*$^{cre+}$ keratinocytes. We found that both gene (Figure 3-1G) and protein (Figure 3-1H) expression was increased in *Setdb2*$^{fl/fl}$ *K14*$^{cre+}$ keratinocytes, validating the role of *Setdb2*-mediated regulation of inflammatory cytokines in keratinocytes. Collectively, these findings indicate that IFNβ signaling in keratinocytes regulates Setdb2/H3K9me3-mediated suppression of inflammation in keratinocytes and may lead to improved wound closure during the early phases of wound healing.

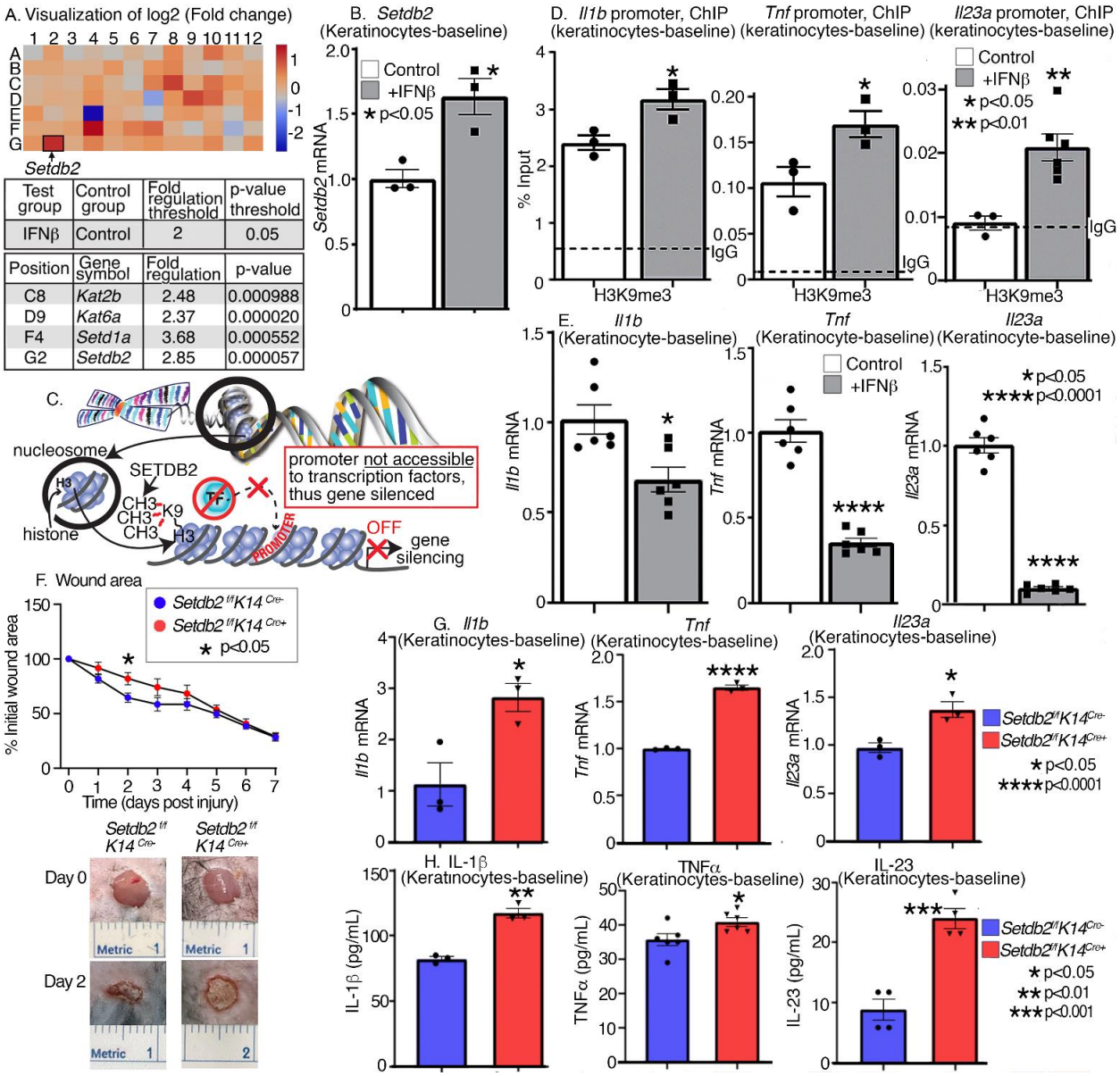


Figure 3-1: IFNβ decreases inflammatory cytokine gene expression via *Setdb2* in keratinocytes

(A) Gene expression of chromatin-modifying enzymes was analyzed using PCR array plates in keratinocytes isolated from C57BL/6 mice stimulated with or without rIFNβ (20 U/mL) for 8 hr. Enzymes that were upregulated (red) and downregulated (blue) are shown. The threshold was set to a 2-fold difference. Data are expressed as fold over control (n = 4 biological replicates). (B) Keratinocytes were isolated from C57BL/6 mice and stimulated with or without rIFNβ (20 U/mL) for 8 hours. *Setdb2* expression was examined via qPCR (n = 3 biological replicates). (C) Schematic of SETDB2-mediated H3K9 trimethylation of gene promoters. (D) Keratinocytes isolated from C57BL/6 mice were stimulated with or without rIFNβ (20 U/mL) for 8 hours. ChIP analysis for H3K9me3 or IgG control was performed at *Il1b, Tnf,* and *Il23a* promoters (n = 3-6 technical replicates). (E) Keratinocytes isolated from C57BL/6 mice were stimulated with or without rIFNβ (20 U/mL) for 8 hours. *Il1b, Tnf,* and *Il23a* expression was examined via qPCR (n = 6 technical replicates). (F) 6 mm punch biopsy wounds were created on DIO *Setdb2*$^{fl/fl}$ *K14*$^{cre+}$ and littermate controls. The change in wound area was recorded daily and analyzed with ImageJ software (2 wounds per mouse, n = 6 mice per group). Representative photographs of the wounds from day 2 are shown. (G) Keratinocytes were isolated from *Setdb2*$^{fl/fl}$ *K14*$^{cre+}$ and *Setdb2*$^{fl/fl}$ *K14*$^{cre-}$ mice, stimulated with rIFNβ (20 U/mL) for 8 or 16 hours. *Il1b, Tnf,* and *Il23a* expression was examined via qPCR (n = 3 biological replicates). (H) Keratinocytes were isolated from *Setdb2*$^{fl/fl}$

K14^{cre+} and *Setdb2*$^{fl/fl}$ *K14*$^{cre-}$ mice, cultured, scratched with a p20 pipette tip, and stimulated with rIFNβ (20 U/mL) for 24 or 48 hours. IL-1β, TNF-α, and IL-23A protein expression was measured from cell lysates (n = 5-6 biological replicates). Data were analyzed for variances, and 2-tailed Student's t test or 1-way ANOVA was performed. *P < 0.05, **P < 0.01, ***P < 0.001, ****P < 0.0001. Data are presented as mean ± SEM. All data are representative of 3 independent experiments.

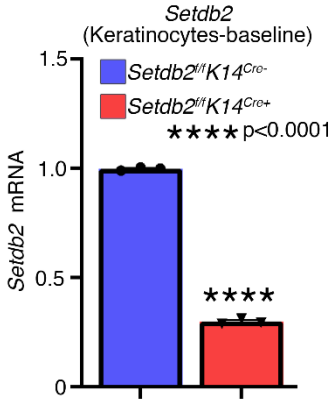


Figure 3-2: Confirmation of decreased Setdb2 expression in keratinocyte-specific *Setdb2*-deficient mice (*Setdb2*$^{fl/fl}$ *K14*$^{cre+}$)
Keratinocytes were isolated from *Setdb2*$^{fl/fl}$ *K14*$^{cre+}$ and *Setdb2*$^{fl/fl}$ *K14*$^{cre-}$ mice. *Setdb2* expression was examined via qPCR (n = 3 biological replicates).

3.4.2 IFNβ Regulates Setdb2 in Keratinocytes via JAK/STAT1

Our group and others have shown that STAT proteins are elevated in wounds (202); however, the regulation of SETDB2 and the signaling pathways in keratinocytes during tissue repair are unknown. Since IFNβ signals primarily through this JAK/STAT pathway, we assessed the relevance of the JAK/STAT pathway on IFNβ-induced *Setdb2* expression in wound keratinocytes using both pharmacologic and genetic tools. Keratinocytes were isolated from C57BL/6 mice and stimulated with IFNβ (rIFNβ) (20 U/mL) and either treated with vehicle only (DMSO) or with a JAK1/3 inhibitor (tofacitinib, 50 nM) for 8 hours. We found keratinocytes demonstrated an increase in *Setdb2* gene transcription following stimulation with IFNβ and blockade of JAK1/3 with tofacitinib reduced *Setdb2* expression in keratinocytes following stimulation (Figure 3-3A). Consistent with these findings, SETDB2 protein levels correlated with

gene expression patterns (Figure 3-3B). Next, we isolated keratinocytes from mice deficient in the interferon-α/β receptor (*Ifnar*$^{-/-}$) and mice deficient in STAT1 (*Stat1*$^{-/-}$) and stimulated them for 8 hours with rIFNβ (20 U/mL). Keratinocytes stimulated with IFNβ from mice deficient in IFNAR (*Ifnar*$^{-/-}$) and STAT1 (*Stat1*$^{-/-}$) displayed reduced *Setdb2* gene (Figure 3-3C) and protein (Figure 3-3D) expression. Further, *Tnf, Il1b*, and *Il23a* gene (Figure 3-3E) and protein (Figure 3-3F) expression was increased in keratinocytes stimulated with rIFNβ (20 U/mL) from mice deficient in IFNAR (*Ifnar*$^{-/-}$) and STAT1 (*Stat1*$^{-/-}$).

Taken together, these results indicate that IFNβ induces *Setdb2* expression in keratinocytes through the JAK/STAT1 pathway, suggesting a potential regulatory role in controlling inflammatory cytokine expression and inflammatory keratinocyte phenotype.

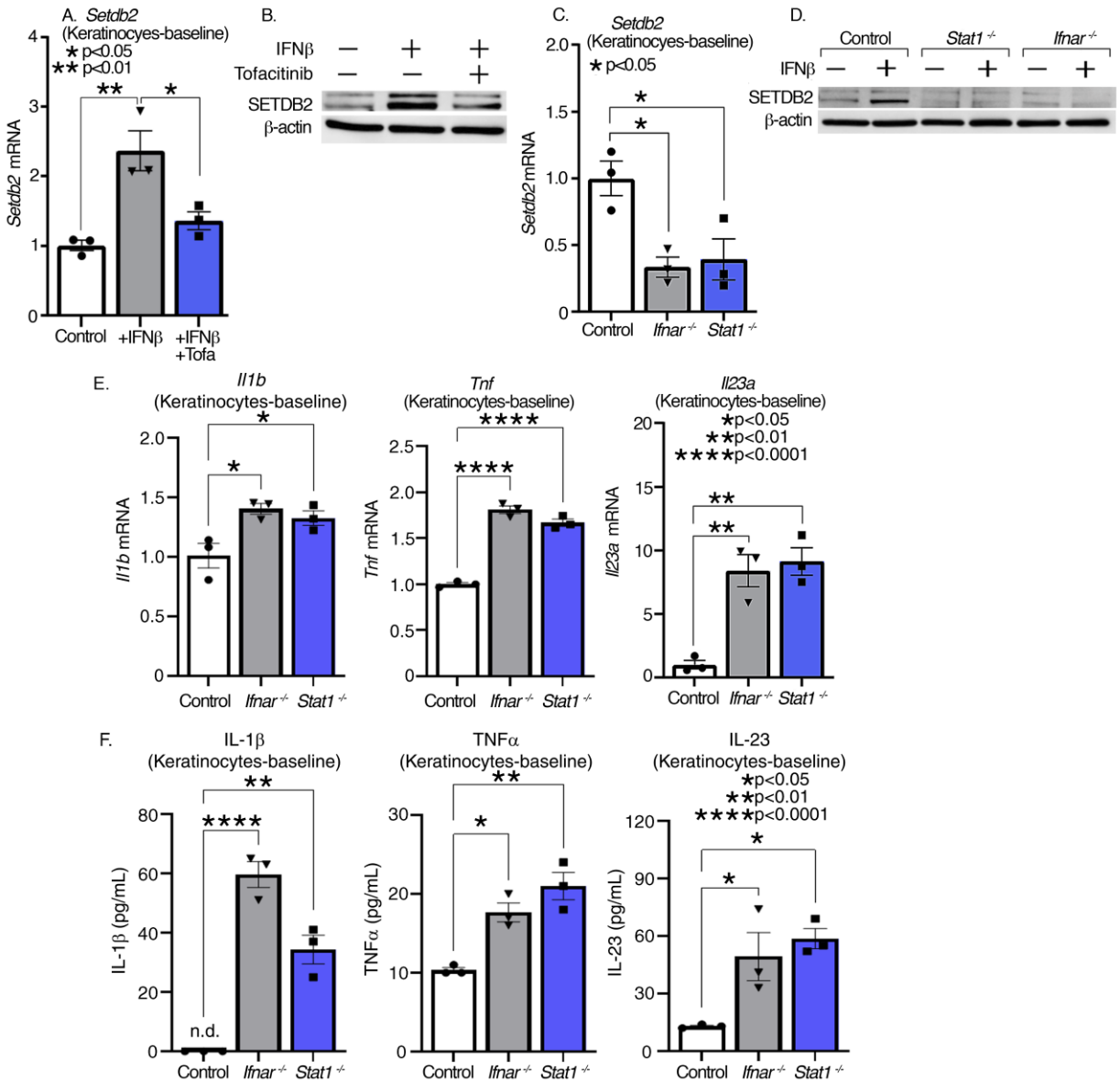


Figure 3-3: IFNβ regulates *Setdb2* in keratinocytes via JAK/STAT1

(A) Keratinocytes were isolated from C57BL/6 mice and treated with medium only, with rIFNβ (20 U/mL) alone, or with rIFNβ (20 U/mL) and tofacitinib (50 nM) for 8 hours and *Setdb2* expression was examined via qPCR (n = 3 biological replicates). (B) Keratinocytes were isolated from C57BL/6 mice and treated with medium only, with rIFNβ (20 U/mL) alone, or with rIFNβ (20 U/mL) and tofacitinib (50 nM) for 16 hours. SETDB2 protein expression was measured from lysates (n = 3 mice per group, pooled, repeated in triplicate). Representative densitometry plot is shown. (C) Keratinocytes were isolated from C57BL/6, *Stat1*$^{-/-}$, and *Ifnar*$^{-/-}$ mice and treated with or without rIFNβ (20 U/mL) for 8 hours. *Setdb2* expression was examined by qPCR (n = 3 biological replicates). (D) Keratinocytes were isolated from C57BL/6, *Stat1*$^{-/-}$, and *Ifnar*$^{-/-}$ mice and treated with or without rIFNβ (20 U/mL) for 16 hours. SETDB2 protein expression was measured from lysates (n = 3 mice per group, pooled, repeated in triplicate). Representative densitometry plot is shown. (E) Keratinocytes were isolated from C57BL/6, *Stat1*$^{-/-}$, and *Ifnar*$^{-/-}$ mice and treated with rIFNβ (20 U/mL) for 8, 16, or 24 hours. *Il1b, Tnf,* and *Il23a* expression was examined by qPCR (n = 3 biological replicates). (F) Keratinocytes were isolated from C57BL/6, *Stat1*$^{-/-}$, and *Ifnar*$^{-/-}$ mice, cultured, scratched with a p20 pipette tip, and treated with rIFNβ (20 U/mL) for 48 hours. IL-1β, TNF-α, and IL-23A protein expression was measured from cell lysates (n = 3 biological replicates). N.D., not detected (below the limit of quantification).

Data were analyzed for variances, and 1-way ANOVA was performed. *$P < 0.05$, **$P < 0.01$, ****$P < 0.0001$. Data are presented as mean ± SEM. All data are representative of 3 independent experiments.

3.4.3 SETDB2 Expression Is Decreased While Inflammatory Cytokine Gene Expression Is Increased in Diabetic Keratinocytes

Given that inflammatory keratinocytes are increased in diabetic wounds (16, 109, 203), we sought to examine if SETDB2 was altered in diabetic keratinocytes. As a translational corollary, we analyzed our single-cell RNA-seq dataset from T2D and non-T2D patient wounds for *SETDB2* expression in keratinocytes (21, 69, 76, 171). Cluster analysis was performed using uniform manifold approximation and projection (UMAP) as previously described (21, 131); where 16 cell clusters were identified in wounds following injury. We identified 4 clusters of keratinocytes, including keratinized, differentiated, cycling, and basal keratinocytes (Figure 3-4A). Diabetic human keratinocytes from the basal keratinocyte cluster exhibited increased expression of *TNF*, *IL1B*, and *IL23A* (Figure 3-4B), demonstrating a heightened inflammatory profile. Next, to assess whether SETDB2 is linked to this inflammatory state, all diabetic keratinocyte cells were subsetted from the Seurat object for downstream analysis. For each keratinocyte, an inflammation score was calculated as the mean expression level of three inflammatory genes (*TNF, IL1B*, and *IL23A*). Cells with inflammation scores above the median were classified as *inflammatory* while cells with scores below the median were classified as *non-inflammatory*. *SETDB2* expression was then compared between inflammatory and non-inflammatory cells across four keratinocyte subsets, as well as within the total keratinocyte population, using a dot plot. We found that *inflammatory* keratinocytes displayed decreased *SETDB2* expression (Figure 3-4C), further linking its role in regulating inflammation in keratinocytes.

To validate these findings, we used our murine model of diabetes, diet-induced obesity (DIO) mice, that were generated by feeding mice with a high fat diet (HFD) for 12 – 16 weeks to

simulate a “prediabetic” state that is physiologically similar to humans (173). Mice were subjected to 6 mm punch biopsy wounds and keratinocytes were isolated on day 5 post-injury for analysis of *Setdb2* gene and protein expression. Both Setdb2 gene expression and protein were significantly decreased in DIO wound keratinocytes compared with controls (Figures 3-4D, E). Further, ChIP assays revealed that there was decreased Setdb2-H3K9me3 marks at inflammatory cytokine gene promoters including *Tnf, Il23a, Il1b,* and *Il12a* in DIO keratinocytes (Figure 3-4F). Consistent with the observed decrease in H3K9me3-mediated suppression, inflammatory cytokine gene (*Tnf, Il23a, Il1b,* and *Il12a*) expression was increased in DIO keratinocytes (Figure 3-4G). Together, these findings demonstrate that both human and murine diabetic keratinocytes display decreased SETDB2 expression and increased inflammatory cytokine expression, suggesting that loss of SETDB2 may contribute to excessive inflammatory signaling and increased inflammatory keratinocytes and impaired wound healing in the diabetic setting.

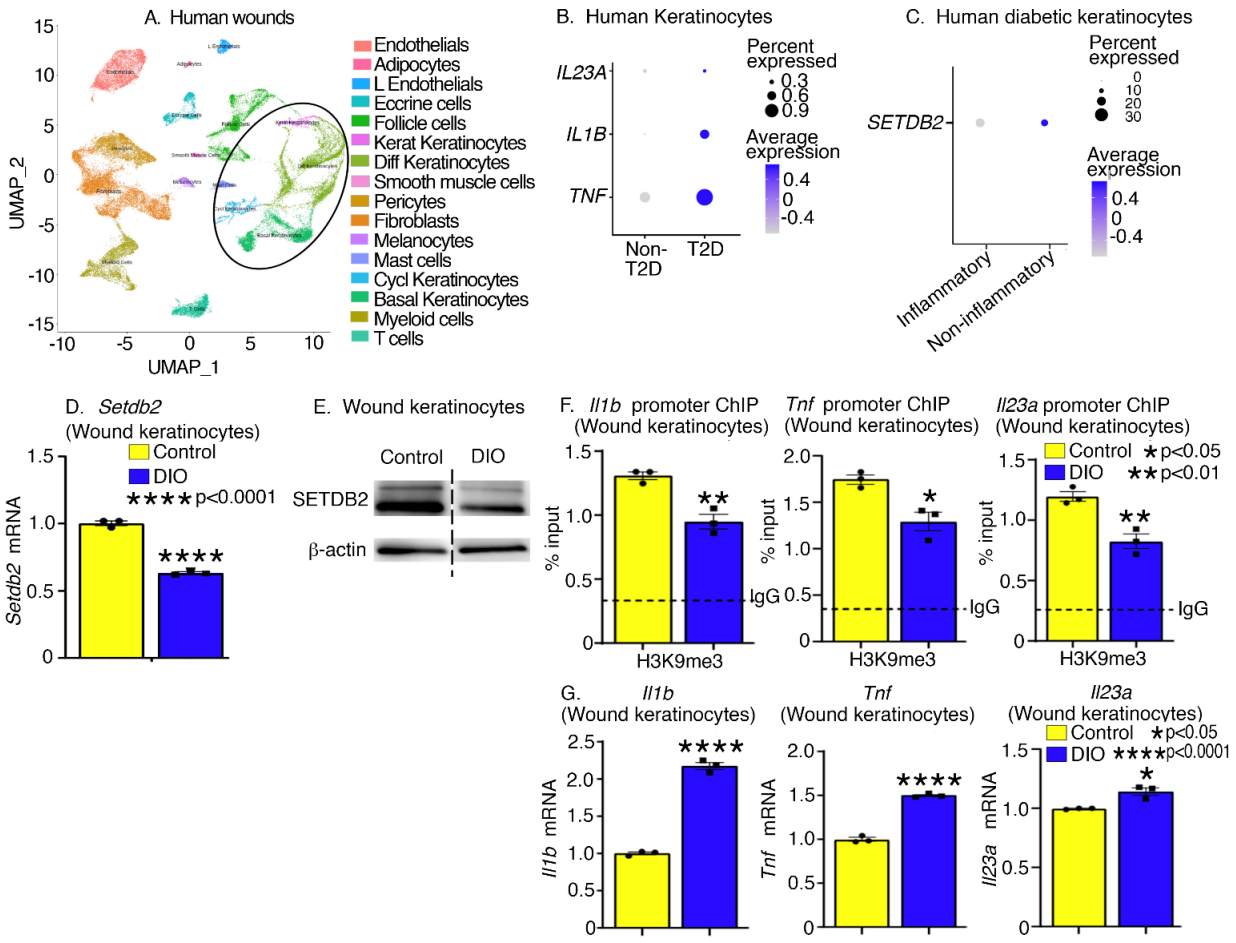


Figure 3-4: SETDB2 expression is decreased while inflammatory cytokine gene expression is increased in diabetic keratinocytes

(A) Cluster analysis was performed using the UMAP technique of single cell sequencing of T2D (N = 6) and nondiabetic wound (N = 6) samples. The black box outlines the keratinocyte populations: basal cells, cycling cells, differentiated cells, keratinized cells. (B) Dot plot demonstrating *IL1B, TNF,* and *IL23A* expression within keratinocyte populations in human T2D and non-T2D samples. Dot size corresponds to the proportion of cells within the group expressing the gene, while the dot color corresponds to expression level. (C) Dot plot demonstrating *SETDB2* expression within *Inflammatory* and *non-inflammatory* keratinocyte subsets in human T2D and non-T2D samples. Dot size corresponds to the proportion of cells within the group expressing the gene, while the dot color corresponds to expression level. (D) Wound keratinocytes were isolated from day 5 wounds from control and DIO mice and *Setdb2* expression was examined via qPCR (n = 3 technical replicates). (E) Wound keratinocytes were isolated from day 5 wounds from control and DIO mice and SETDB2 protein expression was examined via western blot. Representative densitometry is shown. (F) Wound keratinocytes were isolated from day 5 wounds from control and DIO mice and *Il1b, Tnf,* and *Il23a* expression was examined via qPCR (n = 3 technical replicates). (H) Wound keratinocytes were isolated from day 5 wounds from control and DIO mice. ChIP analysis for H3K9me3 or IgG control was performed at *Il1b, Tnf,* and *Il23a* promoters (n = 3 technical replicates). Data were analyzed for variances, and 2-tailed t-test was performed. *$P < 0.05$, **$P < 0.01$, ****$P < 0.0001$. Data are presented as mean ± SEM. All data are representative of 3 independent experiments.

3.4.4 Manipulation of IFNβ/SETDB2 Axis in Keratinocytes Results in Decreased Inflammation and Improved Wound Healing

Previous work from our lab has demonstrated that type I interferon levels including IFNβ are decreased in the diabetic wound environment (15, 21); however, the role of IFNβ signaling on wound keratinocytes is unknown. To address this, we used a well-established murine model of T2D, *db/db* mice, which lack a functional leptin receptor (172), we wounded mice and isolated keratinocytes on day 5 as previously described (133) and performed bulk RNA-Seq. Analysis of bulk RNA-Seq of diabetic wound keratinocytes demonstrated decreased interferon-stimulated gene (ISG) and JAK-STAT pathways in the diabetic wound keratinocytes compared to littermate controls (*db/+*) (Figures 3-5A, B), confirming that IFNβ signaling is compromised in keratinocytes in the diabetic context.

To examine the potential impact of restoring IFNβ signaling in keratinocytes, we wounded DIO mice and isolated keratinocytes on day 5 as previously described (133). We then stimulated diabetic wound keratinocytes *ex vivo* with rIFNβ (20 U/mL). IFNβ treatment decreased inflammatory cytokine (*Tnf, Il1b, Il23a*) expression (Figure 3-5C), demonstrating that impaired IFNβ/JAK/STAT signaling contributes to increased inflammatory cytokine production in diabetic wound keratinocytes.

Since the reduction of the IFNβ/JAK/STAT/SETDB2 pathway appears to be playing a pathologic role in diabetic wound keratinocytes, we examined if inducing this pathway via daily subcutaneous injections of IFNβ into wounds would improve wound healing rates *in vivo* in our DIO murine model. We created 6 mm punch biopsy wounds and administered daily injections of rIFNβ (0.25 μg) or PBS, and wound closure was monitored daily using NIH ImageJ software as we have previously described (15, 21, 68, 69, 76, 115, 130, 131, 164, 171, 191, 201). We found

that there was increased wound healing in DIO mice treated with local wound rIFNβ injections, especially during earlier timepoints days 1 through 4 (Figure 3-5D). Next, we confirmed that keratinocytes isolated from diabetic mice that received rIFNβ injections displayed increased expression of *Setdb2* (Figure 3-5E). Lastly, wound collagen deposition was assessed on day 7 by quantifying Trichrome staining intensity as a measure of tissue remodeling as we have previously described (21). We found that wounds that received rIFNβ injections displayed increased wound collagen deposition (Figure 3-5F), indicating resolution of inflammation and progression to tissue repair. Overall, these findings demonstrate that modulating the IFNβ/SETDB2 axis in keratinocytes reduces pathologic cytokine production and improves wound healing in the diabetic mice, highlighting a potential therapeutic strategy for improving repair in diabetic wounds.

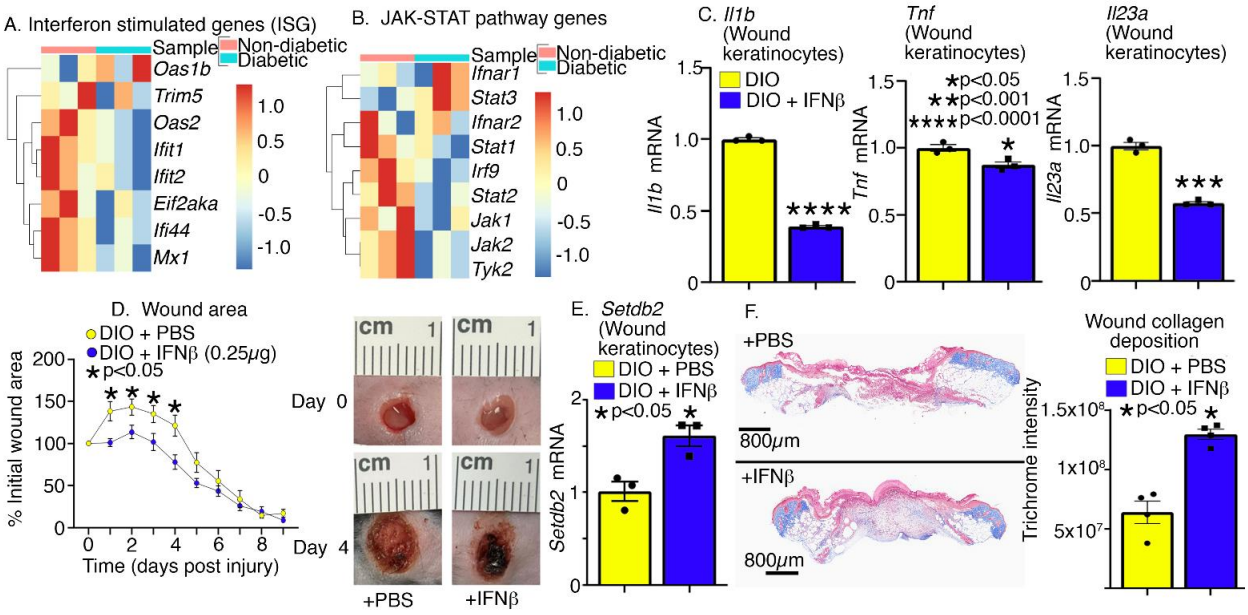


Figure 3-5: Manipulation of IFNβ/SETDB2 axis in keratinocytes results in decreased inflammation and improved wound healing

(A-B) 6 mm punch biopsy wounds were created on diabetic (*db/db*) mice and nondiabetic controls (*db/+*), and wound keratinocytes were isolated on day 5 and samples were processed for bulk RNA sequencing. Heatmap reflecting the expression profiles for selective genes (rows) across different samples (columns; stratified by diabetes status) from (A) interferon stimulated genes (ISG) and (B) JAK-STAT pathway genes in keratinocytes Gene Ontology pathway analysis with downregulation in *db/db* diabetic wound keratinocytes (n = 3 mice) compared to *db/+* control wound keratinocytes (n = 3 mice). (C) 6 mm punch biopsy wounds were created on diabetic (DIO) mice, and wound

keratinocytes were isolated on day 5. Wound keratinocytes were stimulated with rIFNβ (20 U/mL) *ex vivo* for 8 hours. *Il1b, Tnf,* and *Il23a* expression was examined by qPCR (n = 3 technical triplicates). (D) 6 mm punch biopsy wounds were created on diabetic (DIO) mice. Wound closure in DIO mice subjected to daily subcutaneous rIFNβ (0.25 μg) (gray) or PBS (white) injections near the wound edge was quantified using ImageJ software (n = 5 mice/group). Representative images from day 4 are shown. (E) Wound keratinocytes were isolated on day 7 from DIO mice that were administered daily injections with rIFNβ (0.25 μg) (gray) or PBS (white). *Setdb2* expression was examined by qPCR (n = 3 mice pooled per group, repeated in technical replicates). (F) Trichrome staining intensity to measure wound collagen deposition in day 7 wounds from DIO mice that were administered daily injections with rIFNβ (0.25 μg) (gray) or PBS (white) was calculated using ImageJ software (n = 4 mice per group). Data were analyzed for variances, and 2-tailed t-test was performed. *$P < 0.05$, ***$P < 0.001$, ****$P < 0.0001$. Data are presented as mean ± SEM. All data are representative of 2-3 independent experiments.

3.5 Discussion

In this study, we reveal a new epigenetic mechanism through which type I interferon signaling suppresses keratinocyte-mediated inflammation during wound repair. We demonstrate that IFNβ induces expression of the histone methyltransferase SETDB2 via JAK/STAT1 signaling, leading to H3K9me3 deposition at inflammatory cytokine promoters and subsequent transcriptional repression in wound keratinocytes. In diabetic wounds, disruption of this IFNβ/JAK/STAT1/SETDB2 axis results in excessive keratinocyte inflammatory cytokine production that contributes to impaired healing, as summarized in our working model (Figure 3-6). Importantly, therapeutic restoration of IFNβ signaling in diabetic mice enhanced SETDB2 expression in keratinocytes, reduced keratinocyte inflammation, and improved wound closure, suggesting a targetable pathway for diabetic wounds. This discovery aligns with emerging evidence that epigenetic mechanisms serve as master regulators of cellular plasticity in tissue repair and that chromatin modifications fundamentally control cell fate decisions during wound healing (204, 205).

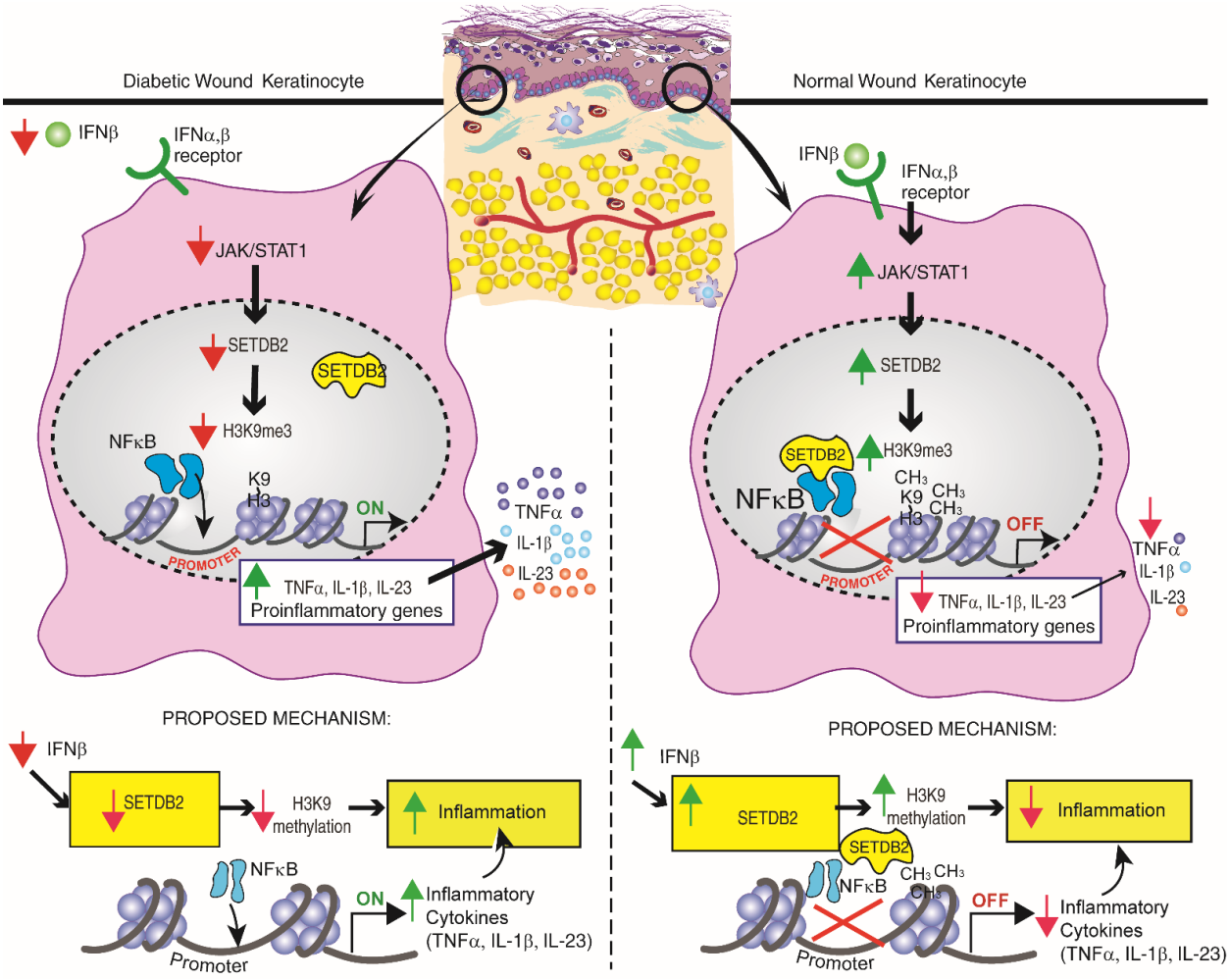


Figure 3-6: Schematic of IFNβ-mediated SETDB2 regulation of keratinocyte inflammatory cytokine gene expression in normal and diabetic wound keratinocytes

(Left) In diabetic wounds, decreased IFNβ availability leads to impaired IFNβ/JAK/STAT1 signaling and decreased SETDB2 expression and activity. Loss of SETDB2-dependent H3K9me3 at inflammatory cytokine gene promoters results in increased proinflammatory gene expression and a sustained inflammatory keratinocyte phenotype. (Right) In non-diabetic wounds, sufficient IFNβ signaling activates the IFNβ/JAK/STAT1 pathway, inducing SETDB2 expression. SETDB2-mediated H3K9me3 deposition at inflammatory cytokine gene promoters functions as an epigenetic checkpoint that restrains keratinocyte inflammation and promotes proper wound repair.

Our findings position SETDB2 as a critical epigenetic checkpoint controlling keratinocyte inflammatory responses. While keratinocytes have long been recognized as initiators of wound inflammation through cytokine and chemokine production (19, 20, 100, 108, 186-188), the mechanisms restraining this inflammatory potential remain poorly understood. Previous work by our group established that CMEs regulate immune cell phenotypes during wound repair (15, 56,

68, 69, 115, 131, 164, 171, 201); however, epigenetic control of structural cells like keratinocytes has been largely underexplored. By demonstrating that SETDB2 deposits repressive H3K9me3 marks at key inflammatory gene promoters, we show how keratinocytes modulate their inflammatory output in a temporally controlled manner—allowing early cytokine production yet preventing persistent inflammation that hinders re-epithelialization. The H3K9me3 mark has been established as a fundamental repressive modification that maintains cellular identity and prevents aberrant gene activation (206). In skin, H3K9 methylation patterns are dynamically regulated during differentiation and have been implicated in maintaining epidermal homeostasis (207). Recent advances in chromatin profiling have revealed that wound-edge keratinocytes undergo extensive chromatin remodeling, with loss of heterochromatin marks associated with enhanced migratory and proliferative capacity (208).

The identification of IFNβ as an upstream regulator of SETDB2 provides mechanistic insight into how type I interferons modulate wound inflammation. Although JAK/STAT signaling is implicated in inflammatory skin disease (196-199), its regulation of wound keratinocytes was not previously understood. We show that IFNβ induces SETDB2 through STAT1, linking interferon signaling directly to chromatin modification. This pathway appears especially important during the early inflammatory phase when cytokine expression requires tight temporal control. Our results demonstrate that keratinocyte-specific *Setdb2* deficiency delays wound closure, further supporting this requirement. Type I interferons have been recognized as critical coordinators of tissue repair, with roles extending beyond antiviral immunity to include regulation of cell proliferation, differentiation, and inflammatory responses in a context-dependent manner (209). In epithelial tissues, interferon signaling has been shown to regulate barrier function and antimicrobial peptide production (210). The connection between interferon signaling and

chromatin modification has been established in immune cells, where STAT-dependent recruitment of chromatin remodelers shapes transcriptional responses (211).

The dysregulation of the IFNβ/SETDB2 axis in diabetic wounds provides a molecular explanation for the chronic inflammatory state characteristic of impaired diabetic healing. Our findings in both human T2D patient wounds and murine diabetic models consistently showed decreased SETDB2 expression coupled with increased inflammatory cytokine expression in keratinocytes. This aligns with our previous work demonstrating reduced type I interferon levels in diabetic wounds (15, 21), but extends these observations by defining downstream epigenetic consequences in keratinocytes. The correlation between decreased SETDB2 expression and increased inflammatory marker expression in human diabetic keratinocyte subsets suggests this mechanism is clinically relevant. Moreover, bulk RNA-seq analysis revealing diminished interferon-stimulated gene and JAK/STAT pathway activity in *db/db* keratinocytes indicates a broader suppression of interferon responsiveness that likely contributes to multiple aspects of impaired diabetic wound repair beyond inflammation. Metabolic dysfunction has been shown to alter epigenetic landscapes in multiple cell types, with hyperglycemia inducing changes in histone modifications through altered metabolite availability (212). In diabetic complications, aberrant histone methylation patterns have been linked to persistent gene expression changes that contribute to metabolic memory (213).

Our therapeutic findings highlight the importance of cell-specific targeting when modulating interferon pathways. The observation that systemic JAK inhibitors may impair wound repair-associated epithelial responses in pre-clinical settings (214) underscores that indiscriminate suppression of interferon signaling may harm key reparative populations such as keratinocytes. In contrast, localized restoration of IFNβ improved healing by re-establishing SETDB2-mediated

repression of inflammatory genes in keratinocytes. This supports a broader framework in which reprogramming the epigenetic state of specific cell types—rather than blocking individual cytokines—may more effectively reverse chronic wound pathology. The concept of epigenetic reprogramming as a therapeutic strategy has gained traction, with evidence that transient modulation of chromatin states can induce lasting cellular changes (215).

Several limitations merit consideration when interpreting these findings. First, given that IFNβ levels are reduced in diabetic wounds (21), identifying the upstream mechanisms suppressing type I interferon production in diabetic skin represents a critical knowledge gap. Prior work from our group demonstrated dysregulated plasmacytoid dendritic cell (pDC) responses in diabetes (115), marked by increased NF-κB-driven inflammatory cytokine production rather than type I IFN secretion. This shift may contribute to the IFNβ deficiency observed in this study, but further investigation is required. Mitochondrial dysfunction, which is prevalent in diabetic tissues (216), has been linked to impaired interferon responses through disruption of mitochondrial DNA-sensing pathways (217). Second, while we demonstrated that IFNβ treatment improves diabetic wound healing, the systemic effects of subcutaneous IFNβ administration likely extend beyond keratinocytes to influence other cell types including immune cells and fibroblasts. The relative contributions of SETDB2 modulation in different cell populations remain to be determined. Additionally, our ChIP analyses examined selected inflammatory gene promoters; comprehensive mapping of SETDB2 genomic targets through ChIP-seq would provide deeper insight into its regulatory scope. The diabetic wound microenvironment contains multiple factors beyond hyperglycemia that could influence epigenetic regulation, including hypoxia, oxidative stress, and altered mechanical forces (1). Lastly, our murine models (DIO and *db/db* mice) may not fully recapitulate the complexity of human T2D, particularly regarding disease duration and

comorbidities. Our analyses focused primarily on day 5 post-wounding, capturing early inflammatory events but potentially missing later repair phases where SETDB2 might play additional roles.

In conclusion, this study establishes the IFNβ/JAK/STAT1/SETDB2 axis as a critical epigenetic mechanism controlling keratinocyte inflammatory responses during wound repair. Loss of this regulatory pathway in diabetes results in excessive keratinocyte-mediated inflammation that impairs healing. The demonstration that IFNβ treatment can restore SETDB2 function and improve diabetic wound closure provides proof-of-principle for therapeutic targeting of this pathway. As chronic wounds affect millions of diabetic patients worldwide with limited treatment options, strategies to modulate keratinocyte epigenetic states through the IFNβ/SETDB2 axis represent a promising avenue for developing novel therapeutics. These findings underscore the importance of understanding cell-specific epigenetic regulation in diabetic complications and highlight how restoring normal epigenetic control mechanisms may overcome pathologic cellular phenotypes in chronic disease states. Understanding how systemic metabolic disease corrupts local tissue epigenetic programs may reveal common therapeutic targets across diabetic end-organ complications.

Chapter 4 – Discussion and Future Directions

4.1.1 Summary of Dissertation Findings

This dissertation establishes a comprehensive framework for understanding how cytokine signaling drives epigenetic programs in keratinocytes in T2D wounds, fundamentally altering their capacity for migration, proliferation, and immune regulation. The findings from Chapters 2 and 3 reveal that keratinocyte dysfunction in diabetic wounds is not merely a passive consequence of the hyperglycemic environment but rather results from active epigenetic remodeling driven by specific cytokine-chromatin modifier axes.

The IL-17A/JMJD3 pathway identified in Chapter 2 and the IFNβ/SETDB2 mechanism elucidated in Chapter 3 represent complementary but distinct modes of epigenetic dysregulation in diabetic wounds. Elevated IL-17A signaling promotes JMJD3-mediated removal of repressive H3K27me3 marks, resulting in increased expression of anti-migratory and inflammatory genes in keratinocytes. In parallel, decreased IFNβ signaling in diabetic wounds leads to decreased SETDB2 expression and loss of H3K9me3-mediated repression at inflammatory gene loci, permitting excessive inflammatory gene expression. Together, these alterations drive an epigenetic state in keratinocytes that is characterized by impaired migration and increased inflammation, which may contribute to delayed re-epithelialization and wound chronicity. The spatial and temporal interplay of these pathways likely influences whether wounds progress toward resolution or persist as chronic non-healing lesions.

Importantly, our findings demonstrate that keratinocytes function as both targets and mediators of epigenetic dysfunction in diabetic wounds. Keratinocytes not only respond to cytokines through epigenetic changes but also produce factors that propagate dysfunction to neighboring cells (21, 76). This positions keratinocytes as central orchestrators of the dysregulated wound microenvironment, challenging the traditional view of these cells as passive structural components. The bidirectional communication between keratinocytes and immune cells, mediated through cytokine-epigenetic signaling cascades, establishes self-reinforcing loops that maintain pathological wound states.

4.1.2 Keratinocyte Epigenetic Regulation in Chronic Wounds

The epigenetic mechanisms identified in this dissertation build upon and extend prior work on inflammatory regulation in wound healing, including studies from our group and others examining chromatin-modifying enzymes in immune cells. JMJD3 has been extensively studied in macrophages, where it promotes inflammatory gene expression and polarization programs (69, 76, 131). Our findings expand the functional scope of JMJD3 by demonstrating a keratinocyte-intrinsic role in regulating genes that directly impair migration. Specifically, we identify integrin α3 (*Itga3*) and TIMP1 (*Timp1*) as previously unrecognized JMJD3-dependent targets whose upregulation contributes to an anti-migratory keratinocyte phenotype. These data highlight how H3K27me3 removal by JMJD3 can enforce maladaptive epithelial programs in the diabetic wound environment.

In contrast, Chapter 3 identifies SETDB2 as a key epigenetic regulator that normally constrains keratinocyte inflammatory gene expression through H3K9 trimethylation. Importantly, IFNβ signaling and SETDB2 expression are decreased in diabetic wounds, resulting in loss of repressive H3K9me3 marks at inflammatory gene loci and increased keratinocyte cytokine

production. This mechanism provides insight into how diminished anti-inflammatory epigenetic control contributes to the sustained inflammatory milieu characteristic of chronic diabetic wounds. Along with prior studies from our group and others implicating dysregulated inflammatory signaling in diabetic wounds (66), these findings point to defective inflammatory resolution as a key feature of impaired healing.

Recent studies have demonstrated that diabetic wound keratinocytes exhibit genome-wide DNA hypermethylation associated with suppression of epithelial-mesenchymal transition programs (218). In parallel, our findings identify histone modification changes in diabetic keratinocytes, indicating that multiple layers of epigenetic regulation may contribute to altered keratinocyte states in chronic wounds. Together, these observations suggest that interactions between DNA methylation and histone modifications may establish an epigenetic landscape that predisposes keratinocytes toward non-healing phenotypes.

The keratinocyte-immune cell crosstalk described in this work further supports the evolving view of keratinocytes as active immune regulators rather than passive structural cells. Prior studies from our group demonstrated that keratinocyte-derived IL-1α induces JMJD3 expression in macrophages, promoting inflammasome activation and inflammatory amplification (76). Our reciprocal findings show that immune-derived cytokines, including IL-17A and IFNβ, directly reprogram keratinocyte chromatin states, establishing bidirectional epigenetic communication as a defining feature of the wound microenvironment. Dysregulation of this crosstalk likely amplifies pathological signaling across multiple cell types in diabetic wounds.

Finally, the role of IL-17A in driving keratinocyte dysfunction through JMJD3 is consistent with prior work from our group identifying a potential plasmacytoid dendritic cell (pDC)-T_H17 differentiation axis in diabetic wounds (115). In this study, pDC-derived IL-6 and TGF-β promotes

skewing of $CD4^+$ T cells toward a T_H17 phenotype, potentially resulting in sustained IL-17A signaling within diabetic wounds. This framework provides mechanistic context for how epigenetically regulated cytokine production in upstream immune populations may indirectly drive keratinocyte epigenetic remodeling and dysfunction. Together, these studies highlight the integrated and multicellular nature of epigenetic dysregulation in chronic wound healing.

4.1.3 WHSC1 as a Potential Epigenetic Regulator of Keratinocyte Proliferation

Having identified epigenetic regulators of keratinocyte inflammation and migration, investigation of epigenetic control of keratinocyte proliferation represents a logical extension of this work. Our preliminary studies, presented at the 2025 Society for Investigative Dermatology meeting, identify Wolf-Hirschhorn syndrome candidate 1 (WHSC1/NSD2/MMSET) as a critical regulator of keratinocyte proliferation and differentiation in wound healing.

WHSC1, an epigenetic enzyme that catalyzes modifications at the histone H3 at lysine 36 site (H3K36me2) (219), demonstrates dynamic expression patterns during keratinocyte differentiation. Previous studies have implicated WHSC1 in promoting tumor progression across multiple cancer types through regulation of cell survival and cell cycle programs (220-224). However, the role of WHSC1 in normal keratinocyte biology, particularly in the context of normal and pathologic wound healing, has not been previously explored.

We first developed an *in vitro* calcium switch model in this study to compare epigenetic programs in basal (proliferative) and differentiated (non-proliferative) keratinocytes. Primary keratinocytes were isolated from the epidermal layer of tails of C57BL/6 mice via trypsinization and cultured for 1 day in low calcium (LoCa) medium with 0.05 mM Ca^{2+} concentration. *In vitro* differentiation was induced by switching to a high calcium (HiCa) medium with 0.3 mM Ca^{2+} concentration overnight. Using this *in vitro* calcium switch model, we validated basal and

differentiated states through morphological assessment (Figure 4-1A), reduced proliferative capacity measured by alamarBlue assays (Figures 4-1B, C), a cycling marker PCR array (Figure 4-1D), and qPCR analysis of proliferation and differentiation genes (Figure 4-1E). Basal keratinocytes cultured without calcium switch exhibited increased expression of proliferation-associated genes (*E2f7*, *Cdc7*, *Pcna*), whereas high-calcium–treated keratinocytes showed increased expression of differentiation markers (*Flg*, *Vim*) (Figure 4-1E). Within this validated system, we performed an unbiased epigenetic super array and found that WHSC1 was one of the enzymes that displayed decreased expression in differentiated keratinocytes compared to basal keratinocytes (Figure 4-2A). We further confirmed that WHSC1 expression was significantly downregulated following high-calcium-induced differentiation (Figure 4-2B). These findings suggest that WHSC1 may contribute to regulation of the keratinocyte proliferation-differentiation transition, a process critical for effective wound re-epithelialization.

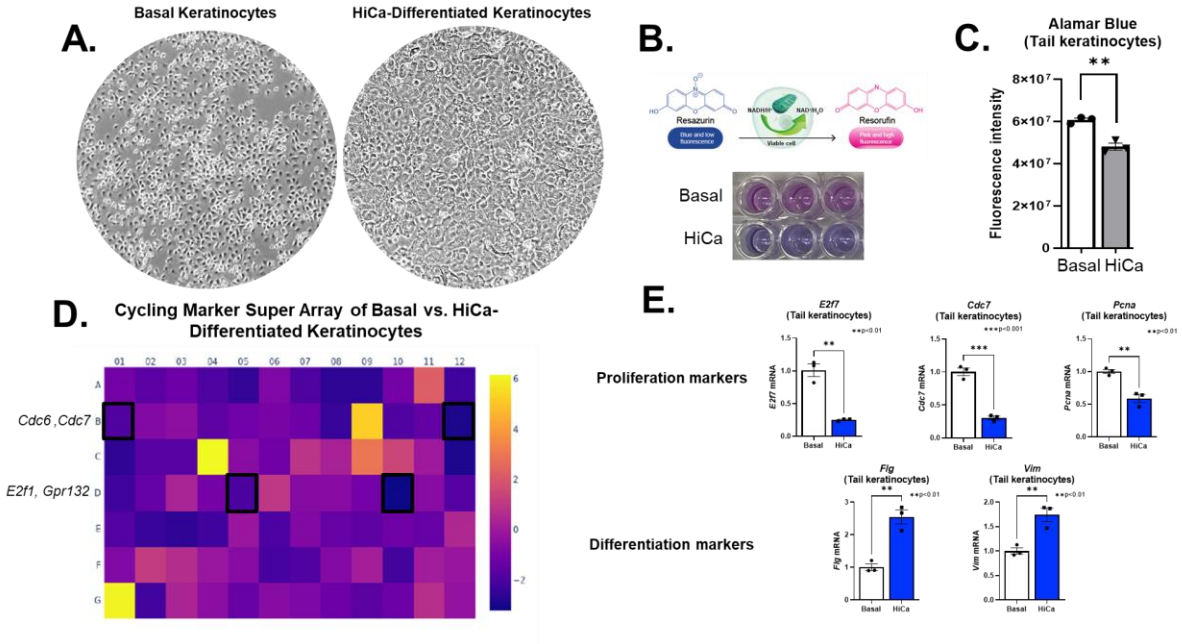


Figure 4-1: HiCa-differentiated keratinocytes display decreased proliferation rates and proliferative gene expression (A) Images of cultured basal vs. *in vitro* HiCa-differentiated primary murine keratinocytes (B) Schematic of alamarBlue reaction and image of basal and differentiated keratinocytes after alamarBlue treatment (C) Quantification of alamarBlue fluorescence intensity (N=3/group) (D) Cycling marker PCR array of basal and differentiated keratinocytes (E) qPCR of select proliferation (*E2f7, Cdc7, Pcna*) and differentiation (*Flg, Vim)* markers (N=3/group).

Data were analyzed for variances, and 2-tailed student t-test was performed. **p < 0.01 and ***p < 0.001. Data are presented as mean and SEM.

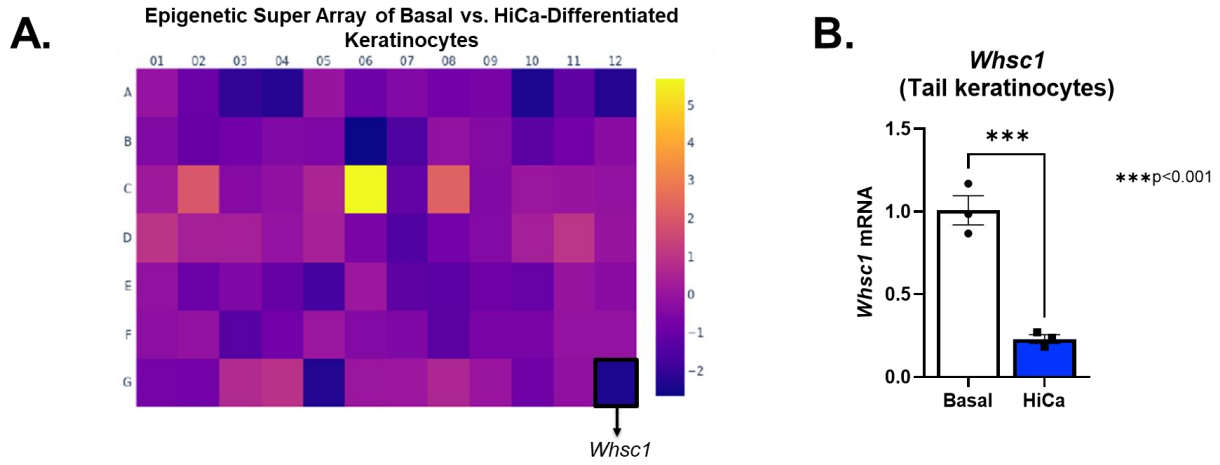


Figure 4-2: HiCa-differentiated keratinocytes display decreased *Whsc1*
(A) Epigenetic enzyme gene PCR array of basal and differentiated keratinocytes (B) qPCR of *Whsc1* in basal and differentiated keratinocytes (N=3/group). Data were analyzed for variances, and 2-tailed student t-test was performed. ***p < 0.001. Data are presented as mean and SEM.

Single-cell RNA sequencing analysis of human wound tissue revealed elevated WHSC1 expression specifically in cycling keratinocytes, with decreased expression in differentiated keratinocyte populations (Figures 4-3A, B). Comparative transcriptomic analysis of WHSC1-high versus WHSC1-low keratinocyte subsets identified enrichment of proliferation markers including *CDC7*, *E2F7*, *E2F2*, and *PCNA* in WHSC1-high cells, while differentiation markers such as filaggrin (*FLG*) and vimentin (*VIM*) were enriched in WHSC1-low populations (Figure 4-3C). These expression patterns position WHSC1 as a master regulator maintaining keratinocytes in a proliferative state.

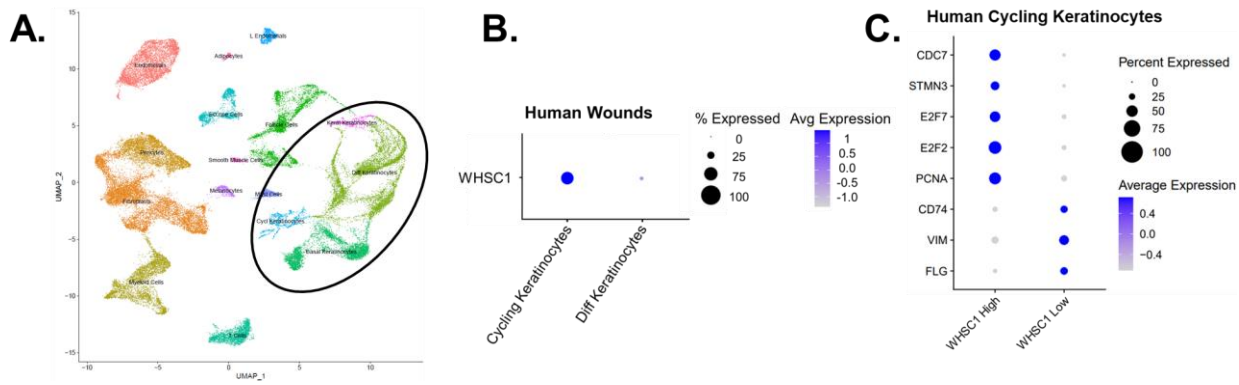


Figure 4-3: WHSC1 gene expression is increased in proliferative keratinocytes in human wounds
(A) Human single cell transcriptional profiling of diabetic wounds (N=10) versus control wounds (N=10). (B) Dot plot of *WHSC1* expression in cycling and differentiated keratinocytes. Dot size corresponds to the proportion of cells within the group expressing *WHSC1*, and dot color corresponds to expression level. (C) Dot plot of cycling (*CDC7, STMN3, E2F7, E2F2, PCNA)* and differentiation *(CD74, VIM, FLG)* marker expression in WHSC1-High and WHSC1-Low expressing cells from the cycling keratinocyte subset.

Genetic and functional validation using both siRNA-mediated knockdown and pharmacological inhibition with LEM-14 (150 μM) confirmed WHSC1's role in promoting keratinocyte proliferation. 75% siRNA-knockdown of *Whsc1* (Figure 4-4A) resulted in decreased expression of proliferative genes (*E2f2, E2f7, Cdc7*) and increased expression of differentiation gene *Flg* (Figure 4-4B). Pharmacological inhibition of WHSC1 induced morphological changes in primary murine keratinocytes consistent with reduced proliferation, including decreased cell spreading and cell density (Figure 4-4C), and was accompanied by significant downregulation of proliferation-associated genes (*E2f2*, *Cdc7*, *E2f7*, *Pcna*) and upregulation of differentiation markers (*Flg*, *Vim*) (Figure 4-4D). WHSC1 is a histone methyltransferase that adds H3K36me2 methyl marks, thereby activating transcription (Figure 4-4E). Chromatin immunoprecipitation assays demonstrated that WHSC1 inhibition decreased H3K36me2 marks at proliferative gene promoters, confirming direct epigenetic regulation (Figure 4-4F). Functionally, WHSC1 inhibition reduced keratinocyte proliferation rates as measured by alamarBlue assays (Figures 4-5A, B) and impaired wound closure in scratch assays (Figures 4-5C, D).

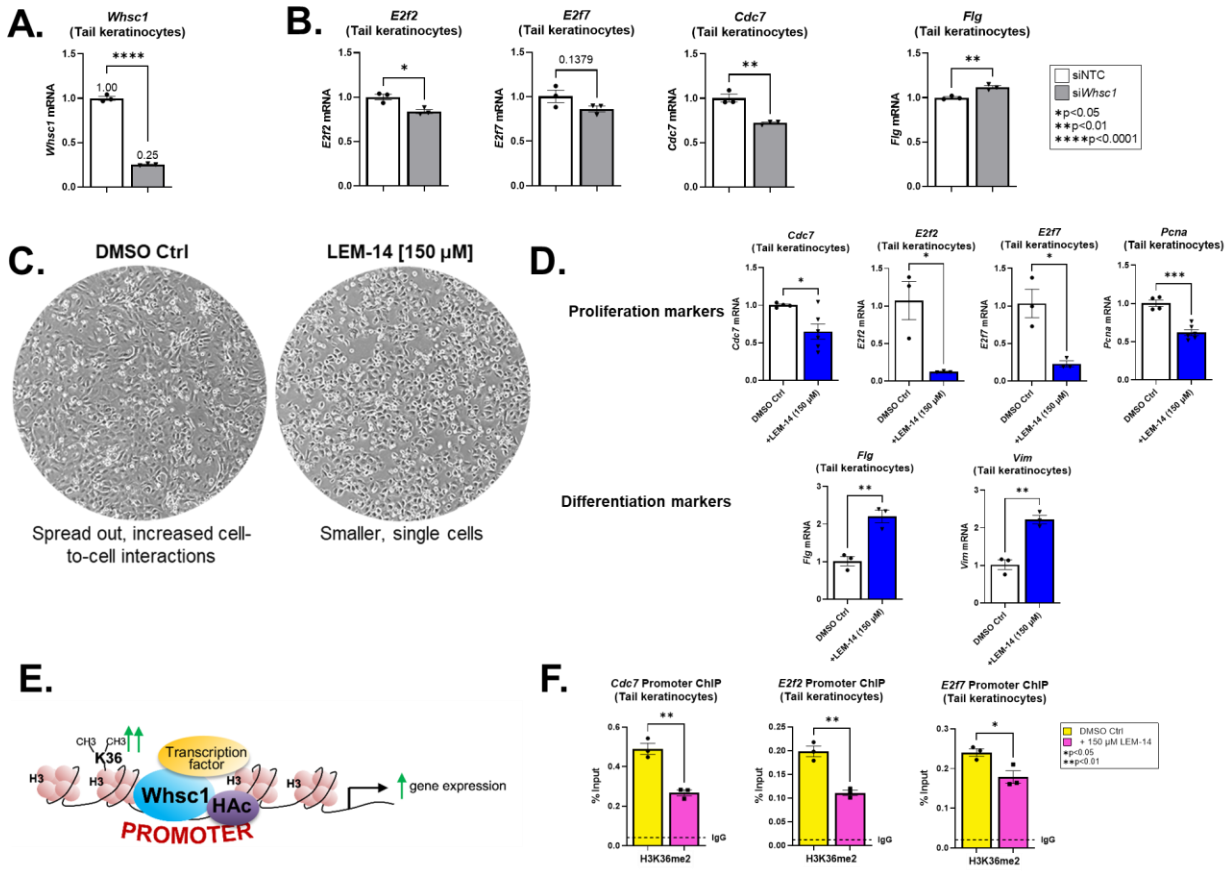


Figure 4-4: siRNA targeting and pharmacological inhibition of *Whsc1* results in decreased proliferative gene expression via reduction of K36me2

(A) Cultured primary murine keratinocytes were transfected with non-targeting control siRNA (siNTC) or si*Whsc1* (Accell, Dharmacon) for 72 hr. 75% knockdown of *Whsc1* was confirmed via qPCR (N=3/group) (B) Proliferative (*E2f2, E2f7, Cdc7*) and differentiation (*Flg)* marker expression was analyzed via qPCR (N=3/group). (C) Representative image of cultured primary murine keratinocytes treated with DMSO only or LEM-14 (150 µM) for 24 hr (D) DMSO control or LEM-14 (150 µM) treated murine keratinocytes were analyzed for proliferative (*Cdc7, E2f2, E2f7, Pcna*) and differentiation (*Flg, Vim*) marker expression via qPCR (N=3-6/group) (E) Schematic of WHSC1-mediated regulation of gene expression (F) ChIP of the H3K36me2 mark on *Cdc7, E2f2, E2f7* gene promoters in tail keratinocytes treated with DMSO only or LEM-14 (150 µM) for 6 hr (N=3/group). Data were analyzed for variances, and 2-tailed student t-test was performed. *p < 0.05, **p < 0.01, ***p < 0.001 and ****p < 0.0001. Data are presented as mean and SEM.

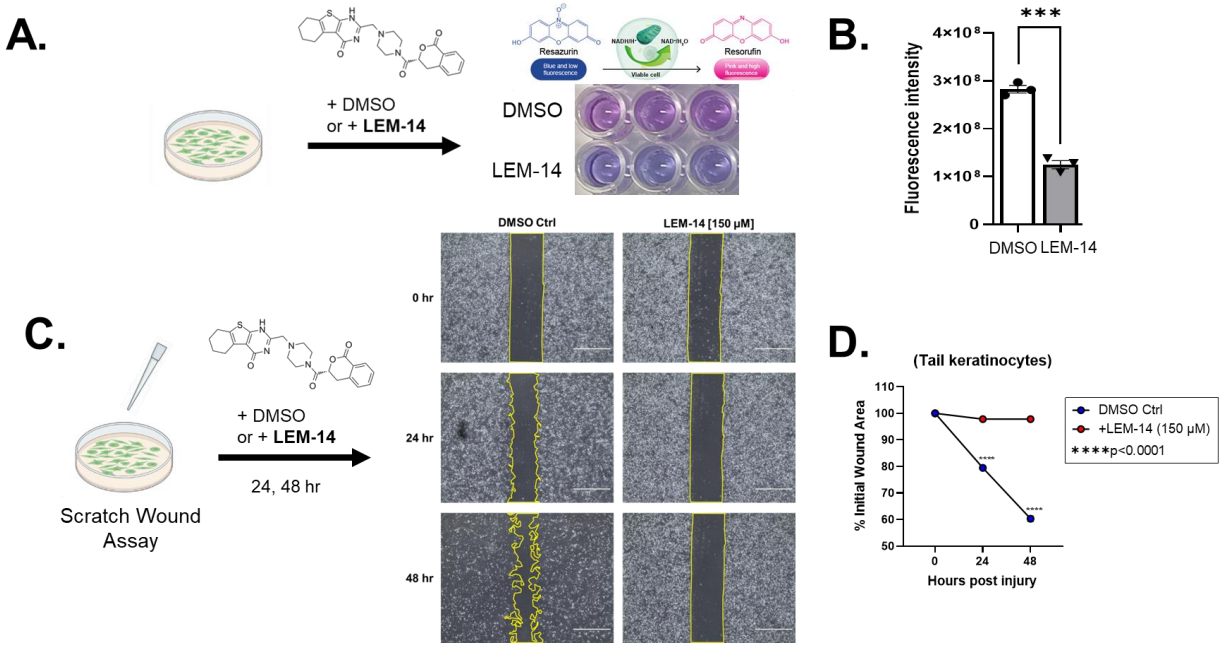


Figure 4-5: Pharmacological inhibition of *Whsc1* results in decreased proliferation and wound closure rates
(A) Schematic of alamarBlue reaction and image of 24 hr DMSO only or LEM-14 (150 µM) treated tail keratinocytes after alamarBlue treatment (B) Quantification of alamarBlue fluorescence intensity (N=3/group) (C) Cultured tail keratinocytes were scratched with sterile 20 µl pipette tips. Wells were washed once and replaced with medium containing DMSO only or LEM-14 (150 µM). Representative images of scratch wound areas at 0, 24, 48 hr (D) Wound area was measured using ImageJ software. Comparisons were made using images taken at the same location of each well. %T0 Wound Area was calculated using the following equation: $\%T0\ \text{Wound Area} = \frac{A(T24\ \text{or}\ 48)}{A(T0)} \times 100\%$ (N=3/group). Data were analyzed for variances, and 2-tailed student t-test was performed. ***p < 0.001 and ****p < 0.0001. Data are presented as mean and SEM.

The calcium-dependent regulation of WHSC1 provides mechanistic insight into how the wound microenvironment controls keratinocyte behavior. Primary murine keratinocytes were treated with the calcium-sensing receptor inhibitor CalHex-231 (40 µM), and effective inhibition of calcium-dependent intracellular signaling was confirmed by Ca^{2+} flux fluorescence assays (Figure 4-6A) and associated morphological changes indicative of impaired differentiation, including reduced cell spreading (Figure 4-6B). Treatment with CalHex-231 prevented calcium-induced WHSC1 downregulation and maintained proliferative gene expression while decreasing differentiation gene expression even under high-calcium conditions (Figure 4-6C). This suggests

that calcium gradients within healing wounds, disrupted in diabetic conditions, may contribute to aberrant WHSC1 regulation and impaired re-epithelialization.

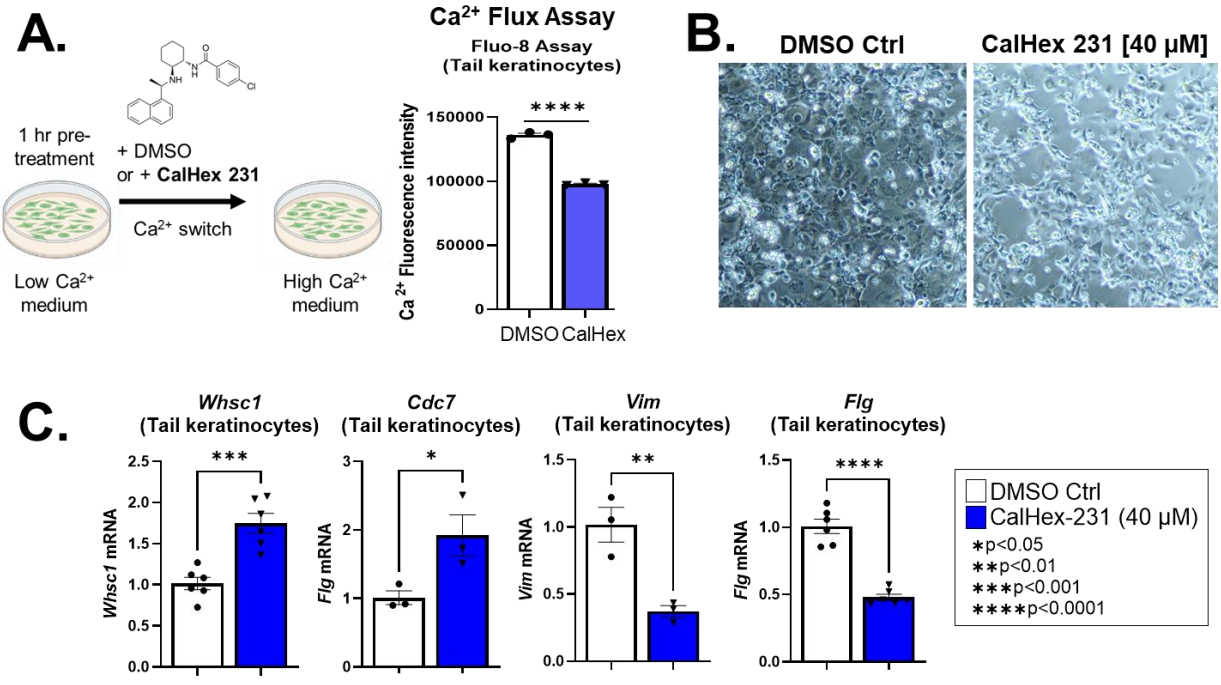


Figure 4-6: Inhibition of calcium signaling results in increased *Whsc1* and proliferative gene expression
(A) Schematic of CalHex-231 treatment of cultured tail keratinocytes. Fluo-8 reagent was added 10 min after switching to HiCa medium to confirm decreased Ca^{2+} influx (B) Representative images of 24 hr DMSO only or CalHex-231 (40 µM) treated keratinocytes (C) *Whsc1,* proliferative (*Cdc7*) and differentiation (*Vim, Flg*) marker expression was analyzed via qPCR *(*N=3-6/group) Data were analyzed for variances, and 2-tailed student t-test was performed. *p < 0.05, **p < 0.01, ***p < 0.001, and ****p < 0.0001. Data are presented as mean and SEM.

In vivo validation using a murine wound healing model demonstrated that subcutaneous administration of LEM-14 (1 mg/kg daily) significantly delayed wound closure compared to vehicle controls (Figures 4-7A, B). While these findings suggest that appropriate WHSC1 activity is necessary for normal wound healing, they also raise the possibility that dysregulated WHSC1 in diabetic wounds could contribute to impaired healing. Further investigation is warranted to determine whether WHSC1 expression or activity is altered in diabetic versus normal wounds and whether targeted modulation could enhance healing.

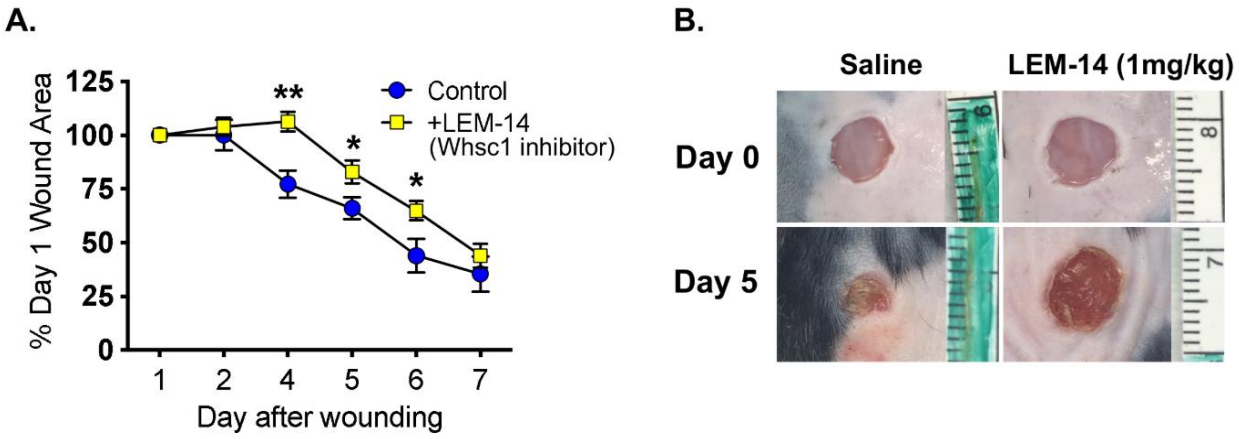


Figure 4-7: Pharmacological inhibition of WHSC1 results in delayed wound repair
(A) 4 mm punch biopsy wounds were created on C57Bl/6 mice. Mice were subcutaneously injected with saline or LEM-14 (1 mg/kg). The change in wound area was recorded daily and analyzed with ImageJ software. (N=6/group) Data were analyzed for variances, and one-way ANOVA was performed. *$p < 0.05$ and **$p < 0.01$. Data are presented as mean and SEM.

These preliminary findings identify WHSC1 as a novel epigenetic regulator controlling the critical balance between keratinocyte proliferation and differentiation during wound healing. The integration of WHSC1 with the JMJD3 and SETDB2 pathways suggests a comprehensive epigenetic network wherein distinct chromatin-modifying enzymes coordinate different aspects of keratinocyte function—migration, inflammation, and proliferation—to orchestrate successful wound repair.

4.1.4 Broader Impact and Translational Implications

The identification of targetable epigenetic mechanisms underlying keratinocyte dysfunction in diabetic wounds has significant implications for developing novel therapeutic strategies. Current treatments for chronic diabetic wounds primarily focus on wound debridement, infection control, and growth factor supplementation, with limited success in addressing the fundamental cellular dysfunction (48, 59, 60, 189, 204). Our findings suggest that epigenetic

reprogramming represents an underexplored therapeutic avenue with the potential to restore normal keratinocyte function.

The druggability of chromatin-modifying enzymes offers immediate translational potential. In our previous work, cell-specific nanoparticle delivery of JMJD3 inhibitors such as GSK-J4 have shown efficacy in preclinical models (69), and recent findings suggest that topical application to target wound-edge keratinocytes could enhance re-epithelialization (225). Similarly, selective modulation of SETDB2 activity could restore appropriate inflammatory responses without triggering excessive inflammation. The development of these wound-specific delivery systems could enable precise spatial and temporal control of epigenetic modulation.

Beyond diabetic wounds, our findings have implications for other chronic inflammatory skin conditions characterized by keratinocyte dysfunction. Psoriasis, atopic dermatitis, and other inflammatory dermatoses involve aberrant keratinocyte responses to cytokine signaling (123). The epigenetic mechanisms identified here may contribute to pathological keratinocyte states in these conditions, suggesting broader therapeutic applications for epigenetic modulators.

The concept of epigenetic memory in wound healing raises important considerations for therapeutic timing (213, 226). Our findings suggest that early intervention to prevent establishment of pathological epigenetic states may be more effective than attempting to reverse established dysfunction. This has implications for diabetic patient management, where prophylactic epigenetic modulation in high-risk patients could prevent wound chronicity.

The integration of our findings with emerging technologies such as CRISPR-based epigenome editing offers exciting possibilities for precision medicine approaches (227). The ability to selectively modify histone marks at specific genomic loci could enable targeted restoration of normal gene expression patterns without affecting global chromatin states. Recent

advances in tissue nanotransfection technology (228) demonstrate the feasibility of delivering epigenetic modulators directly to wound tissue, potentially enabling *in situ* epigenetic reprogramming.

4.1.5 Limitations and Future Directions

While this dissertation provides important mechanistic insights, several limitations must be acknowledged. First, the majority of our experiments utilized *in vitro* systems that, while allowing precise mechanistic dissection, may not fully recapitulate the complex wound microenvironment. Future studies should validate these findings using more sophisticated model systems, including organotypic skin cultures and humanized mouse models that better represent human wound healing physiology.

Second, our studies focused primarily on histone modifications, yet epigenetic regulation encompasses DNA methylation, non-coding RNAs, and chromatin remodeling complexes. The interplay between these different epigenetic mechanisms remains incompletely understood. Future work should employ integrated multi-omics approaches combining ChIP-seq, ATAC-seq, bisulfite sequencing, and RNA-seq to comprehensively map the epigenetic landscape of diabetic wound keratinocytes.

Third, the heterogeneity of keratinocyte populations in wounds presents analytical challenges. Our single-cell RNA sequencing data reveal distinct keratinocyte subsets with varying epigenetic states, yet our functional studies primarily used bulk populations. Future investigations should employ single-cell epigenomics techniques to resolve subset-specific epigenetic programs and their functional consequences.

The temporal dynamics of epigenetic changes during wound healing require further investigation. Our studies provide snapshots at specific time points, but wound healing is a

dynamic process where the timing of epigenetic modifications may be critical. Longitudinal studies tracking epigenetic changes from injury through resolution or chronicity would provide valuable insights into therapeutic windows for intervention.

Future therapeutic development should focus on several key areas:

1) Combination Epigenetic Therapy: Given the multiple epigenetic alterations identified, combination approaches targeting different chromatin modifiers (229) may be necessary. The development of dual inhibitors or sequential treatment protocols could address the complex epigenetic dysfunction in diabetic wounds.
2) Cell-Type Specific Delivery: Technologies for selective delivery of epigenetic modulators to specific cell populations within wounds would minimize off-target effects (69, 225). Keratinocyte-specific promoters driving expression of epigenetic modifiers could enable precise therapeutic targeting.
3) Biomarker Development: Identification of epigenetic biomarkers predicting wound healing outcomes could enable personalized treatment strategies. Circulating cell-free DNA bearing specific histone modifications or DNA methylation patterns (230) could serve as non-invasive indicators of wound epigenetic states.
4) Prevention Strategies: Understanding the establishment of pathological epigenetic states could inform preventive interventions in high-risk diabetic patients. Prophylactic modulation of epigenetic regulators before wound occurrence represents an unexplored therapeutic paradigm.
5) Systems Biology Approaches: Integration of epigenetic data with metabolomic, proteomic, and transcriptomic datasets using systems biology approaches could reveal

emergent properties of the wound healing system not apparent from studying individual pathways.

The role of metabolic dysfunction in driving epigenetic changes warrants further investigation. Hyperglycemia, advanced glycation end products, and altered lipid metabolism in diabetes may directly influence chromatin-modifying enzyme activity (49, 94, 101, 176, 231). Understanding these metabolic-epigenetic connections could identify upstream interventions to prevent epigenetic dysfunction.

Finally, translation of these findings to clinical applications will require careful consideration of safety and efficacy. While epigenetic modulators show promise, their effects on normal wound healing and potential for off-target consequences must be thoroughly evaluated. The development of wound-specific, temporally controlled epigenetic interventions represents both a significant challenge and opportunity for advancing diabetic wound care.

4.1.6 Conclusions

This dissertation establishes epigenetic dysregulation as a fundamental mechanism underlying keratinocyte dysfunction in T2D wound healing. The identification of the IL-17A/JMJD3 and IFNβ/SETDB2 axes, along with preliminary findings on WHSC1-mediated proliferation control, provides a comprehensive framework for understanding how inflammatory signals are translated into alterations in keratinocyte gene expression programs. These findings position chromatin-modifying enzymes as promising therapeutic targets for restoring normal keratinocyte function and promoting healing in chronic diabetic wounds.

The broader implications of this work extend beyond wound healing to fundamental understanding of how cells integrate environmental signals through epigenetic mechanisms. The demonstration that cytokines can drive lasting changes in cellular behavior through histone

modifications highlights epigenetics as a critical mediator of cellular plasticity and dysfunction. As the global burden of diabetes continues to rise, understanding and targeting these epigenetic mechanisms becomes increasingly important for developing effective treatments for diabetic complications.

Bibliography

1. Gurtner, G. C., Werner, S., Barrandon, Y. & Longaker, M. T. Wound repair and regeneration. *Nature* **453**, 314-321 (2008).
2. Eming, S. A., Martin, P. & Tomic-Canic, M. Wound repair and regeneration: mechanisms, signaling, and translation. *Sci Transl Med* **6**, 265sr266 (2014).
3. Werner, S., Krieg, T. & Smola, H. Keratinocyte-fibroblast interactions in wound healing. *J Invest Dermatol* **127**, 998-1008 (2007).
4. Shaw, T. J. & Martin, P. Wound repair: a showcase for cell plasticity and migration. *Curr Opin Cell Biol* **42**, 29-37 (2016).
5. Rodrigues, M., Kosaric, N., Bonham, C. A. & Gurtner, G. C. Wound Healing: A Cellular Perspective. *Physiol Rev* **99**, 665-706 (2019).
6. Nurden, A. T. The biology of the platelet with special reference to inflammation, wound healing and immunity. *Front Biosci (Landmark Ed)* **23**, 726-751 (2018).
7. Barrientos, S., Stojadinovic, O., Golinko, M. S., Brem, H. & Tomic-Canic, M. Growth factors and cytokines in wound healing. *Wound Repair Regen* **16**, 585-601 (2008).
8. Ramirez, H., Patel, S. B. & Pastar, I. The Role of TGFβ Signaling in Wound Epithelialization. *Adv Wound Care (New Rochelle)* **3**, 482-491 (2014).
9. Wilgus, T. A. Inflammation as an orchestrator of cutaneous scar formation: a review of the literature. *Plast Aesthet Res* **7** (2020).
10. Wang, J. Neutrophils in tissue injury and repair. *Cell Tissue Res* **371**, 531-539 (2018).

11. Wilgus, T. A., Roy, S. & McDaniel, J. C. Neutrophils and Wound Repair: Positive Actions and Negative Reactions. *Adv Wound Care (New Rochelle)* **2**, 379-388 (2013).

12. Gerlach, B. D. *et al.* Efferocytosis induces macrophage proliferation to help resolve tissue injury. *Cell Metab* **33**, 2445-2463.e2448 (2021).

13. Koh, T. J. & DiPietro, L. A. Inflammation and wound healing: the role of the macrophage. *Expert Rev Mol Med* **13**, e23 (2011).

14. Krzyszczyk, P., Schloss, R., Palmer, A. & Berthiaume, F. The Role of Macrophages in Acute and Chronic Wound Healing and Interventions to Promote Pro-wound Healing Phenotypes. *Front Physiol* **9**, 419 (2018).

15. Kimball, A. S. *et al.* The Histone Methyltransferase Setdb2 Modulates Macrophage Phenotype and Uric Acid Production in Diabetic Wound Repair. *Immunity* **51**, 258-271.e255 (2019).

16. Wolf, S. J., Melvin, W. J. & Gallagher, K. Macrophage-mediated inflammation in diabetic wound repair. *Semin Cell Dev Biol* **119**, 111-118 (2021).

17. Landén, N. X., Li, D. & Ståhle, M. Transition from inflammation to proliferation: a critical step during wound healing. *Cell Mol Life Sci* **73**, 3861-3885 (2016).

18. Tonnesen, M. G., Feng, X. & Clark, R. A. Angiogenesis in wound healing. *J Investig Dermatol Symp Proc* **5**, 40-46 (2000).

19. Jiang, Y. *et al.* Cytokinocytes: the diverse contribution of keratinocytes to immune responses in skin. *JCI Insight* **5** (2020).

20. Piipponen, M., Li, D. & Landén, N. X. The Immune Functions of Keratinocytes in Skin Wound Healing. *Int J Mol Sci* **21** (2020).

21. Wolf, S. J. *et al.* IFN-κ is critical for normal wound repair and is decreased in diabetic wounds. *JCI Insight* **7** (2022).

22. Gröne, A. Keratinocytes and cytokines. *Vet Immunol Immunopathol* **88**, 1-12 (2002).

23. Kennedy-Crispin, M. *et al.* Human keratinocytes' response to injury upregulates CCL20 and other genes linking innate and adaptive immunity. *J Invest Dermatol* **132**, 105-113 (2012).

24. Harper, E. G. *et al.* Th17 cytokines stimulate CCL20 expression in keratinocytes in vitro and in vivo: implications for psoriasis pathogenesis. *J Invest Dermatol* **129**, 2175-2183 (2009).

25. Hassanshahi, A. *et al.* Macrophage-Mediated Inflammation in Skin Wound Healing. *Cells* **11** (2022).

26. Guda, P. R. *et al.* Nanoscopic and Functional Characterization of Keratinocyte-Originating Exosomes in the Wound Fluid of Non-Diabetic and Diabetic Chronic Wound Patients. *Nano Today* **52** (2023).

27. Sharma, A. *et al.* Mitochondrial Bioenergetics of Functional Wound Closure is Dependent on Macrophage-Keratinocyte Exosomal Crosstalk. *ACS Nano* **18**, 30405-30420 (2024).

28. Zhou, X. *et al.* Exosome-Mediated Crosstalk between Keratinocytes and Macrophages in Cutaneous Wound Healing. *ACS Nano* **14**, 12732-12748 (2020).

29. Than, U. T. T., Guanzon, D., Leavesley, D. & Parker, T. Association of Extracellular Membrane Vesicles with Cutaneous Wound Healing. *Int J Mol Sci* **18** (2017).

30. Breitkreutz, D., Koxholt, I., Thiemann, K. & Nischt, R. Skin basement membrane: the foundation of epidermal integrity--BM functions and diverse roles of bridging molecules nidogen and perlecan. *Biomed Res Int* **2013**, 179784 (2013).

31. Pastar, I. *et al.* Epithelialization in Wound Healing: A Comprehensive Review. *Adv Wound Care (New Rochelle)* **3**, 445-464 (2014).

32. Mauldin, E. A. & Peters-Kennedy, J. Integumentary System. *Jubb, Kennedy & Palmer's Pathology of Domestic Animals: Volume 1*, 509-736.e501 (2016).

33. Longmate, W. M. The epidermal integrin-mediated secretome regulates the skin microenvironment during tumorigenesis and repair. *Matrix Biol* **134**, 175-183 (2024).

34. Jimenez, P. A. & Rampy, M. A. Keratinocyte growth factor-2 accelerates wound healing in incisional wounds. *J Surg Res* **81**, 238-242 (1999).

35. Johnson, K. E. & Wilgus, T. A. Vascular Endothelial Growth Factor and Angiogenesis in the Regulation of Cutaneous Wound Repair. *Adv Wound Care (New Rochelle)* **3**, 647-661 (2014).

36. Leong, A. & Kim, M. The Angiopoietin-2 and TIE Pathway as a Therapeutic Target for Enhancing Antiangiogenic Therapy and Immunotherapy in Patients with Advanced Cancer. *Int J Mol Sci* **21** (2020).

37. Joussen, A. M. *et al.* Angiopoietin/Tie2 signalling and its role in retinal and choroidal vascular diseases: a review of preclinical data. *Eye (Lond)* **35**, 1305-1316 (2021).

38. Eelen, G., Treps, L., Li, X. & Carmeliet, P. Basic and Therapeutic Aspects of Angiogenesis Updated. *Circ Res* **127**, 310-329 (2020).

39. Davis, G. E. & Senger, D. R. Endothelial extracellular matrix: biosynthesis, remodeling, and functions during vascular morphogenesis and neovessel stabilization. *Circ Res* **97**, 1093-1107 (2005).

40. Witjas, F. M. R., van den Berg, B. M., van den Berg, C. W., Engelse, M. A. & Rabelink, T. J. Concise Review: The Endothelial Cell Extracellular Matrix Regulates Tissue Homeostasis and Repair. *Stem Cells Transl Med* **8**, 375-382 (2019).

41. Aman, J. & Margadant, C. Integrin-Dependent Cell-Matrix Adhesion in Endothelial Health and Disease. *Circ Res* **132**, 355-378 (2023).

42. Xue, M. & Jackson, C. J. Extracellular Matrix Reorganization During Wound Healing and Its Impact on Abnormal Scarring. *Adv Wound Care (New Rochelle)* **4**, 119-136 (2015).

43. Hinz, B. The role of myofibroblasts in wound healing. *Curr Res Transl Med* **64**, 171-177 (2016).

44. Lau, P., Cruz, S., Keswani, S. & Olutoye, O. O. in *Pediatric Surgery: A Comprehensive Textbook for Africa* (eds Emmanuel A. Ameh *et al.*) 73-88 (Springer International Publishing, 2020).

45. Magliano, D. J., Boyko, E. J. & committee, I. D. F. D. A. t. e. s. in *Idf diabetes atlas* (International Diabetes Federation

© International Diabetes Federation, 2021., 2021).

46. Armstrong, D. G., Boulton, A. J. M. & Bus, S. A. Diabetic Foot Ulcers and Their Recurrence. *N Engl J Med* **376**, 2367-2375 (2017).

47. Beeson, S. A. *et al.* Analysis of 5-year Mortality following Lower Extremity Amputation due to Vascular Disease. *Plast Reconstr Surg Glob Open* **11**, e4727 (2023).

48. Baltzis, D., Eleftheriadou, I. & Veves, A. Pathogenesis and treatment of impaired wound healing in diabetes mellitus: new insights. *Adv Ther* **31**, 817-836 (2014).

49. El-Osta, A. *et al.* Transient high glucose causes persistent epigenetic changes and altered gene expression during subsequent normoglycemia. *J Exp Med* **205**, 2409-2417 (2008).

50. Zhang, P. *et al.* Global epidemiology of diabetic foot ulceration: a systematic review and meta-analysis (†). *Ann Med* **49**, 106-116 (2017).

51. Bellia, A., Meloni, M., Andreadi, A., Uccioli, L. & Lauro, D. Geographic and Ethnic Inequalities in Diabetes-Related Amputations. *Front Clin Diabetes Healthc* **3**, 855168 (2022).

52. Raghav, A. *et al.* Financial burden of diabetic foot ulcers to world: a progressive topic to discuss always. *Ther Adv Endocrinol Metab* **9**, 29-31 (2018).

53. Pop-Busui, R. *et al.* Diabetic Neuropathy: A Position Statement by the American Diabetes Association. *Diabetes Care* **40**, 136-154 (2017).

54. Beckman, J. A., Creager, M. A. & Libby, P. Diabetes and atherosclerosis: epidemiology, pathophysiology, and management. *Jama* **287**, 2570-2581 (2002).

55. Dowey, R., Iqbal, A., Heller, S. R., Sabroe, I. & Prince, L. R. A Bittersweet Response to Infection in Diabetes; Targeting Neutrophils to Modify Inflammation and Improve Host Immunity. *Front Immunol* **12**, 678771 (2021).

56. Kimball, A. *et al.* Ly6C(Hi) Blood Monocyte/Macrophage Drive Chronic Inflammation and Impair Wound Healing in Diabetes Mellitus. *Arterioscler Thromb Vasc Biol* **38**, 1102-1114 (2018).

57. Hadian, Y., Bagood, M. D., Dahle, S. E., Sood, A. & Isseroff, R. R. Interleukin-17: Potential Target for Chronic Wounds. *Mediators Inflamm* **2019**, 1297675 (2019).

58. Schilrreff, P. & Alexiev, U. Chronic Inflammation in Non-Healing Skin Wounds and Promising Natural Bioactive Compounds Treatment. *Int J Mol Sci* **23** (2022).

59. Margolis, D. J., Allen-Taylor, L., Hoffstad, O. & Berlin, J. A. Diabetic neuropathic foot ulcers: predicting which ones will not heal. *Am J Med* **115**, 627-631 (2003).

60. Nowak, M., Mehrholz, D., Barańska-Rybak, W. & Nowicki, R. J. Wound debridement products and techniques: clinical examples and literature review. *Postepy Dermatol Alergol* **39**, 479-490 (2022).

61. Deng, X., Gould, M. & Ali, M. A. A review of current advancements for wound healing: Biomaterial applications and medical devices. *J Biomed Mater Res B Appl Biomater* **110**, 2542-2573 (2022).

62. Papanas, N. & Maltezos, E. Benefit-risk assessment of becaplermin in the treatment of diabetic foot ulcers. *Drug Saf* **33**, 455-461 (2010).

63. Dutra Alves, N. S. *et al.* Advances in regenerative medicine-based approaches for skin regeneration and rejuvenation. *Front Bioeng Biotechnol* **13**, 1527854 (2025).

64. Ortega, M. A. *et al.* A General Overview on the Hyperbaric Oxygen Therapy: Applications, Mechanisms and Translational Opportunities. *Medicina (Kaunas)* **57** (2021).

65. Ridiandries, A., Tan, J. T. M. & Bursill, C. A. The Role of Chemokines in Wound Healing. *Int J Mol Sci* **19** (2018).

66. Bauer, T. M., Moon, J. Y., Shadiow, J., Buckley, S. D. & Gallagher, K. A. Mechanisms of Impaired Wound Healing in Type 2 Diabetes: The Role of Epigenetic Factors. *Arterioscler Thromb Vasc Biol* **45**, 632-642 (2025).

67. den Dekker, A., Davis, F. M., Kunkel, S. L. & Gallagher, K. A. Targeting epigenetic mechanisms in diabetic wound healing. *Transl Res* **204**, 39-50 (2019).

68. Kimball, A. S. *et al.* The Histone Methyltransferase MLL1 Directs Macrophage-Mediated Inflammation in Wound Healing and Is Altered in a Murine Model of Obesity and Type 2 Diabetes. *Diabetes* **66**, 2459-2471 (2017).

69. Audu, C. O. *et al.* Macrophage-specific inhibition of the histone demethylase JMJD3 decreases STING and pathologic inflammation in diabetic wound repair. *Cell Mol Immunol* **19**, 1251-1262 (2022).

70. Na, J. *et al.* Histone H3K27 Demethylase JMJD3 in Cooperation with NF-κB Regulates Keratinocyte Wound Healing. *J Invest Dermatol* **136**, 847-858 (2016).

71. Holliday, R. & Pugh, J. E. DNA modification mechanisms and gene activity during development. *Science* **187**, 226-232 (1975).

72. Yan, J. *et al.* Diabetes impairs wound healing by Dnmt1-dependent dysregulation of hematopoietic stem cells differentiation towards macrophages. *Nat Commun* **9**, 33 (2018).

73. Yang, X. *et al.* Epigenetic regulation of macrophage polarization by DNA methyltransferase 3b. *Mol Endocrinol* **28**, 565-574 (2014).

74. Phillipson, M. & Kubes, P. The Healing Power of Neutrophils. *Trends Immunol* **40**, 635-647 (2019).

75. Matarazzo, L., Hernandez Santana, Y. E., Walsh, P. T. & Fallon, P. G. The IL-1 cytokine family as custodians of barrier immunity. *Cytokine* **154**, 155890 (2022).

76. Wolf, S. J. *et al.* Diabetic Wound Keratinocytes Induce Macrophage JMJD3-Mediated Nlrp3 Expression via IL-1R Signaling. *Diabetes* **73**, 1462-1472 (2024).

77. Werner, S. & Grose, R. Regulation of wound healing by growth factors and cytokines. *Physiol Rev* **83**, 835-870 (2003).

78. Al Sadoun, H. Macrophage Phenotypes in Normal and Diabetic Wound Healing and Therapeutic Interventions. *Cells* **11** (2022).

79. da Silva, M. D. *et al.* IL-10 cytokine released from M2 macrophages is crucial for analgesic and anti-inflammatory effects of acupuncture in a model of inflammatory muscle pain. *Mol Neurobiol* **51**, 19-31 (2015).

80. Werner, S. Keratinocyte growth factor: a unique player in epithelial repair processes. *Cytokine Growth Factor Rev* **9**, 153-165 (1998).

81. Bonan, N. F. *et al.* Inhibition of HGF/MET signaling decreases overall tumor burden and blocks malignant conversion in Tpl2-related skin cancer. *Oncogenesis* **8**, 1 (2019).

82. Larjava, H., Salo, T., Haapasalmi, K., Kramer, R. H. & Heino, J. Expression of integrins and basement membrane components by wound keratinocytes. *J Clin Invest* **92**, 1425-1435 (1993).

83. Kleiser, S. & Nyström, A. Interplay between Cell-Surface Receptors and Extracellular Matrix in Skin. *Biomolecules* **10** (2020).

84. Bermudez, D. M. *et al.* Impaired biomechanical properties of diabetic skin implications in pathogenesis of diabetic wound complications. *Am J Pathol* **178**, 2215-2223 (2011).

85. Werner, S., Breeden, M., Hübner, G., Greenhalgh, D. G. & Longaker, M. T. Induction of keratinocyte growth factor expression is reduced and delayed during wound healing in the genetically diabetic mouse. *J Invest Dermatol* **103**, 469-473 (1994).

86. Werner, S. *et al.* Differential splicing in the extracellular region of fibroblast growth factor receptor 1 generates receptor variants with different ligand-binding specificities. *Mol Cell Biol* **12**, 82-88 (1992).

87. Law, B., Fowlkes, V., Goldsmith, J. G., Carver, W. & Goldsmith, E. C. Diabetes-induced alterations in the extracellular matrix and their impact on myocardial function. *Microsc Microanal* **18**, 22-34 (2012).

88. DiPietro, L. A. Angiogenesis and wound repair: when enough is enough. *J Leukoc Biol* **100**, 979-984 (2016).

89. Liu, Z. *et al.* Spatiotemporal single-cell roadmap of human skin wound healing. *Cell Stem Cell* **32**, 479-498.e478 (2025).

90. Cambier, S., Gouwy, M. & Proost, P. The chemokines CXCL8 and CXCL12: molecular and functional properties, role in disease and efforts towards pharmacological intervention. *Cell Mol Immunol* **20**, 217-251 (2023).

91. Rousselle, P., Braye, F. & Dayan, G. Re-epithelialization of adult skin wounds: Cellular mechanisms and therapeutic strategies. *Adv Drug Deliv Rev* **146**, 344-365 (2019).

92. Hyter, S. *et al.* Endothelin-1 is a transcriptional target of p53 in epidermal keratinocytes and regulates ultraviolet-induced melanocyte homeostasis. *Pigment Cell Melanoma Res* **26**, 247-258 (2013).

93. Sych, K. *et al.* Expression of PKM2 in wound keratinocytes is coupled to angiogenesis during skin repair in vivo and in HaCaT keratinocytes in vitro. *J Mol Med (Berl)* **101**, 151-169 (2023).

94. Wang, Z. *et al.* Metabolic reprogramming in skin wound healing. *Burns Trauma* **12**, tkad047 (2024).

95. Havran, W. L. & Jameson, J. M. Epidermal T cells and wound healing. *J Immunol* **184**, 5423-5428 (2010).

96. LeBlanc, G., Kreissl, F. K., Melamed, J., Sobel, A. L. & Constantinides, M. G. The role of unconventional T cells in maintaining tissue homeostasis. *Semin Immunol* **61-64**, 101656 (2022).

97. Roan, F., Obata-Ninomiya, K. & Ziegler, S. F. Epithelial cell-derived cytokines: more than just signaling the alarm. *J Clin Invest* **129**, 1441-1451 (2019).

98. Li, H. *et al.* Epigenetic control of IL-23 expression in keratinocytes is important for chronic skin inflammation. *Nat Commun* **9**, 1420 (2018).

99. Hasheminia, A., Mann, S., Liblik, K. & El-Diasty, M. The CCL17/CCL22-CCR4 Axis in Pain Pathogenesis: A Comprehensive Review of Immune-Mediated Mechanisms and Therapeutic Opportunities. *Mol Neurobiol* **63**, 174 (2025).

100. Lan, C. C., Liu, I. H., Fang, A. H., Wen, C. H. & Wu, C. S. Hyperglycaemic conditions decrease cultured keratinocyte mobility: implications for impaired wound healing in patients with diabetes. *Br J Dermatol* **159**, 1103-1115 (2008).

101. Ward, M. S., Fortheringham, A. K., Cooper, M. E. & Forbes, J. M. Targeting advanced glycation endproducts and mitochondrial dysfunction in cardiovascular disease. *Curr Opin Pharmacol* **13**, 654-661 (2013).

102. Caturano, A. *et al.* Oxidative Stress in Type 2 Diabetes: Impacts from Pathogenesis to Lifestyle Modifications. *Curr Issues Mol Biol* **45**, 6651-6666 (2023).

103. Xu, F. *et al.* CXCL10 secreted by SPRY1-deficient epidermal keratinocytes fuels joint inflammation in psoriatic arthritis via CD14 signaling. *J Clin Invest* **135** (2025).

104. Rauschenberger, T. *et al.* T Cells Control Chemokine Secretion by Keratinocytes. *Front Immunol* **10**, 1917 (2019).

105. Haensel, D. *et al.* Defining Epidermal Basal Cell States during Skin Homeostasis and Wound Healing Using Single-Cell Transcriptomics. *Cell Rep* **30**, 3932-3947.e3936 (2020).

106. Zhu, B. M. *et al.* SOCS3 negatively regulates the gp130-STAT3 pathway in mouse skin wound healing. *J Invest Dermatol* **128**, 1821-1829 (2008).

107. Panatta, E. *et al.* Kruppel-like factor 4 regulates keratinocyte senescence. *Biochem Biophys Res Commun* **499**, 389-395 (2018).

108. Dekoninck, S. & Blanpain, C. Stem cell dynamics, migration and plasticity during wound healing. *Nat Cell Biol* **21**, 18-24 (2019).

109. Wang, Y. & Graves, D. T. Keratinocyte Function in Normal and Diabetic Wounds and Modulation by FOXO1. *J Diabetes Res* **2020**, 3714704 (2020).

110. Caley, M. P., Martins, V. L. & O'Toole, E. A. Metalloproteinases and Wound Healing. *Adv Wound Care (New Rochelle)* **4**, 225-234 (2015).

111. Petrie, R. J., Doyle, A. D. & Yamada, K. M. Random versus directionally persistent cell migration. *Nat Rev Mol Cell Biol* **10**, 538-549 (2009).

112. Kelly, G. *et al.* Dysregulated cytokine expression in lesional and nonlesional skin in hidradenitis suppurativa. *Br J Dermatol* **173**, 1431-1439 (2015).

113. Li, L. *et al.* High Glucose Suppresses Keratinocyte Migration Through the Inhibition of p38 MAPK/Autophagy Pathway. *Front Physiol* **10**, 24 (2019).

114. Moura, J. *et al.* Impaired T-cell differentiation in diabetic foot ulceration. *Cell Mol Immunol* **14**, 758-769 (2017).

115. Audu, C. O. *et al.* Histone demethylase JARID1C/KDM5C regulates Th17 cells by increasing IL-6 expression in diabetic plasmacytoid dendritic cells. *JCI Insight* **9** (2024).

116. Wang, Q. *et al.* Dysregulation of circulating CD4+CXCR5+ T cells in type 2 diabetes mellitus. *Apmis* **123**, 146-151 (2015).

117. Cai, B. *et al.* Micro-inflammation characterized by disturbed Treg/Teff balance with increasing sIL-2R in patients with type 2 diabetes. *Exp Clin Endocrinol Diabetes* **121**, 214-219 (2013).

118. Dworacka, M. *et al.* Circulating CD3+56+ cell subset in pre-diabetes. *Exp Clin Endocrinol Diabetes* **122**, 65-70 (2014).

119. Hu, W. *et al.* Skin γδ T Cells and Their Function in Wound Healing. *Front Immunol* **13**, 875076 (2022).

120. Lavoz, C. *et al.* Could IL-17A Be a Novel Therapeutic Target in Diabetic Nephropathy? *J Clin Med* **9** (2020).

121. Ma, J. *et al.* Interleukin 17A promotes diabetic kidney injury. *Sci Rep* **9**, 2264 (2019).

122. Mu, X. *et al.* IL-17 in wound repair: bridging acute and chronic responses. *Cell Commun Signal* **22**, 288 (2024).

123. Furue, M., Furue, K., Tsuji, G. & Nakahara, T. Interleukin-17A and Keratinocytes in Psoriasis. *Int J Mol Sci* **21** (2020).

124. Majumder, S. & McGeachy, M. J. IL-17 in the Pathogenesis of Disease: Good Intentions Gone Awry. *Annu Rev Immunol* **39**, 537-556 (2021).

125. Gurczynski, S. J. & Moore, B. B. IL-17 in the lung: the good, the bad, and the ugly. *Am J Physiol Lung Cell Mol Physiol* **314**, L6-l16 (2018).

126. Jaenisch, R. & Bird, A. Epigenetic regulation of gene expression: how the genome integrates intrinsic and environmental signals. *Nat Genet* **33 Suppl**, 245-254 (2003).

127. Kashgari, G. *et al.* GRHL3 activates FSCN1 to relax cell-cell adhesions between migrating keratinocytes during wound reepithelialization. *JCI Insight* **6** (2021).

128. Kobayashi, T. *et al.* TRAF6 is a critical factor for dendritic cell maturation and development. *Immunity* **19**, 353-363 (2003).

129. Kroetz, D. N. *et al.* Type I Interferon Induced Epigenetic Regulation of Macrophages Suppresses Innate and Adaptive Immunity in Acute Respiratory Viral Infection. *PLoS Pathog* **11**, e1005338 (2015).

130. Davis, F. M. *et al.* Epigenetic regulation of the PGE2 pathway modulates macrophage phenotype in normal and pathologic wound repair. *JCI Insight* **5** (2020).

131. Davis, F. M. *et al.* Palmitate-TLR4 signaling regulates the histone demethylase, JMJD3, in macrophages and impairs diabetic wound healing. *Eur J Immunol* **50**, 1929-1940 (2020).

132. Boniakowski, A. M. *et al.* SIRT3 Regulates Macrophage-Mediated Inflammation in Diabetic Wound Repair. *J Invest Dermatol* **139**, 2528-2537.e2522 (2019).

133. Lichti, U., Anders, J. & Yuspa, S. H. Isolation and short-term culture of primary keratinocytes, hair follicle populations and dermal cells from newborn mice and keratinocytes from adult mice for in vitro analysis and for grafting to immunodeficient mice. *Nat Protoc* **3**, 799-810 (2008).

134. Dickson, M. A. *et al.* Human keratinocytes that express hTERT and also bypass a p16(INK4a)-enforced mechanism that limits life span become immortal yet retain normal growth and differentiation characteristics. *Mol Cell Biol* **20**, 1436-1447 (2000).

135. Vang Mouritzen, M. & Jenssen, H. Optimized Scratch Assay for In Vitro Testing of Cell Migration with an Automated Optical Camera. *J Vis Exp* (2018).

136. Martinotti, S. & Ranzato, E. Scratch Wound Healing Assay. *Methods Mol Biol* **2109**, 225-229 (2020).

137. Bolger, A. M., Lohse, M. & Usadel, B. Trimmomatic: a flexible trimmer for Illumina sequence data. *Bioinformatics* **30**, 2114-2120 (2014).

138. Kim, D., Langmead, B. & Salzberg, S. L. HISAT: a fast spliced aligner with low memory requirements. *Nat Methods* **12**, 357-360 (2015).

139. Liao, Y., Smyth, G. K. & Shi, W. featureCounts: an efficient general purpose program for assigning sequence reads to genomic features. *Bioinformatics* **30**, 923-930 (2014).

140. Robinson, M. D., McCarthy, D. J. & Smyth, G. K. edgeR: a Bioconductor package for differential expression analysis of digital gene expression data. *Bioinformatics* **26**, 139-140 (2010).

141. Ishii, M. *et al.* Epigenetic regulation of the alternatively activated macrophage phenotype. *Blood* **114**, 3244-3254 (2009).

142. Li, B. *et al.* Transcriptome analysis of psoriasis in a large case-control sample: RNA-seq provides insights into disease mechanisms. *J Invest Dermatol* **134**, 1828-1838 (2014).

143. Tsoi, L. C. *et al.* Analysis of long non-coding RNAs highlights tissue-specific expression patterns and epigenetic profiles in normal and psoriatic skin. *Genome Biol* **16**, 24 (2015).

144. Dobin, A. *et al.* STAR: ultrafast universal RNA-seq aligner. *Bioinformatics* **29**, 15-21 (2013).

145. Anders, S., Pyl, P. T. & Huber, W. HTSeq--a Python framework to work with high-throughput sequencing data. *Bioinformatics* **31**, 166-169 (2015).

146. Love, M. I., Huber, W. & Anders, S. Moderated estimation of fold change and dispersion for RNA-seq data with DESeq2. *Genome Biol* **15**, 550 (2014).

147. Tsoi, L. C. *et al.* Progression of acute-to-chronic atopic dermatitis is associated with quantitative rather than qualitative changes in cytokine responses. *J Allergy Clin Immunol* **145**, 1406-1415 (2020).

148. Butler, A., Hoffman, P., Smibert, P., Papalexi, E. & Satija, R. Integrating single-cell transcriptomic data across different conditions, technologies, and species. *Nat Biotechnol* **36**, 411-420 (2018).

149. Konieczny, P. *et al.* Interleukin-17 governs hypoxic adaptation of injured epithelium. *Science* **377**, eabg9302 (2022).

150. Wikramanayake, T. C., Borda, L. J., Miteva, M. & Paus, R. Seborrheic dermatitis-Looking beyond Malassezia. *Exp Dermatol* **28**, 991-1001 (2019).

151. Smits, J. P. H. *et al.* Immortalized N/TERT keratinocytes as an alternative cell source in 3D human epidermal models. *Sci Rep* **7**, 11838 (2017).

152. Koike, Y., Yozaki, M., Utani, A. & Murota, H. Fibroblast growth factor 2 accelerates the epithelial-mesenchymal transition in keratinocytes during wound healing process. *Sci Rep* **10**, 18545 (2020).

153. Meyer, M. *et al.* FGF receptors 1 and 2 are key regulators of keratinocyte migration in vitro and in wounded skin. *J Cell Sci* **125**, 5690-5701 (2012).

154. Margadant, C. *et al.* Integrin alpha3beta1 inhibits directional migration and wound re-epithelialization in the skin. *J Cell Sci* **122**, 278-288 (2009).

155. Kim, J. P., Zhang, K., Kramer, R. H., Schall, T. J. & Woodley, D. T. Integrin receptors and RGD sequences in human keratinocyte migration: unique anti-migratory function of alpha 3 beta 1 epiligrin receptor. *J Invest Dermatol* **98**, 764-770 (1992).

156. Hodivala-Dilke, K. M., DiPersio, C. M., Kreidberg, J. A. & Hynes, R. O. Novel roles for alpha3beta1 integrin as a regulator of cytoskeletal assembly and as a trans-dominant inhibitor of integrin receptor function in mouse keratinocytes. *J Cell Biol* **142**, 1357-1369 (1998).

157. deHart, G. W., Healy, K. E. & Jones, J. C. The role of alpha3beta1 integrin in determining the supramolecular organization of laminin-5 in the extracellular matrix of keratinocytes. *Exp Cell Res* **283**, 67-79 (2003).

158. Rousselle, P., Montmasson, M. & Garnier, C. Extracellular matrix contribution to skin wound re-epithelialization. *Matrix Biol* **75-76**, 12-26 (2019).

159. Arpino, V., Brock, M. & Gill, S. E. The role of TIMPs in regulation of extracellular matrix proteolysis. *Matrix Biol* **44-46**, 247-254 (2015).

160. Rohani, M. G. & Parks, W. C. Matrix remodeling by MMPs during wound repair. *Matrix Biol* **44-46**, 113-121 (2015).

161. Huang, S. M. *et al.* High glucose environment induces M1 macrophage polarization that impairs keratinocyte migration via TNF-α: An important mechanism to delay the diabetic wound healing. *J Dermatol Sci* **96**, 159-167 (2019).

162. Chiricozzi, A. *et al.* Integrative responses to IL-17 and TNF-α in human keratinocytes account for key inflammatory pathogenic circuits in psoriasis. *J Invest Dermatol* **131**, 677-687 (2011).

163. Korbecki, J., Maruszewska, A., Bosiacki, M., Chlubek, D. & Baranowska-Bosiacka, I. The Potential Importance of CXCL1 in the Physiological State and in Noncancer Diseases of the Cardiovascular System, Respiratory System and Skin. *Int J Mol Sci* **24** (2022).

164. Gallagher, K. A. *et al.* Epigenetic changes in bone marrow progenitor cells influence the inflammatory phenotype and alter wound healing in type 2 diabetes. *Diabetes* **64**, 1420-1430 (2015).

165. Swaidani, S., Liu, C., Zhao, J., Bulek, K. & Li, X. TRAF Regulation of IL-17 Cytokine Signaling. *Front Immunol* **10**, 1293 (2019).

166. Qian, Y., Kang, Z., Liu, C. & Li, X. IL-17 signaling in host defense and inflammatory diseases. *Cell Mol Immunol* **7**, 328-333 (2010).

167. Chang, S. H., Park, H. & Dong, C. Act1 adaptor protein is an immediate and essential signaling component of interleukin-17 receptor. *J Biol Chem* **281**, 35603-35607 (2006).

168. Xu, S. & Cao, X. Interleukin-17 and its expanding biological functions. *Cell Mol Immunol* **7**, 164-174 (2010).

169. Dalpatraj, N., Naik, A. & Thakur, N. GSK-J4: An H3K27 histone demethylase inhibitor, as a potential anti-cancer agent. *Int J Cancer* **153**, 1130-1138 (2023).

170. Qiu, A. W., Cao, X., Zhang, W. W. & Liu, Q. H. IL-17A is involved in diabetic inflammatory pathogenesis by its receptor IL-17RA. *Exp Biol Med (Maywood)* **246**, 57-65 (2021).

171. Melvin, W. J. *et al.* The histone methyltransferase Mixed-lineage-leukemia-1 drives T cell phenotype via Notch signaling in diabetic tissue repair. *JCI Insight* **9** (2024).

172. Tartaglia, L. A. *et al.* Identification and expression cloning of a leptin receptor, OB-R. *Cell* **83**, 1263-1271 (1995).

173. Parekh, P. I., Petro, A. E., Tiller, J. M., Feinglos, M. N. & Surwit, R. S. Reversal of diet-induced obesity and diabetes in C57BL/6J mice. *Metabolism* **47**, 1089-1096 (1998).

174. Liu, Y. *et al.* Fibroblasts: Immunomodulatory factors in refractory diabetic wound healing. *Front Immunol* **13**, 918223 (2022).

175. Ling, C. & Rönn, T. Epigenetics in Human Obesity and Type 2 Diabetes. *Cell Metab* **29**, 1028-1044 (2019).

176. Nilsson, E. *et al.* Altered DNA methylation and differential expression of genes influencing metabolism and inflammation in adipose tissue from subjects with type 2 diabetes. *Diabetes* **63**, 2962-2976 (2014).

177. De Santa, F. *et al.* The histone H3 lysine-27 demethylase Jmjd3 links inflammation to inhibition of polycomb-mediated gene silencing. *Cell* **130**, 1083-1094 (2007).

178. Liu, T., Zhang, L., Joo, D. & Sun, S. C. NF-κB signaling in inflammation. *Signal Transduct Target Ther* **2**, 17023- (2017).

179. Zhang, X., Yin, M. & Zhang, L. J. Keratin 6, 16 and 17-Critical Barrier Alarmin Molecules in Skin Wounds and Psoriasis. *Cells* **8** (2019).

180. Rajarathnam, K., Schnoor, M., Richardson, R. M. & Rajagopal, S. How do chemokines navigate neutrophils to the target site: Dissecting the structural mechanisms and signaling pathways. *Cell Signal* **54**, 69-80 (2019).

181. Ma, X. X. *et al.* The role of neutrophils in diabetic ulcers and targeting therapeutic strategies. *Int Immunopharmacol* **124**, 110861 (2023).

182. Takagi, N. *et al.* IL-17A promotes neutrophilic inflammation and disturbs acute wound healing in skin. *Exp Dermatol* **26**, 137-144 (2017).

183. Wan, R. *et al.* Diabetic wound healing: The impact of diabetes on myofibroblast activity and its potential therapeutic treatments. *Wound Repair Regen* **29**, 573-581 (2021).

184. Wang, J. & Ding, X. IL-17 signaling in skin repair: safeguarding metabolic adaptation of wound epithelial cells. *Signal Transduct Target Ther* **7**, 359 (2022).

185. Zhang, T. *et al.* EZH2-dependent epigenetic modulation of histone H3 lysine-27 contributes to psoriasis by promoting keratinocyte proliferation. *Cell Death Dis* **11**, 826 (2020).

186. Hu, S. C. & Lan, C. E. High-glucose environment disturbs the physiologic functions of keratinocytes: Focusing on diabetic wound healing. *J Dermatol Sci* **84**, 121-127 (2016).

187. Brazil, J. C., Quiros, M., Nusrat, A. & Parkos, C. A. Innate immune cell-epithelial crosstalk during wound repair. *J Clin Invest* **129**, 2983-2993 (2019).

188. Barker, J. N., Mitra, R. S., Griffiths, C. E., Dixit, V. M. & Nickoloff, B. J. Keratinocytes as initiators of inflammation. *Lancet* **337**, 211-214 (1991).

189. Falanga, V. Wound healing and its impairment in the diabetic foot. *Lancet* **366**, 1736-1743 (2005).

190. Guenther, M. G., Levine, S. S., Boyer, L. A., Jaenisch, R. & Young, R. A. A chromatin landmark and transcription initiation at most promoters in human cells. *Cell* **130**, 77-88 (2007).

191. Melvin, W. J. *et al.* Coronavirus induces diabetic macrophage-mediated inflammation via SETDB2. *Proc Natl Acad Sci U S A* **118** (2021).

192. Torrano, J., Al Emran, A., Hammerlindl, H. & Schaider, H. Emerging roles of H3K9me3, SETDB1 and SETDB2 in therapy-induced cellular reprogramming. *Clin Epigenetics* **11**, 43 (2019).

193. Zhang, X. *et al.* Deficiency of histone lysine methyltransferase SETDB2 in hematopoietic cells promotes vascular inflammation and accelerates atherosclerosis. *JCI Insight* **6** (2021).

194. Rayamajhi, M., Humann, J., Kearney, S., Hill, K. K. & Lenz, L. L. Antagonistic crosstalk between type I and II interferons and increased host susceptibility to bacterial infections. *Virulence* **1**, 418-422 (2010).

195. Rawlings, J. S., Rosler, K. M. & Harrison, D. A. The JAK/STAT signaling pathway. *J Cell Sci* **117**, 1281-1283 (2004).

196. Kahn, J. S., Deverapalli, S. C. & Rosmarin, D. M. JAK-STAT signaling pathway inhibition: a role for treatment of discoid lupus erythematosus and dermatomyositis. *Int J Dermatol* **57**, 1007-1014 (2018).

197. Qi, F., Liu, F. & Gao, L. Janus Kinase Inhibitors in the Treatment of Vitiligo: A Review. *Front Immunol* **12**, 790125 (2021).

198. Alves de Medeiros, A. K. *et al.* JAK3 as an Emerging Target for Topical Treatment of Inflammatory Skin Diseases. *PLoS One* **11**, e0164080 (2016).

199. Amano, W. *et al.* The Janus kinase inhibitor JTE-052 improves skin barrier function through suppressing signal transducer and activator of transcription 3 signaling. *J Allergy Clin Immunol* **136**, 667-677.e667 (2015).

200. Turnier, J. L. & Kahlenberg, J. M. The Role of Cutaneous Type I IFNs in Autoimmune and Autoinflammatory Diseases. *J Immunol* **205**, 2941-2950 (2020).

201. Mangum, K. D. *et al.* The STAT3/SETDB2 axis dictates NF-κB-mediated inflammation in macrophages during wound repair. *JCI Insight* **9** (2024).

202. Alexander, K. A. *et al.* Inhibition of JAK1/2 Tyrosine Kinases Reduces Neurogenic Heterotopic Ossification After Spinal Cord Injury. *Front Immunol* **10**, 377 (2019).

203. Hosseini Mansoub, N. The role of keratinocyte function on the defected diabetic wound healing. *Int J Burns Trauma* **11**, 430-441 (2021).

204. Eming, S. A., Wynn, T. A. & Martin, P. Inflammation and metabolism in tissue repair and regeneration. *Science* **356**, 1026-1030 (2017).

205. Shaw, T. & Martin, P. Epigenetic reprogramming during wound healing: loss of polycomb-mediated silencing may enable upregulation of repair genes. *EMBO Rep* **10**, 881-886 (2009).

206. Nicetto, D. & Zaret, K. S. Role of H3K9me3 heterochromatin in cell identity establishment and maintenance. *Curr Opin Genet Dev* **55**, 1-10 (2019).

207. Kang, S., Long, K., Wang, S., Sada, A. & Tumbar, T. Histone H3 K4/9/27 Trimethylation Levels Affect Wound Healing and Stem Cell Dynamics in Adult Skin. *Stem Cell Reports* **14**, 34-48 (2020).

208. Naik, S. *et al.* Inflammatory memory sensitizes skin epithelial stem cells to tissue damage. *Nature* **550**, 475-480 (2017).

209. Gregorio, J. *et al.* Plasmacytoid dendritic cells sense skin injury and promote wound healing through type I interferons. *J Exp Med* **207**, 2921-2930 (2010).

210. Pott, J. *et al.* IFN-lambda determines the intestinal epithelial antiviral host defense. *Proc Natl Acad Sci U S A* **108**, 7944-7949 (2011).

211. Ivashkiv, L. B. & Donlin, L. T. Regulation of type I interferon responses. *Nat Rev Immunol* **14**, 36-49 (2014).

212. Keating, S. T. & El-Osta, A. Epigenetics and metabolism. *Circ Res* **116**, 715-736 (2015).

213. Reddy, M. A., Zhang, E. & Natarajan, R. Epigenetic mechanisms in diabetic complications and metabolic memory. *Diabetologia* **58**, 443-455 (2015).

214. Veltkamp, S. H. C. & Voorneveld, P. W. The Cell-Specific Effects of JAK1 Inhibitors in Ulcerative Colitis. *J Clin Med* **14** (2025).

215. Avgustinova, A. & Benitah, S. A. Epigenetic control of adult stem cell function. *Nat Rev Mol Cell Biol* **17**, 643-658 (2016).

216. Chen, Y. *et al.* Mitochondrial quality control in diabetes mellitus and complications: molecular mechanisms and therapeutic strategies. *Cell Death Dis* **16**, 652 (2025).

217. West, A. P. *et al.* Mitochondrial DNA stress primes the antiviral innate immune response. *Nature* **520**, 553-557 (2015).

218. Singh, K. *et al.* Genome-wide DNA hypermethylation opposes healing in patients with chronic wounds by impairing epithelial-mesenchymal transition. *J Clin Invest* **132** (2022).

219. Goto, N. *et al.* ISWI chromatin remodeling complexes recruit NSD2 and H3K36me2 in pericentromeric heterochromatin. *J Cell Biol* **223** (2024).

220. Yan, J. *et al.* WHSC1 is involved in DNA damage, cellular senescence and immune response in hepatocellular carcinoma progression. *J Cell Mol Med* **27**, 1436-1441 (2023).

221. Sengupta, D. *et al.* NSD2 dimethylation at H3K36 promotes lung adenocarcinoma pathogenesis. *Mol Cell* **81**, 4481-4492.e4489 (2021).

222. Wang, Y. *et al.* Histone methyltransferase WHSC1 inhibits colorectal cancer cell apoptosis via targeting anti-apoptotic BCL2. *Cell Death Discov* **7**, 19 (2021).

223. Chen, D. *et al.* H3K36me2 methyltransferase NSD2/WHSC1 promotes triple-negative breast cancer metastasis via activation of ULK1-dependent autophagy. *Autophagy* **21**, 1824-1842 (2025).

224. Chen, D. *et al.* Circ-FOXO3 inhibits triple-negative breast cancer growth and metastasis via regulating WHSC1-H3K36me2-Zeb2 axis. *Cell Signal* **117**, 111079 (2024).

225. Li, J. *et al.* Topical Lyophilized Targeted Lipid Nanoparticles in the Restoration of Skin Barrier Function following Burn Wound. *Mol Ther* **26**, 2178-2188 (2018).

226. Kato, M. & Natarajan, R. Epigenetics and epigenomics in diabetic kidney disease and metabolic memory. *Nat Rev Nephrol* **15**, 327-345 (2019).

227. Fadul, S. M., Arshad, A. & Mehmood, R. CRISPR-based epigenome editing: mechanisms and applications. *Epigenomics* **15**, 1137-1155 (2023).

228. Shakra, M. Y. Tissue nanotransfection and cellular reprogramming in regenerative medicine and antimicrobial dynamics. *Front Bioeng Biotechnol* **13**, 1558735 (2025).

229. Juergens, R. A. *et al.* Combination epigenetic therapy has efficacy in patients with refractory advanced non-small cell lung cancer. *Cancer Discov* **1**, 598-607 (2011).

230. Yasui, K. *et al.* Circulating cell-free DNA methylation patterns as non-invasive biomarkers to monitor colorectal cancer treatment efficacy without referencing primary site mutation profiles. *Mol Cancer* **23**, 1 (2024).

231. Zhang, J. *et al.* AGE-induced keratinocyte MMP-9 expression is linked to TET2-mediated CpG demethylation. *Wound Repair Regen* **24**, 489-500 (2016).